Development of Small Molecular Weight Bioactive Compounds and Polysaccharide from Marine Macroalgae belonging to the Family Sargassaceae.

Synopsis of the

Ph. D Thesis

Submitted to

MANGALORE UNIVERSITY

for the award of the degree of

DOCTOR OF PHILOSOPHY

in

CHEMISTRY

by

Mr. Shubhajit Dhara

RESEARCH FELLOW

(Ref. No. MU/EXB/Ph.D/CR.80/Chem./2020-21/E.13, dated 20th November, 2020)

Under the Faculty of Science and Technology

MANGALORE UNIVERSITY

MANGALAGANGOTHRI – 574 199

Dakshina Kannada Dist. Karnataka, India

Central Marine Fisheries Research Institute

Post Box No. 1603, Ernakulam North PO

Kochi- 682 018, Kerala

India

NAME OF THE GUIDE: DR. KAJAL CHAKRABORTY

Principal Scientist (Organic Chemistry)

Central Marine Fisheries Research Institute (CMFRI)

April 2023

ABSTRACT

Marine organisms, mainly marine macroalgae, are potential reservoirs of naturally-derived chemical compounds with potent pharmacological properties and additional health benefits. Among various brown marine macroalgae those belonging to the family Sargassaceae, particularly *Sargassum* and *Turbinaria*, are ubiquitous in the coastal shelf areas and represent an untapped reservoir of bioactive compounds with valuable pharmaceutical applications. The present study envisaged isolating and characterizing small molecular weight lead pharmacophores and polysaccharides from *Turbinaria conoides* {(J.Agardh) Kützing, 1860}, *Turbinaria ornata* {(Turner) J.Agardh, 1848}, *Sargassum tenerrimum* (J.Agardh, 1848), and *Sargassum ilicifolium* {(Turner) C. Agardh, 1820} belonging to family Sargassaceae involving chemical profiling coupled with the evaluation of biological activity concerning inflammation, hyperglycemia, and hypertension.

Pharmacological potencies of ethyl acetate/methanol (EtOAc/MeOH) extract of four different brown algal species (*Turbinaria conoides*, *Turbinaria ornata*, *Sargassum tenerrimum* and *Sargassum ilicifolium*) was evaluated against hyperglycemic, hypertensive, inflammation and free radical scavenging by various *in vitro* studies. Among the studied algal species, crude organic extract of *T. ornata* exhibited more significant attenuation potential against pro-inflammatory 5-lipoxygenase (5-LOX) enzyme (IC_{50} 1.11 mg mL^{-1}) along with starch degrading enzyme α-amylase and proteolytic enzyme dipeptidyl peptidase-4 (DPP-4) (IC_{50} 0.42 and 0.24 mg mL^{-1}, respectively) in comparison with other studied species. Crude extract of *T. conoides* showed maximum enzyme inhibitory potential (IC_{50} 1.09 mg mL^{-1}) against cyclooxygenase-2 (COX-2). Organic crude extracts of *Sargassum* species recorded with lesser angiotensin-converting enzyme (ACE-I) inhibitory potential (IC_{50} 0.27-0.33 mg mL^{-1}) than those exhibited by *Turbinaria* species (IC_{50} 0.18-0.22 mg mL^{-1}). Principle component analysis (PCA) statistical study revealed positive correlations between anti-inflammatory, antioxidant, anti-hyperglycemic and anti-hypertensive activities of tested macroalgal extracts. It was established that non-phenolic compounds in algal crude extracts could be responsible for bioactivities. The proton nuclear magnetic resonance (NMR) spectra of crude macroalgal extracts showed a direct correlation between the number of electronegative functionalities (appeared at the downfield region) and bioactivities. Therefore, crude EtOAc/MeOH extracts of *T. conoides*, *T. ornata* and *S. ilicifolium* were fractionated by repeated column chromatography to obtain different types of previously undescribed compounds. Chemical structures of isolated compounds were ascertained by detailed spectroscopic analyses, such as one and two-dimensional NMR spectroscopy, Fourier transform infrared (FT-IR), and mass spectroscopy. The bioactivities of isolated compounds were evaluated by different *in vitro* analyses. Different electronic, steric and hydrophobic parameters were used to determine structure-bioactivity correlation analyses

The organic extract of *Turbinaria conoides*, harvested from the Gulf of Manner region of Indian peninsular was chromatographically fractionated to yield three substituted 2*H*-pyran derivatives, namely methyl-2^1-yl-[5′,6′-dihydro-5′-yl-{5^4-(4-hydroxybenzoyl)-oxy-(5^2-methylbutyl)}-3′-methyl-2*H*-pyran]-2^1-methyl butanoate (compound **1**), 11-[(3′,6′-dihydro-4′-methyl-2′-oxo-2*H*-pyran-3′-yl)methyl]-1′-methylhexyl benzoate (compound **2**), and [6-ethyl-3,4-dimethyl-(tetrahydro-2′,2′,6′-trimethyl-2*H*-pyran-3′-yl)-2,5-cycloheptadiene]-1′-propanoate (compound **3**). The compounds **1** and **2** bearing 2*H*-pyranyl-4-hydroxybenzoyl and 2*H*-pyranyl-1′-methylhexylbenzoate moieties exhibited potential antioxidant activities (IC_{50} 0.54-0.69 mg mL^{-1}). Likewise, potential bioactivity of the 2*H*-pyran derivative **1** against 5-lipoxygenase (IC_{50} ~ 1 mg mL^{-1}) along with higher index of selectivity (COX-1 $inhibitory_{IC50}$/COX-2 $inhibitory_{IC50}$ 1.88) indicated their selective anti-inflammatory properties against inducible inflammatory mediators than that displayed by commercially available non-steroidal anti-inflammatory drug (ibuprofen, 0.44). Structure-activity relationship analysis of the studied compounds showed that the anti-oxidative and anti-inflammatory potentials were

directly proportional to their electronic properties. The previously undescribed 2*H*-pyranoids might constitute potential anti-oxidative and anti-inflammatory pharmacophores for medicinal applications.

Bioactivity-guided chromatographic fractionation of the organic extract of *T. conoides* resulted in three previously undescribed macrocyclic lactone homologues, named 6-ethyl-9,18,19-trihydroxy-24,28-dimethyl-22,25-dioxabicyclo[19.3.1]pentacosa-5,11,14-triene-1-one (compound **4**), 6-ethyl-9,18,19-trihydroxy-28-dimethyl-22,25-dioxabicyclo[19.3.1]pentacosa-5,11,14-triene-1-one-29-yl)isobutyl acetate (compound **5**), and (6-ethyl-9,18,19-trihydroxy-28-dimethyl-22,25-dioxabicyclo[19.3.1]pentacosa-5,11,14-triene-1-one-29-yl)methyl acetate (compound **6**). Compound **4** displayed more significant attenuation potential against COX-2 (IC_{50} 1.75 mM) and 5-LOX (IC_{50} 4.24 mM) than other analogues. The higher selectivity index of compound **4** (COX-1 $inhibitory_{IC50}$/COX-2 $inhibitory_{IC50}$ 1.79) recognized its selective attenuation potential against the inducible COX-2 enzyme. A superior inhibition potential of compound **4** was observed against ACE-I (IC_{50} 1.23 mM) and protein tyrosine phosphatase-1B (PTP-1B, IC_{50} 1.39 mM). *In silico* molecular docking study of compound **4** with the allosteric sites of the targeted enzymes exhibited the least binding energy of -14.51 to -11.27 kcal mol^{-1} compared to those exhibited by other studied macrolide homologues. Drug-likeness and predictive pharmacokinetic parameters of compound **4** exhibited an acceptable oral bioavailability. These reports inferred that compound **4** encompassing pentacosa macrocyclic moiety, could be a promising therapeutic lead to inhibit the enzymes related to the development and progression of pathological conditions leading to inflammation, hypertension and type-2 diabetes.

Chromatographically fractionated crude extract of *Turbinaria conoides* (family Sargassaceae) yielded an undescribed furanyl-substituted isochromanyl metabolite, which was characterized as methyl 4-[8-{[4-ethyl-2,3-dihydrofuran-3-yl]methyl}-1-oxo-3,4-dihydro-1*H*-2-benzopyran-3-yl]butanoate (compound **7**). The isochromanyl derivative possessed comparable attenuation potential against 5-LOX (IC_{50} 3.70 μM) with standard 5-LOX inhibitor drug (IC_{50} 2.41 μM). Noticeably, the index of anti-inflammatory selectivity of compound **7** (~1.7) was considerably more significant than that exhibited by the standard agent (1.06). Antioxidant properties of compound **7** against oxidants (IC_{50} ~ 24 μM) further supported its potential anti-inflammatory property. Greater electronic properties (topological polar surface area of 61.8) along with comparatively lesser docking parameters of compound **7** with aminoacyl residues of targeted enzymes (COX-2 and 5-LOX) (binding energy of -11.05 and -9.40 kcal mol^{-1}, respectively) recognized its prospective anti-inflammatory potential. To develop seaweed-based natural anti-inflammatory leads, the present study isolated compound **7** as promising 5-LOX and COX-2 inhibitor, which could be used for pharmaceutical and biotechnological applications.

Bioactive compounds with ACE-I attenuation potential are deemed as therapeutic agents for hypertension owing to their capacity to suppress the conversion of angiotensin-I into the vasoconstrictor angiotensin-II. In an aim to develop natural ACE-I inhibitors from marine algae, three 6, 6-spiroketals, named as 6ª-methylpent-5ª-en-3ª-yl-1ª-(4′,6′,6-trimethyl-3-oxodecahydrospiro [furo-3,4-c] pyran-7, 2′-pyran-3′-yl) acetate (compound **8**), pent-4ª-en-3ª-yl-1ª-(7-acetoxy-6′-methyl-4-oxodecahydrospiro [isochromene-8,2′-pyran]-3′-yl) acetate (compound **9**) and 6ª-methylocta-1ª-(4′-acetoxy-6′-methyl-4-oxodecahydrospiro-[isochromene-8,2′-pyran]-3′-yl)-1ª,5ª-diene (compound **10**) were isolated from the organic extract of the spiny brown marine macroalga *Turbinaria ornata*. Compound **8** exhibited comparatively greater ACE-I attenuation potential (IC_{50} 4.5 μM) than those displayed by other studied spiroketals (IC_{50} 4.7–4.9 μM). Greater antioxidant properties of compound **8** against oxidants (IC_{50} 1.1-1.3 mM) also substantiated its potential attenuation property against ACE-I enzyme. Structure-activity correlation studies showed that electronic properties (topological polar surface area, 71) and balanced hydrophilic-lipophilic parameters (partition coefficient of logarithmic octanol-water ~3.2) of compound **8** appeared to play pivotal roles in the inhibition of the targeted enzyme. Predicted

drug-likeness and other physicochemical parameters appeared to attribute to the acceptable oral bioavailability of spiroketal derivatives. Additionally, the least binding energy of compound **8** (-10.5 kcal/mol) coupled with the maximum number of hydrogen-bonding interactions with allosteric sites of the zinc-dependent angiotensin converting enzyme could recognize its potential therapeutic application against hypertensive diseases.

Chemical investigation of Phaeophytan marine macroalga *Turbinaria ornata* resulted in the characterization of three 2-furanone analogues, which were characterized as 6,7-dihydroxy-8-methyl-3-(5'-methyloct-4'-en-1'-yl)-3,4,5,6,7,8-hexahydrocyclooct-1-en-[1,2-c]furan-11-one (compound **11**), 4-hydroxy-3-isopropyl-7,8-dimethyl-6-(pentan-2'-acetate)-3,4,5,6,7,8-hexahydrocycloocta-1-en-[1,2-c]furan-11-one (compound **12**), and 6-acetoxy-8-ethyl-5-methoxy-3-(2'-methylhex-4'-en-1'-yl)-3,4,5,6,7-pentahydrocycloocta-1,7-dien-[1,2-c]furan-11-one (compound **13**). Inhibitory property of compound **12** against PTP-1B was significantly greater (IC_{50} 2.42 mM) than those exhibited by other studied analogues. Greater electronic properties along with molecular docking experiments corroborated the attenuation property of compound **12** against PTP-1B, by exhibiting minimum binding energy of -11.80 kcal mol^{-1} compared to other studied analogues. The results demonstrated that previously undescribed compound **12** might be used as a prospective natural anti-hyperglycemic lead to alleviating the likelihood of higher postprandial blood glucose levels.

Phytochemical analysis of the organic extract from intertidal brown seaweed *Sargassum ilicifolium* characterized an undescribed xenicane-type compound, elucidated as 3-(17-hydroxy-14-methylhept-13-en-10-yl)-6-methylhexahydro-1*H*-cyclonona[c]furan-4,19-diyl diacetate (compound **14**). The studied compound exhibited prospective free radical quenching potential (IC_{50} 1.2-1.4 mM) in comparison with commercial antioxidant (α-tocopherol, IC_{50} > 1.40 mM). Attenuation property of compound **14** against pro-inflammatory enzyme, 5-LOX (IC_{50} 4.70 mM) was comparable with that displayed by the nonsteroidal anti-inflammatory agent ibuprofen (IC_{50} 4.51 mM). Compound **14** showed a greater selectivity index (1.42) than ibuprofen's (0.44), recognizing the former's selective attenuation potential against the inducible COX-2 and 5-LOX enzymes. Higher electronic parameters (topological polar surface area, 82.06) and balanced hydrophobic-hydrophilic property (octanol-water partition coefficient 2.94) coupled with docking score (-11.17 kcal mol^{-1}) and lower binding energy (-9.61 kcal mol^{-1}) with the active site of 5-lipoxygenase supported the significant anti-inflammatory properties of the studied xenicane-type compound.

Naturally occurring polysaccharide-structured nanoparticles have developed as promising materials for treating bone health disorders. Silver nanoparticle (ST-Ag^{NP})-structured from sulfated polygalacto-fucopyranose isolated from *Sargassum tenerrimum* demonstrated potential activities associated with osteogenesis. Subsequent treatment with ST-Ag^{NP}, activity of alkaline phosphatase (63 mU/mg) was raised in osteoblast stem cells (human mesenchymal, hMSC) than those exhibited by control treatment (30 mU/mg). The intense growth of mineralized nodule on the surface of hMSC was apparent following treatment with ST-Ag^{NP}, with an intensity difference from 0.46 (obtained from normal control cells) to 3.64 fold (obtained after treatment with ST-Ag^{NP}). An increased population of bone morphogenic protein-2 (23%) and osteocalcin-positive cells (50%) on M2 macrophages were apparent following treatment with ST-Ag^{NP} (0.25 mg mL^{-1}). Glucocorticoid-induced *in vivo* animal model studies of ST-Ag^{NP} exhibited significant recovery of serum biochemical parameters along with serum estradiol (75 pg/mL) and parathyroid hormone (7.4 pg/mL) compared to disease control (46.5 and 13 pg/mL, respectively). Disease-induced groups treated with ST-Ag^{NP} showed the disappearance of osteoporotic cavities in the trabecular bone. Following treatment with ST-Ag^{NP}, serum calcium and phosphorus contents were significantly recovered.

Tumor protein, or cellular tumor antigen *p53*, is considered a critical transcriptional regulation factor, which can suppress the growth of tumor cells by activating other functional genes. The current study appraised the *p53* activation pathways, which could be used as an alternative therapeutic strategy for treating hepatocellular and ductal carcinoma. Algal polysaccharides have been used as emerging sources of bioactive natural pharmacophores. A sulfated galactofucan characterized as [→1)-*O*-4-sulfonato-*α*-fucopyranose-(3 → 1)-*α*-fucopyranose-(3→] as the main branch with [→1)-6-*O*-acetyl-*β*-galactopyranose-(4→] as side chain isolated from *Turbinaria ornata* exhibited prospective apoptosis on HepG2 (hepatocellular carcinoma) and MCF7 (ductal carcinoma) cells. Annexin V-fluorescein isothiocyanate-propidium iodide study displayed higher early apoptosis in MCF7 and HepG2 cell lines (56 and 24.2%, respectively) treated with sulfated galactofucan (at IC_{50} concentration) than those administered with standard camptothecin. Upregulation of the *p53* gene expression (1.5-1.8 fold upregulation compared to standard control) was perceived in sulfated galactofucan treated HepG2 and MCF7 cells.

Sulfated polysaccharides are effective immunostimulating agents by activating several intracellular signaling pathways. A sulfated (1→3)/(1→4)-linked galactofucan with promising immunomodulatory effects was purified from *Turbinaria conoides*. The immune-enhancing potential of sulfated (1→3)/(1→4)-linked galactofucan (100-400 mg/kg BW) was evaluated on cyclophosphamide-induced immunosuppressed animals by increasing bone marrow cellularity (10-13 cells/femur/mL x 10^6), *α*-esterase activity (1200-1700 number of positive cells/4000 BMC), interferon-*γ* (1.31-1.49 pg/mL), interleukin-2 (3.49-3.99 pg/mL) secretion, and WBC count (> 3000 cells/cu mm). The proliferation of lymphocytes for *in vitro* and *in vivo* conditions was enhanced by administering sulfated (1→3)/(1→4)-linked galactofucan besides regulating the secretion of pro-inflammatory cytokines (interleukin-6/1*β*/12, tumor necrosis factor-*α*, transforming growth factor-*β*), and an inducible isoform of nitric oxide synthase. A promising reduction of viral copy formation was observed by administering sulfated (1→3)/(1→4)-linked galactofucan (< 2×10^7 number) on SARS CoV-2 (delta variant) induced Vero cells in comparison with the infected group (> 5×10^7 number).

After repeated chromatographic fractionation, organic extracts of *T. conoides*, *T. ornata* and *S. ilicifolium* yielded 14 previously undescribed compounds with potential pharmacological properties against various oxidative stress-induced disorders with potential pharmacological properties against various oxidative stress-induced disorders. Further, three sulfated polysaccharides were isolated from *S. tenerrimum*, *T. ornata*, and *T. conoides*, whereas their bioactivities were evaluated by *in vitro* and *in vivo* models. The sulfated polygalacto-fucopyranose isolated from *S. tenerrimum* has been used to develop polysaccharide-based nanoparticle, which might be a good therapeutic lead to reduce the risk of bone health disorders. A sulfated galactofucan isolated from *T. ornata* could be used as an alternative therapeutic approach against ductal and hepatocellular carcinoma. The sulfated (1→3)/(1→4)-linked galactofucan isolated from *T. conoides* might be a potent naturally-derived alternative for health benefits against inflammation, autoimmune disorders and SARS-CoV-2 infection.

The pharmacologically active small molecular metabolites and polysaccharide leads developed from the marine macroalgal species belonging to *T. conoides*, *T. ornata*, *S. ilicifolium* and *S. tenerrimum* can be considered promising therapeutic candidates against different oxidative stress-induced diseases to promote well-being, and thus, support achieving many of the 'Development Challenges' directly linked to the United Nations Sustainability Development Goals (SDG) envisaging to ensure a healthy life.

The present investigation entitled "**Development of small molecular weight bioactive compounds and polysaccharide from marine macroalgae belonging to the family Sargassaceae.**" has been discussed under seven chapters. The primary sections discussed the acknowledgements, abbreviations, contents, abstract, list of tables and list

of figures. The chapters are divided into nine followed by references and the list of publications, which were detailed as follows:

CHAPTER 1: INTRODUCTION

This is a prefatory chapter, which was dealt with an introduction on the importance and significance of marine macroalgae. This chapter explained the bioactive potencies of marine macroalgae belonging to the family Sargassaceae along with the importance of small molecular weight bioactive compounds and polysaccharides.

The marine ecosystem comprises around fifty percent of the global biodiversity, inhabiting 75% of the earth's surface and containing a large assemblage of different species or organisms. Marine organisms have gained more significant attraction for several years because of their remarkable biodiversity. They are a promising natural reservoir of specialized pharmacologically active lead molecules with diverse chemical structures. The development of marine organisms in an extremely stressful underwater environment helps them to reinforce their natural defence system. Therefore, they can potentially produce a large variety of bioactive compounds. Bioactive metabolites obtained from marine organisms were beneficial as functional food and pharmaceutical agent (Peñalver et al., 2020). Several novel pharmacophores with unique chemical structures and bioactivities were developed from marine organisms during the last few decades. Marine organism-derived functional food ingredients have potential pharmaceutical advantages and are endowed with pluralities of bioactivities against different diseases. An increasing interest in marine natural products and functional food ingredients, as evidenced by scientific publications and patents in the last decade, has appropriately demonstrated the possibilities of bioactive compounds from those to maintain and improve human health and well-being (Demunshi et al., 2010). Bioprospecting of previously undescribed natural products, mainly from the marine environment, has been improved considerably over the previous few decades, resulting in an investigation of newer secondary metabolites. It has been stated that marine organisms were the most prominent sources of natural products and, therefore, have been favourite choices of natural product chemists. Newer natural compounds of marine origin have delivered promising bioactive compounds with previously undescribed structures/skeletons, and these could be used as promising nutraceuticals and therapeutic agents against various ailments (Lordan et al., 2011). Many newer natural compounds have been reported for their bioactivities and as candidate molecules for potential drugs, even though only a few qualified as drug candidates. During the past few years, various bio-potential components have been isolated, identified and characterized from different marine organisms, such as mollusks, angiosperms, phytoplankton, zooplankton, marine macroalgae (also named as seaweeds), etc. Oceans are known as the "lungs of the Earth" due to photosynthetic marine plankton (algae) and cyanobacteria providing a major share of atmospheric oxygen. Therefore, naturally occurring macroalgal-based bioactive pharmacophores are used against various chronic diseases as an alternative treatment approach (Pradhan et al., 2020). The aquatic environment covers 80% of global plant diversities, and numerous species (~150 k) have been recorded in tropical and intertidal zones of oceans, which are considered pivotal sources of marine natural products (Hakim et al., 2020). Marine macroalgae are non-flowering stem-less plant-like flora attached to hard bottom substances (such as dead corals, rocks, pebbles, and shells) through holdfast. Nearly 8000 macroalgal species were discovered in the world's coastal areas (with 270 m depth). A total of 350 species of red algae, 90 species of brown algae, and 25 species of green algae are observed in the global coastline and recognized as commercially important macroalgae due to potential biochemical constituents (Chakraborty et al., 2012). About 1800 species of brown macroalgae have been recognized worldwide, in which 95% of those species are mostly distributed in temperate to cold waters. Major marine algae sources are found in southwestern and central-east Pacific regions along with the south-eastern, north-western and western-central Atlantic. Widespread distribution of marine macroalgae has

been observed through the Indian coastline and its maritime states {Andaman and Nicobar Islands-1500*, Andhra Pradesh-975*, Maharashtra-720*, Kerala-590*, Orissa-450*, Karnataka-280*, West Bengal-157*, Lakshadweep Islands-120*, and Goa-104* (* approx. in km)} (Pati et al., 2016). Tamil Nadu and Gujarat areas are enriched with maximum macroalgal diversity (Ganesan et al., 2019). Gujarat (surrounded by 1600 km coastline) harbours a total of 198 species that belong to different phyla. In contrast, Tamil Nadu has a coastline of ~1076 km and a current survey reported the presence of 282 algal species (of which 56, 80, and 146 species were identified from Ochrophyta, Chlorophyta, and Rhodophyta, respectively) (Ganesan et al., 2019; Mantri et al., 2020). Marine organisms, such as macroalgae, molluscs, bryozoans, ascidians, cnidarians, and sponges, exist in abyssal to the intertidal environmental zone. Marine macroalgae constitute a major share (~ 10%) in marine environments. Marine macroalgae offer important contributions to benthic community habitat by playing ecological and biological roles in the marine ecosystem (Williams et al., 2007). Since the pre-historic time, in many countries, macroalgae (enriched with vitamins and micronutrients) have been used as food source of the daily diet, due to their nutritional values. In many Asian countries, the population of macroalgae has made it a favoured biomass for commodity goods development. Also, commercial macroalgae aquaculture provides socio-economic advantages to rural coastal communities. The production after commercial culture has achieved a milestone of 31.2 million tonnes per year (95% accounts for farming, market value of US$ 11.7 billion) (FAO, 2018). The demand for marine macroalgae has increased globally other than traditional uses and the occurrence of diverse bioactive phytoconstituents exhibiting their applications in biomedical and pharmaceutical industries (Rebours et al., 2014; Hafting et al., 2015; Lomartire et al., 2022; Venkatesan et al., 2015). Other than several properties (photosynthetic storage, photosynthetic membranes, morphology), majorly marine macroalgae can be classified as Phaeophyceae (Brown algae), Rhodophyceae (Red algae) and Chlorophyceae (Green algae), based on their pigment content. Brown algal species were found as the largest group compared to other species. Owing to the degree of calcification, most of the macroalgae possess with soft tissues. Their cell wall controls the formation of calcium layer in macroalgae attached polysaccharides. The photosynthesis property of macroalgae is similar to terrestrial plants. Still, due to their non-complex cellular structure and underwater habitat, marine macroalgae are more effective in solar energy to biomass conversion (Klnc et al., 2013). Among harvested macroalgae, nearly 13% have been used to produce commercial hydrocolloids (agar, alginate, fucoidan, carrageenan etc.), whereas 75 and 12 % are being used for food and agriculture sector, respectively (Hardouin et al., 2014). Macroalgae are possessed with abundant nutrients, such as minerals, dietary fibers, vitamins, peptides/proteins, fatty acids, polyphenols etc. (Cardoso et al., 2015). The nutritional components of macroalgae can be affected and varied by season, geographic location, species, etc., but comprise the rich carbohydrate content in the cellular polysaccharide. Marine macroalgal species have been extensively utilized to produce low molecular weight bioactive and phycocolloids in food, pharmaceuticals, and other industries. Noticeably, most species belonging to the class of Phaeophyceae have yet to be majorly explored for their pharmacological and biochemical potencies. Recently, the importance of these macroalgal species (belonging to the class Phaeophyceae) and their pharmacological potentials have drawn substantial interest among researchers.

1.2. Marine organisms as potent sources of bioactive metabolites

According to WoRMS (World Register of Marine Species), the marine ecosystem contains almost 2,40,000 species, signifying a diverse source of unique bioactive compounds with pharmacological potencies that can be used to treat various human ailments. The importance of marine natural products (MNPs) had increased after the isolation of spongothymidine and spongouridine from a Caribbean sponge *Tethya crypta*, which led to the development of cytarabine (anti-leukemia agent) and vidarabine (antiviral agent), respectively (Sagar et al., 2010). Over 5 million species of the world in about 30 different phyla reside in the oceans. Because of the diversities of marine organisms and

habitats, marine natural products enfold various chemical classes, including terpenes, shikimates, polyketides, acetogenins, peptides, and alkaloids of varying structures. Many natural products of interest to the pharmaceutical industry are secondary metabolites, and several such compounds, derived from marine organisms, have been in clinical trials as experimental drugs. Over the past 50 years, numerous novel compounds have been isolated from marine flora and fauna having biological activities such as antibacterial, antiviral, antitumor, antiparasitic, anticoagulants, antimicrobial, anti-inflammatory and cardiovascular compounds. Recently, the technology of target-based drug discovery has taken a more excellent pace by using various advanced methodologies (Kanase et al., 2018). It is appropriate to state that marine natural products have had an important impact on chemistry, pharmaceutical and drug development areas over the past few years and be valuable sources for newer bioactive templates in upcoming years. The marine flora and fauna remain largely unexplored. Approximately 71% of the molecular entities listed in the Dictionary of Marine Natural Products have novel molecular structures compared to ~40% of those in the Dictionary of Natural Products. In NCI preclinical cytotoxicity screen, marine organisms show a higher incidence of anti-tumor potential: 1% vs 0.1% for terrestrial organisms. The number of new marine compounds reported yearly is increasing by>1000.

Naturally derived bioactives (from marine sources) were mainly isolated from macroalgae, sponges, echinoderms, mollusks, bryozoans, polychaetes, cnidarians, and ascidians with promising efficacy against various disorders. Sponges are considered one of the primary sources of various lipidic components along with steroids, terpenoids, alkaloids, cyclic peptides, and amino acid derivatives (Anjum et al., 2016). Several unusual polyoxygeneted and polyhydroxylated steroid compounds attenuating platelet aggregation and inflammation were isolated from marine sponges *Petrosia contignata*, *Xestospongia bergquisicta* and *Clathria lissosclera* (Nair et al., 2015). Chemical investigation of the coral-derived fungus *Penicillium sclerotiorin* separated napthoquinone-attached polyketides with significant anti-inflammatory activities (Liu et al., 2019a). In some instances, protein hydrolysate-derived peptides obtained from marine organisms (squids, sea cucumber, tuna, etc.) exhibited more significant antioxidant properties than synthetic antioxidants (Ngo et al., 2012). Marine fungi of phycomycetes group were reported as very good producers of long chain omega-3 polyunsaturated fatty acids (PUFAs), γ-linolenic acid, arachidonic acid (AA), docosahexaenoic acid (DHA), and eicosapentaenoic acid (EPA) (Shahidi et al., 2018). Those bioactive metabolites from marine organisms were utilized as potential pharmacological lead molecules, including substituents of synthetic antioxidants. Fucoidan, a sulfated acidic polysaccharide isolated from brown algae's cell wall, has gained attention because of its promising therapeutic potential in the pharmaceutical and food industries (Wang et al., 2019). Likewise, oligosaccharide obtained from the sea-cucumber *Apostichopus japonicus* showed *in vitro* superoxide and hydroxyl free radical quenching activities, whereas *in vivo* animal model study resulted in anti-hyperlipidemic property (Liu et al., 2012). Polysaccharides derived from marine sources exhibited several pharmaceutical and biotechnological applications in biomaterial fabrications, wound healing dressings and porous scaffolds. Another polysaccharide chitosan, obtained from crab and shrimp shells, is used (primarily as a hydrogel) in drug delivery systems, and previous literature reported that self-regulated chitosan-based microgels showed sufficient attenuation in blood glucose levels of type-1 diabetes (Nair et al., 2015; Gu et al., 2013). Extensive investigation on marine molluscs showed their values as functional foods, nutraceuticals, etc. (Chakraborty et al., 2020). Bioactive compounds from oyster sauces and blue mussels were observed to decrease hypertension, whereas ground abalone cells were used for eye treatment (Wijesekara et al., 2010; Kim et al., 2012). Crustacean represents one of the most abundant and commercially available marine arthropods in global markets. It is widely consumed as a value-added health food by Asian people, owing to its nutritional values and several curative potentials (Tou et al., 2007). Marine microbes attached to marine plants and animals (which can be easily cultured) are one of the emerging sources of new bioactive compoundsAnionic exopolysaccharides obtained from various strains of *Alteromonas*, showed their potential as metal-binding capacities and thickening agents (Guezennec et

al., 2002). The contents of DHA and EPA were found in deep-sea bacteria, and these long-chain unsaturated fatty acids were involved in bacterial survival in extreme environmental conditionsBacterial exopolysaccharides were found to possess favourable rheological properties and were resistant to high temperatures, extreme salinities, and pH (Rasmussen et al., 2007). Phytochemical investigations of marine macro and microalgae showed those as an abundant resource of bioactive pharmacophores. They have a prominent role in developing functional food supplements and nutraceuticals. Especially marine macroalgae are endowed with bioactive components, such as peptides, sulfated polysaccharides, phenolics, sterols, lipids, pigments, and several heterocyclic derivatives (Khalid et al., 2018). Several functional foods, nutraceutical supplements, and biomedical products from marine macroalgae provide numerous health benefits for humans and multiple lifestyles and degenerative metabolic disorders, like obesity, diabetes, hypertension, hyperlipidaemia, inflammation, hypothyroid, and reactive oxygen species-mediated diseases (Khalid et al., 2018).

1.3. Marine macroalgae: General

Algae are a heterogeneous group of organisms capable of performing photosynthesis. The algae can be either microscopic unicellular organisms or macroscopic multicellular organisms and are found in various habitats. Among algae, marine macroalgae or seaweeds represent a diverse group of photoautotrophic, multicellular forms occurring in the coastal and sublittoral areas of the marine environment. Unlike terrestrial plants, seaweeds lack actual stems, leaves and roots. Also, they do not possess conducting tissues, and the nutrients are absorbed directly through the surface tissues. Marine macroalgae contain high levels of nutrients, can be cultivated in seawater and do not require arable land, freshwater, or fertilizer; thus, farming these species is widely touted as an activity with a low carbon footprint. Marine macroalgae also grow faster and have yields higher than land plants. Hence, marine macroalgae could be considered a sustainable nutrient source to achieve global nutritional security. The World Wildlife Fund, in collaboration with Knorr Foods, has prepared a list of 50 future foods that can make people and the planet healthier and can lead to global food sustainability. The marine macroalgae species *Porphyra umbilicalis* and *Undaria pinnatifida* has found a place in the list of the future 50 foods (WWF, 2019). The criteria for selecting the future foods were high nutritional value, relative environmental impact, flavour, accessibility, acceptability and affordability, modelled after the Food and Agricultural Organization (FAO) definition of sustainable diets. The marine macroalgae act as excellent habitats and food for several economically important shellfish and crustaceans. They also offer multiple ecosystem services, such as bioremediation for coastal pollution, localized control of coastal water acidification, mitigation of climate change, and nutrient absorption (Langton et al, 2019). Marine macroalgae cultivation has been considered a proven tool to empower women and reduce poverty among the resource-poor coastal communities in many low-income countries (Msuya, 2006; Valderrama, 2012; Mantri et al, 2017; Ginigaddara et al. 2018).

1.3.1. Marine macroalgae as potent source of primary metabolites

Marine macroalgae macro and micro-nutrients include carbohydrates, proteins, lipids, dietary fibre, minerals, and vitamins. Considerable variation has been observed in the chemical composition of marine macroalgae, depending on the species, stage of maturity, and environmental conditions like habitat, light, temperature, season etc. (Maehre et al, 2014). The carbohydrate content in marine macroalgae varies from 20% to 76% of dry weight, depending on the species and primarily forms structural and storage components of the cell (Holdt et al., 2011). Even though marine macroalgae have significantly higher carbohydrate content, a large portion is available as polysaccharide dietary fibre. The dietary fibre in marine macroalgae constitutes about 25–75% of its dry weight (Jiménez-Escrig et al., 2000). The soluble fibre fraction represents about 55–70% of the total dietary fibre of marine macroalgae (Rajapakse et al., 2011). The highest content of soluble dietary fibres is seen in *Chondrus* and *Porphyra* (15 % – 22 %). The marine

macroalgae have protein concentrations up to 47% of their dry weight (Černá et al., 2011 and O' Connor et al., 2020). Marine macroalgal protein is a rich source of amino acids like glycine, alanine, arginine, proline, glutamic, and aspartic acids (Rajapakse et al., 2011; Černá et al., 2011). Leucine and isoleucine are the limiting amino acids in red algae, and the amino acids methionine, cysteine and lysine are often deficient in brown algae (Dawczynski et al., 2007). The protein yield for marine macroalgae ranges from 2.5–7.5 tons per hectare per year. This value is 2-5 times higher than wheat or legumes (O' Connor et al., 2020). The marine macroalgae have lipid content of up to 5% of their dry matter (Khotimchenko et al., 2005; Maehre et al, 2014; Fakhry et al., 2015; Kendel et al., 2015). Lipid composition in marine algae has raised considerable interest due to their high content of PUFAs, specifically α-linolenic (18:3n-3), octadecatetraenoic (18:4n-3), arachidonic (20:4n-6), and eicosapentaenoic acids (20:5n-3) (Dawczynski et al., 2007). Red marine macroalga contains 33 fatty acids, and green algae contain 29 fatty acids (Fouda et al, 2019). Marine macroalga is an excellent source of both water-soluble vitamins and lipid-soluble vitamins. The production of vitamins in marine macroalga depends on environmental factors, especially exposure to sunlight (Leandro et al, 2020). Marine macroalga is considered a good source of B-group vitamins (particularly B1 and B12) and vitamins A and E (Bender et al., 1980; Ortiz et al., 2009; Škrovánková et al., 2011). Marine macroalga is known for its high mineral content, which accounts for up to 40% of its dry weight (Rupérez, 2002; Peñalver et al, 2020). Marine macroalga contains mineral macronutrients such as sodium, calcium, magnesium, potassium, chlorine, sulfur, and phosphorus. The micronutrients include iodine, iron, zinc, copper, selenium, molybdenum, fluoride, manganese, boron, nickel, cobalt etc. Calcium is one of the prominent minerals contributing about 4–7% of the dry matter. Calcium is available as calcium phosphate in marine macroalga, and its bioavailability is more than that of calcium carbonate, the form of calcium available in milk (Rajapakse et al., 2011). Marine macroalga is a well-known food source with rich iodine content (Teas et al, 2004). The highest iodine content is found in brown algae (1500–8000 ppm); red and green algae primarily have a lower iodine content (Rajapakse et al., 2011). Marine macroalga contains significantly higher amounts of iron and copper than meat and spinach (Holland et al., 1993).

1.3.2. Marine macroalgae as potent source of secondary bioactive metabolites

In addition to the primary metabolites, the marine macroalga possesses an array of structurally diverse secondary metabolites with potential biological activities. These bioactive compounds are mainly produced under various stress conditions due to fluctuations in environmental conditions such as changes in temperature, salinity, nutrients, exposure to ultraviolet radiation, pollution etc. The long life expectancy and a lower rate of cardiovascular diseases in Japanese people might be associated with their regular intake of marine macroalgae. Above all, these have been identified as new sources of ingredients for developing nutraceuticals. Studies on natural product chemistry and chemical defense systems of marine macroalgae recognized the presence of bioactive leads with prominent pharmacological activities. The major bioactive compounds isolated from marine macroalga include polysaccharides, phenolics, proteins, peptides, terpenes, terpenoids, carotenoids, sterols, dibutanoids, acetogenins alkaloids etc. (Kumar et al, 2008; Balboa et al, 2013; Yu et al, 2014; Anusree et al., 2017; Chakraborty et al., 2019; Chakraborty et al., 2020). These molecules are mainly responsible for the beneficial properties associated with marine macroalgae. Unique bioactive secondary metabolites from marine resources, particularly from ocean herbs or macroalgae, are acknowledged worldwide for developing lead pharmacophores against different target diseases. The demand for other bioactive macroalgal metabolites is continuously growing as alternatives to synthetic drugs and their derivatives (Lourenço-Lopes et al., 2020). Dietary consumption of macroalgae has been shown to exhibit several biological activities, including antidiabetic, antioxidant, anti-hypertensive, anti-inflammatory, antiviral, immunomodulatory, and others (Afonso et al., 2019). Since significantly earlier times, macroalgae have been used as a traditional diet among the people of coastal

communities, and it is widely consumed in East Asian countries. Studies showed high life expectancies and lower mortality rates among Japanese people due to regular consumption of macroalgae (Muraiet al., 2021). Therefore, macroalgal-derived pharmacophores and functional food ingredients benefit human health because of their nutritional and medicinal importance.

1.4. Major classifications of marine algae

Marine macroalgae, based on their characteristic pigmentation, are classified into three major groups, namely Chlorophyta (green algae), Phaeophyta (brown algae) and Rhodophyta (red algae). The pigments found in green marine macroalgae are chlorophyll a and b, which require good levels of light and are mostly found in littoral waters. Brown marine macroalgae contain chlorophyll a and c and fucoxanthin. The red marine macroalgae have chlorophyll a and d and phycobilins (phycoerythrin and phycocyanin) and require low light levels, thus can be found even in the deepest underwater. About 900 green marine macroalgae, 1500 brown marine macroalgae, and 4000 red marine macroalgae are present worldwide (Dawes et al., 1998). The distribution of marine macroalgae is affected by temperature. Red and green marine macroalgae are generally found in subtropical and tropical waters, whereas brown marine macroalgae are more common in temperate waters (Khan et al., 2003).

Marine macroalgae (seaweeds) are oxygenic photosynthesizers (liberating molecular oxygen as a by-product). They are classified into three groups depending upon their colour difference (due to photosynthetic pigments), belonging to brown, red and green. Other than colour, additionally, they can be differentiated by cell wall compositions, absence/presence of flagella, storage compounds, chloroplast structure, and mitosis ultrastructure (Rindi et al., 2012). Current classification schemes are based on their evolutionary origin. They can be classified based on different kingdoms; brown algae belong to the kingdom Chromista, whereas green and red algae belong to the kingdom Plantae (Cavalier-Smith et al., 2007). Other evolutionary processes were involved in the origin of marine macroalgae, where the primary endosymbiosis process was involved for red and green algae and secondary endosymbiosis for brown algae (Rindi et al., 2012). Macroalgae are situated on rocky shores in coastal habitats and propagate through coastal water surface from 270 m of oceanic water.There are approximately 1800 species of brown algae species are currently classified as Phaeophyceae (including 17 orders) of Ochrophyta phylum (de Reviers et al., 2007). Brown algae are different from the other two algae. Despite that, similarity has been noticed at the macroscopic level, and their growth occurs on rocky seashores. The diversity and abundance of brown algae are found chiefly in cold water, although they are distributed in tropical oceans, and their growth is restricted between polar to temperate waters. Some genera of brown macroalgae, such as *Turbinaria* and *Sargassum* are abundantly available in tropical seawaters. Filamentous brown algae (*Ectocarpus* and *Pylaiella* genus) comprised of branched threads can proliferate in the intertidal zone with an attachment of rocky substance or mixed with larger macroalgae. The appearance of brown algae is mostly like small trees or bushes with branches. Macroalgal species of order Fucales have economic importance due to their habitats in subtidal temperate rocky reefs. Therefore, they produce a supportive environment with great biological diversities (Coleman et al., 2017). The dense belts in the northern Atlantic (for Fucales) sea are a well-known example. Macroalgal species for this order float into the seawater instead of attaching to the rocky bottom. Another order, Laminariales (brown algae), is one of the largest (size-wise) macroalgae popularly known as kelps. *Macrocystis pyrifera*, popularly termed giant Pacific kelp, produce dense forests on the Pacific shores of the USA and Canada. *Lessonia*, *Ecklonia* and *Laminaria* are some of the species that also form similar underwater forests in different regions of the world.

Red algae are one of the oldest known eukaryotic algae. A typical characteristic of this particular group is the lack of centrioles and flagella (or any other flagellar apparatus) during their entire lifetime (Maggs et al., 2007). Due to phycobilins, the colour range of red algae is noticed between bright red to pink. Globally, near about 6000 red algal species are recognized. Red algae belong to a single phylum (Rhodophyta) that can be subdivided into 2 subphyla (Rhodophytina and Cyanidiophytina), 33 orders, and 7 classes (*Bangiophyceae*, *Florideophyceae*, *Cyanidiophyceae*, *Porphyridiophyceae*, *Compsopogonophyceae*, *Stylonematophyceae* and *Rhodellophyceae*) (Yoon et al., 2006; Saunders et al., 2004). The smallest morphological form of red algae is comprised of thin filaments (*Bangia*) or single cells (*Porphyridium*). Red algal species of order Corallinales can store carbonate material in their cell walls and spread as red/pink calcified crusts on rocky shores. Some common red algal species (like *Chondrus*, *Gigartina*, *Gelidium*, *Hypnea*, *Laurencia* and *Gracilaria*) appear like branched plants and bushes.

Green algae constitute a diverse group of species conspicuously dispersed in the oceanic water along with terrestrial and freshwater habitats. Depending on DNA sequencing data, green algae are part of a group called Viridiplantae (Lewis et al., 2004). About 920 species of green algae (classified into a standard class, Ulvophyceae) are distributed in the seawater. The growth of two genera *Chaetomorpha* and *Cladophora* are observed as branched filaments. A typical morphological characteristic of *Ulva* (popularly known as sea lettuce species) is their sheet-like leaves. The appearance of green algae is identified by their nutrient absorbance capacity and faster growth in seawater. The unrestricted growth of green algae results in the deposition of large algal masses in water, called green tides. Sometimes mechanical removal may require the removal of algal biomass. Siphonaleans green algae are composed of a single cell (containing several nuclei), and the species belonging to the genus *Caulerpa* are well-known examples. Some other genera of siphonalen organization are *Acetabularia*, *Codium*, *Udotea*, *Halimeda* and *Valonia*. Various shapes of green algal species belonging to *Halimeda* are observed in tropical areas and islands.

1.5. Diversity and distribution of macroalgae in the Indian coastline

The Indian coastal length is distributed up to more than 7500 km, harbouring many marine macroalgal species (Roy et al., 2020). The vegetation of macroalgal species (mostly tropical algae) is copiously dispersed in the oceanic water. Among several algal species, 271 genera of macroalgae were observed in the Indian water (with an ideal habitation environment). Most are on rocky shores, lagoons, and coral mudflats (Sahayaraj et al., 2014; Subba Rao et al., 2006). The total area of the Indian coastline is comprised of 21 Gulf of Mannar islands and 42 coastal stations. Major macroalgae-enriched beds in southern coastal regions are Mahabalipuram, Tuticorin, Gulf of Mannar, Kanyakumari, Tiruchendur, Kerala, and Visakhapatnam (particularly the eastern coast). Besides that, the Gulf of Kutch, the Veraval region of the western coast, Lakshadweep, Andaman and Nicobar Islands are also essential for algal biomass production (Domettila et al., 2013). A previous report showed a total stock of 97,400 tonnes of macroalgae (wet weight) were recorded from the Tamil Nadu coast, whereas 19,345 and 7500 tonnes of macroalgae (wet weight) were recorded at Lakshadweep and Andhra Pradesh, respectively (Ganeshan et al., 2019). Tamil Nadu and Gujarat are two large maritime states covering approximately half of India's total macroalgal diversity. In the west coast region, particularly in Maharashtra, macroalgal diversity was observed in both, pre and post-monsoon periods. A total of 19 macroalgal species (13 orders, 16 genera, families belonging to Rhodophyta, Chlorophyta, Ochrophyta and Charophyta) were identified from the Uran coast (Pawar et al., 2017). According to FAO (2014) report, global production of macroalgae from wild stocks was ~1.3 million tonnes (between the years 2000-2009) (Ganeshan et al., 2019). Unlike other Southeast Asian countries, marine macroalgae are majorly used In India to produce phycocolloids, such as, *Gelidiella acerosa*, *Gracilaria edulis* are harvested for agar production, whereas, *Turbinaria* and *Sargassum* spp. are the primary source material for the production of alginate. The Palk Bay coast and Gulf of Mannar are considered highly

productive provinces for commercially collecting alginophytes and agarophytes. All these reports/studies implied the presence of various economically essential macroalgae (based upon their commercial production) on the Indian coastline.

1.6. Pharmacological importance of marine macroalgae

Marine macroalgae have been primarily considered a good source of alternative medicines and functional foods in Asian countries. In contrast, in western countries, they are used in the food, pharmaceutical, and cosmetic industries (Suleria et al., 2016). A wide range of pharmacological properties has been exhibited globally by marine macroalgae (macrophytes) (Kathirvel et al., 2022). The phytochemical composition of marine macroalgae may differ based on the species, geographical location, cultivation, atmosphere etc. Chemical investigation of macroalgae resulted in many compounds, such as carotenoids, peptides, polyphenols, terpenes, alkaloids, vitamins, carbohydrates, etc. (El-Beltagi et al., 2022). Polysaccharides are the major carbohydrates present in the algal cell wall, and based on their monosaccharide compositions, interlinkage pattern, and sulfation pattern, polysaccharides can be structurally different. Fucoidan, carrageenan and ulvan are the major polysaccharides isolated from brown, red, and green algae. Natural polysaccharides with unique physical and chemical properties have emerged as an eco-friendly and sustainable alternative to plastics and synthetic polymers (Lim et al., 2021). Polysaccharides contain more than 80% of the total macroalgal weight. Macroalgal polysaccharides are comprised of unique poly-uronides, and other than that, and some exist in methylated, acetylated, sulphated, and pyruvylated form (El-Beltagi et al., 2022). Due to their biological features (such as prevention of free radical formation in cells, regulation of different enzymatic action, and reduction of viral copy formation), sulfated polysaccharides have gained much attention among researchers, and therefore, various applications of sulfated polysaccharides were observed in pharmaceutical industries (El-Beltagi et al., 2022). Macroalgal sulfated polysaccharide-based hydrogels were found to be very useful for controlled drug delivery systems because of their biodegradability and biocompatibility (Sun et al., 2020). Sulfated galactan/xylomannan isolated from red macroalgae showed antiviral effect by preventing the interaction between virus and cell surface, through complex formation (Damonte et al., 2004). Sulfated polysaccharides derived from *Hypnea* spp. showed prospective hypocholesterolemic potential (by reducing cholesterol level) and blood pressure regulatory effect (by maintaining sodium/potassium ratio) (Cherry et al., 2019). Fucose-containing sulfated polysaccharides obtained from brown algal species showed their curative potential against high blood cholesterol level and metabolic syndrome (Cherry et al., 2019). Another study revealed that brown algal sulfated polysaccharide possessed anticancer potential on metastasis tumour by attenuating Vascular Endothelial Growth Factor (VEGF) or matrix metalloproteinases (MMPs) (Mohamed et al., 2012). Alginate is one of non-sulfated polysaccharides from brown algae, which was found to be beneficial for colon cancer prevention, hypertension, and improving gut health (Pérez, et al., 2016; de Morais et al., 2015). Macroalgae contain various natural amino acids, which can act as potential antioxidants, and acidic amino acids were predominantly present in most species (El-Beltagi et al., 2022). Also, amino acids are necessary for the production of body proteins and vital nitrogen-based compounds, and due to their distinct physiological functions they can be used for the treatment of some disorders like multiple sclerosis (Wu et al., 2013). Mycosporine-like amino acids (MAAs) were observed from the species belonging to Rhodophyceae, which showed notable photo-protecting activities (Pereira et al., 2018). Bioactive peptides (through functional foods and nutraceuticals) might enhance immunity against inflammation and oxidative stress-induced disorders (Cicero et al., 2017). Fatty acids are important components of the plasma membrane, which can assist in cell development and gene expression. In contrast, the number of unsaturated bonds in fatty acids determines their activities. Fucoxanthin-enriched brown algal lipids demonstrated anti-obesity activities by decreasing the excess deposition of fat molecules in white adipose tissues (El-Beltagi et al., 2022). Functional lipids

(omega-3 and omega-6 fatty acids) are crucial for human health. In 2004, Food and Drug Administration declared that omega-3-enriched foods are medicinally essential because of their therapeutic potencies against high blood pressure, cardiovascular disorder, diabetes, bone health disorder, and nervous system dysregulation (Francavilla et al., 2010). Phenolic compounds (tannins, flavonoids, polyphenols) are important bioactive constituents that are present in algae. Many phlorotannins were found in brown algae, whereas red algae and green algae contained most phenolic acids, bromophenols and flavonoids (Gómez-Guzmán et al., 2018). Polyphenols isolated from macroalgae were associated with various pharmacological (anti-inflammatory, antidiabetic, antiviral, and antioxidant) properties (Gómez-Guzmán et al., 2018). Additionally, several secondary metabolites with unique chemical structures were isolated from marine algae, and their bioactivities were assessed through *in vivo* model and clinical trial (Rosa et al., 2019). Two different clinical trial studies were scheduled to start in 2019 for fucoxanthin. Among those, one was aimed at fucoxanthin-enriched supplement for the improvement of liver health (ClinicalTrials.gov identifier: NCT03625284), whereas the other one was the effect of fucoxanthin on metabolic syndrome (ClinicalTrials.gov identifier: NCT03613740). Another trial showed marine macroalgae's weight loss properties (reduction of abdominal fat and body weight) in obese Japanese adults (Hitoe et al., 2017). Kahalalaide F is a peptide isolated from the green algal species (*Bryopsis pennata*), which is being tested in clinical trials, especially for its antitumor properties. The result showed that, unlike other chemotherapeutic agents, it did not exhibit severe adverse effects among patients up to the completion of the study (Martín-Algarra et al., 2009; Salazar et al., 2013). Recently, a clinical trial study was examined among 60 healthy adults. Their postprandial cognitive function was checked after consuming brown algal extract (containing 20% of phlorotannins) (Haskell-Ramsay et al., 2018). Test result showed that dietary consumption of algae could be helpful for cognitive benefits. Regular ingestion of *Ulva lactuca* Linnaeus extract (aqueous extract) for three months showed substantial improvement in depression state (caused by anhedonia) (Allaert et al., 2018). A synergistic combination of brown alga (2.5 g of *Undaria pinnatifida*) and spirulina (3 g of *Arthrospira platensis*) was able to increase immune response by reducing HIV viral loading and replication over a three-month period (after regular consumption) (Teas et al., 2012). Development of breast cancer is closely associated with high levels of serum estradiol (E2), and a study report showed that a regular dose (5 g) of brown algae (*Alaria esculenta*) was able to reduce the risk by modulating serum hormone level (Teas et al., 2009). A quick search on ClinicalTrials.gov showed that among 66 results (macroalgae/seaweed-related), six studies are not yet started, 12 are ongoing, and 35 are completed. The results of clinical trial studies showed that consuming brown algae could benefit human health (Rosa et al., 2019). Still, identifying a particular chemical compound (responsible for the curative effect) is necessary to understand the mechanism. Therefore, phytochemical investigation of macroalgae might be helpful for the development of novel pharmacologically active compounds associated with potent bioactive properties.

Polysaccharides are the significant components of seaweeds, and their content ranges between 4–76% of their dry weight. The seaweeds with the highest polysaccharide contents include *Ascophyllum*, *Porphyra*, and *Palmaria* (Paniagua-Michel et al, 2014). Red algae contain unique sulfated galactans, such as agar, agarose, and carrageenans. Some of red algae also include sulfated mannans or neutral xylans, instead of sulfated galactans, as the primary structural polysaccharide (Usov, 2011). The brown algae contain sulfated polysaccharides such as laminarin, alginate, and fucoidan (Dobrinčić et al, 2020; Chakraborty and Anusree, 2020). The primary matrix-sulfated polysaccharides green algae produce are ulvans, galactans and arabinogalactans (Popper et al. 2011). The sulphated polysaccharides exhibit many valuable biological properties like anticoagulant, antiviral, antioxidant, anti-tumour, immunomodulating, anti-hyperlipidemic and anti-hepatotoxic (Wang et al, 2014).

Phenolic compounds are a group of secondary metabolites found in seaweeds. The most inimitable seaweed polyphenol compound is phlorotannins, and other polyphenolic compounds include bromophenols, flavonoids, phenolic terpenoids, and mycosporine-like amino acids (Cotas et al, 2020). Among the marine algae, Laminariacea has the most abundant source of phlorotannins (Rengasamy et al, 2020). Most phenolic compounds possess a broad variety of biological activities such as anti-diabetic, anti-inflammatory, antimicrobial, antiviral, anti-allergic, antioxidant, hypertension, neuroprotective, anti-cancer properties etc. (Guzmán et al, 2018; Santibañez et al, 2018; Alghazeer et al, 2018; Olasehinde et al, 2019). One of the biologically essential peptides extracted from seaweeds is lectins. They are a structurally diverse group of particular, reversibly carbohydrate-binding proteins (Hori et al, 2000). Because of the specific way lectins bind to sugars outside cell surfaces, inhibiting cell proliferation (Gauto et al, 2011; Manning et al, 2017), lectins mainly exhibit biomedical activities like antiviral, anti-cancer, antimicrobial, anti-inflammatory, anti-nociceptive and acaricidal activities (Singh and Walia, 2018).

Halogenated compounds are bioactive secondary metabolites observed in seaweeds (Rocha et al, 2018). Based on their structural characteristics, halogenated organic molecules are generally categorized into terpenoids, non-terpenoid C15-acetogenins (ACGs), indoles, and phenols/aromatics. The halogenated terpenoids, non-terpenoid ACGs, and indoles were mainly discovered from the genus *Laurencia*. In contrast, the halogenated phenols/aromatics were reported primarily as metabolites from other genera of the family, such as *Polysiphonia*, *Rhodomela*, and *Symphyocladia* (Wang et al, 2013). Among the halogenated compounds, terpenes and bromophenols have exhibited the most potential for new drug development *in vivo* studies (Rosa et al, 2020).

Carotenoids consist of two groups, namely xanthophylls and carotenes. Concerning algal lipids, fucoxanthin is a xanthophyll carotenoid found in seaweed lipids and is one of the most studied metabolites due to its health benefits (Cardoso et al, 2015). *Undaria pinnatifida* contains 5–10% fucoxanthin, one of Japan's most well-known edible seaweed. The health benefits of fucoxanthin include biological activities such as antioxidant, anti-cancer, anti-inflammatory, anti-obesity, and neuroprotective activities (Kim and Pangestuti, 2011).

Sterols are an essential structural component of cell membranes (Kim and Van Ta, 2011). Sa´nchez-Machado et al. (2004) reported that fucosterol and fucosterol derivatives are the significant sterols found in brown algae, cholesterol and cholesterol derivatives are found in red algae. Ergosterol and 24-ethyl cholesterol are found in green algae. Fucosterol isolated from brown algae *Pelvitia siliquosa* exhibited antioxidant and anti-diabetic properties (Lee et al, 2003; 2004). Saringosterol, a derivative of fucosterol, separated from the brown algae *Lessonia nigrescens* has been reported to prevent the growth of *Mycobacterium tuberculosis* (Wächter et al, 2001). Thus saringosterol could be a potential candidate for inhibiting tuberculosis. Two sterol glycosides isolated from red algae *Peyssonnelia sp.* showed significant cytotoxicity in human breast cancer (Lin et al, 2010).

1.7. Role of brown marine macroalgae-derived compounds in various lifestyle disorders

The pharmacological importance and enormous array of therapeutic effects of marine macroalgae have already been well known. Most lifestyle disorders correlate with oxidative stress (imbalance between the natural defence system and reactive oxygen species production). Reactive oxygen species (ROS) are produced by several intracellular and extracellular processes involved in cell signalling pathways. Overproduction of ROS can cause structural changes in cellular macromolecules, which deactivate many biological functions by modifying the cell signalling process and implicate the development of various ailments, such as cancer, inflammatory diseases, diabetes, cardiovascular

disorders etc. (Begum et al., 2021). Antioxidants are those substances that prevent ROS-mediated cell damage and also play an essential role in oxidative stress-induced signalling pathways. Brown algae (Phaeophyta) and brown marine macroalgal-derived compounds showed promising antioxidant and other bioactive properties, which could be useful as natural alternatives to manage these disorders (Begum et al., 2021).

Induction of apoptosis is one of the critical approaches to stop the growth of cancer cells. TRAIL (tumor necrosis factor-related apoptosis-inducing ligand) is an integral membrane protein, which binds with death receptors and transmits apoptotic signals into the intracellular zones of cancer cells. An experimental study on gastric cell lines showed anticancer properties of *Hyalogonium fusiforme* extract (alcoholic extract), and the results exhibited that tumour cell apoptosis was activated by the upregulation of tumour necrosis factor-alpha (TNF-α) expression (Annibaldi et al., 2020). The current research study showed that the alcoholic extract of *H. fusiforme* inhibited matrix metalloproteinase (MMP) expression in human hepatoma cancer cells Hep3B, and also was found to regulate metastasis of tumour invasive genes [thrombospondin-1 (TSP-1), claudins, insulin-like growth factor-1 (IGF-1), and cadherin] along with their activity-related genes [tissue inhibitor of metalloproteinases-1,2 (TIMP-1,2)], which induce apoptosis (Kim et al., 2021). Another study showed that apoptosis of human leukemia U937 cells was induced by ethanolic extract of *H. fusiformecan* and outcomes of this results exhibited that cell death was caused by the reduction of apoptosis inhibitors and B-cell lymphoma-2 (Bcl-2) protein (Sakthivel et al., 2019; Kim et al., 2009). Solvent extract of Mediterranean brown algae *Colpomenia sinuosa* exhibited apoptotic and cytotoxic effects on colon cancer cells (HCT-116) (Al Monla et al., 2020). This study revealed that morphological alterations and apoptosis in HCT-116 cells were induced by *C. sinuosa* extract through the generation of reactive oxygen species, *p21* gene upregulation, poly (ADP-ribose) polymerase-1 (PARP-1) cleavage along with caspases 3 and 9 activation. An estrogen receptor-independent experiment was performed (for cytotoxicity study), and cytotoxic effects of three brown algae (*Cystoseira myrica*, *Sargassum swartzii* and *Colpomenia sinuosa*) were evaluated on different cancer cell lines (Khanavi et al., 2010). Another brown alga *Dictyota dichotoma* (collected from Yemen sea-coast), exhibited cytotoxicity in a dose-dependent manner, and cytotoxicity was observed more in some selected cancer cell lines (El-Shaibany et al., 2020). Polysaccharides obtained from brown algae (mainly belonging to *Sargassum* spp.) exhibited anticancer potentials against various cancer cell models (Remyan et al., 2022).

The antioxidant activity of a substance depends on its oxygen scavenging ability, free radical quenching property and chelation ability of metal ions. Brown algae comprise natural antioxidants with a prominent free radical scavenging property. The hydroxyl group (-OH) attached to naturally-derived compounds (especially in phenolic derivatives) can form a stable product by transferring hydrogen to free radicals. The durability of retaining the product's stability defines that particular constituent's antioxidant property (Fernando et al., 2016). The occurrence of phenolic acids (including catechin, gallic acid, coumaric acid, caffeic acid, rutin, quercetin, kaempferol, etc.) was present abundantly in brown algal species, and their antioxidant properties were also reported (Aminina et al., 2020). Benzene (or aromatic) ring structures of a previously mentioned hydroxyl group attached phenolics are one of the significant factors for hydrogen donation and their free radical scavenging properties. An earlier study revealed that the benzene ring associated with but-2-ene moiety could enhance the antioxidant activity by superior hydrogen donation ability and radical stabilization (Balasundram et al., 2006). Phlorotannin is one of the abundantly available hydrophilic metabolites with potent antioxidant properties in brown algae. Additional functional groups at substituted phlorotannins (such as extra -OH group at the third ring of fuhalols, phenyl connectivity in fucols, ether linkage in phlorethols, dibenzodioxin connection in eckols, phenyl and ether groups in fucophloroethol) could also enhance the antioxidant properties (Balasundram et al., 2006; Peron et al., 2013). *In vitro* antioxidant potentials of three brown algae *Sargassum*

plagiophyllum, *Anthophycus longifolius*, and *Sargassum myriocystum* were evaluated by effective stabilization of 2,2-diphenylpicrylhydrazyl (DPPH) and 2,2'-azino-bis(3-ethylbenzothiazoline-6-sulfonic acid) (ABTS) radicals. In contrast, no significant alterations were observed for ferrous ion chelation and hydrogen peroxide scavenging potential (Chakraborty et al., 2017). Secondary metabolites isolated from *Ascophyllum nodosum*, *Padina tetrastromatica* and *Cystoseira schiffneri* exhibited significant antioxidant properties (Liu et al., 2019b; Naveen et al., 2021; Benslima et al., 2021).

Reactive oxygen species (ROS) generally involve many cellular metabolism pathways, primarily those produced by mitochondria (Reuter et al., 2010). Abnormality in cellular function (also known as inflammation) is observed due to the excess production of ROS in the body. Eosinophils and mast cells are two critical inflammatory-inducing cells, which initiate chemical signals (due to ROS release) that can induce signal transduction in various enzymes, cytokines, and proteins related to inflammation, such as cyclooxygenase-2 (COX-2), nuclear factor kappa B (NF-κB), interleukin-1β (IL-1β), nitric oxide synthase (*i*NOS), tumor necrosis factor-α (TNF-α), etc. This induction process results in inflammation in healthy cells. Therefore downregulating the expression of those aforementioned genes along with scavenging the free radicals are necessary to reduce the battery of inflammatory reaction. A binary solvent mixture (DMSO and ethanol) of *Cystoseira amentacea* (obtained from Ligurian Sea) exhibited effective anti-inflammatory effect against inflammatory cytokines (De La Fuente et al., 2020). Sulfated polysaccharide isolated from *Padina commersonii* showed substantial anti-inflammatory properties on LPS-induced macrophages (Asanka Sanjeewa et al., 2019). Interestingly, this experimented result reduced inflammatory responses by blocking TLR/NF-κB signal pathway by the sulfated polysaccharide. Potential anti-inflammatory activities of three brown algae *Cystoseira crinite*, *Cystoseira sedoides*, and *Cystoseira compressa* were evaluated in animal model study, and the experimented outcome was compared with commercial standards (Mhadhebi et al., 2014).

Research studies on antihyperglycemic potential showed that brown marine macroalgae possessed potential inhibitory properties against α-glucosidase and α-amylase, which are two vital enzymes in carbohydrate hydrolysis. Postprandial hyperglycaemia could be reduced by inhibiting these carbolytic enzymes (Nair et al., 2013). Inhibition of protein tyrosine phosphatase-1B, aldose reductase enzymes are also beneficial to prevent postprandial hyperglycaemia (Remyan et al., 2022). Fucoxanthin-containing methanol extract of Malaysian brown algae *Sargassum polycystum* and *Sargassum siliquosum* exhibited α-amylase and α-glucosidase inhibitory properties (Nagappan et al., 2017). A previous study reported more than 85% inhibitory activity of α-amylase enzyme by polyphenols (obtained from *Eisenia bicyclis*). The inhibitory activity of isolated compounds was correlated proportionally with the total number of hydroxyl groups present in that molecule (Okada et al., 2004). Alginate polysaccharide from brown algae was reported as significant α-amylase inhibitors (Zaharudin et al., 2018). Another study showed effective anti-diabetic properties of brown algal (*Sargassum confusum*) oligosaccharides (Yang et al., 2019). The regulation of insulin receptor substrate 1/phosphatidylinositol 3-kinase and c-Jun N-terminal kinase pathways explained the effectiveness towards its anti-diabetic potential. Thus, the phytoconstituents of brown algae could be potential marine natural products for use as therapeutics against several lifestyle disorders.

1.8. Morphological features and distribution of brown marine macroalgae belonging to *Turbinaria* spp.

Turbinaria is a genus of brown algae (class Phaeophyceae; family Sargassaceae, order Fucales) found primarily in tropical marine waters. It is characterized by outwardly branched, monopodially grown axes, comprising partially grown blades, and stable turbinate structures (Fritsch et al., 1959). The specimens of *Turbinaria* genus are represented by upward thalli with complex branches bearing blades. Most of the species are observed as a rigid, solid,

and tough texture with conifer cone-like characteristic of the thallus. Naturally, these leaf-vesicles (blades) are turbinate and crowned with umbrella shaped lamina (Blomquist et al., 1945). Lateral blades (one or two rows) of commonly known *Turbinaria* spp are observed with approximate rectangular or triangular (depending on species), concave or flat outer face. In most species, the proximal part of the blade is terete or slightly narrower towards one end. Presence of air vesicles in blades could enable the vertically remained thallus to float after detaching from the reef (Payri et al., 1982). Thalli are commonly attached with a well-developed holdfast comprising spread hapterous branches originating from main monopodial axes. In mature thalli, short, compactly branched reproductive organs (receptacles) arise on the upper side of the blades. The abundance of *Turbinaria* species is observed in coral reef ecosystems, but its geographical location also outspreads to subtropical areas (rarely distributed in temperate regions). Maximum diversity of *Turbinaria* species was found in the Southeast Asia (12 species) and the Indian Ocean (16 species). In the Pacific region, nine species were accounted for, whereas the Atlantic region (including the Caribbean) has been recorded with three species (*Turbinaria turbinata, Turbinaria ornata, Turbinaria tricostata*). Among all species, *Turbinaria ornata* appears as most abundant species in the Red Sea, East African coast, West Atlantic, and Indo-Pacific region. No records are observed for the presence of *Turbinaria* species throughout the west coast of Africa and Europe.

1.9. Morphological features and distribution of brown marine macroalgae belonging to *Sargassum* spp.

Sargassum (also known as sea holly or gulf-weed) is a genus of brown marine macroalga (class Phaeophyceae) belonging to the family Sargassaceae (order Fucales). The *Sargassum* genus comprises approximately 400 species and is dispersed throughout subtropical and tropical areas of the world (Mattio et al., 2011). Genus *Sargassum* was first identified by C. Agardh (1820), who also established a new classification system for marine macroalgae. The general morphology of *Sargassum* species is characterized by a thallus containing holdfast, one or some branches (main axes) that are divided into leaves, receptacles (reproductive organs), vesicles (aerocysts), etc. According to Camacho (2014), the structural morphology of *Sargassum* species contains conical, discoid holdfast with short, flattened or cylindrical main axes with diversified but simple leaves. Due to sunlight exposure, ostioles (pores or opened conceptacles) can be observed in leaves. Oval or spherical-shaped vesicles were held by pedicel (with different sizes and shapes, such as flattened, foliar or cylindrical). The air bubbles in this species help them float in the oceanic water. Major distribution of *Sargassum* species was observed in the Atlantic islands, the Indian Ocean islands, Pacific islands along with the coastal area of South America, Africa, South-west Asia, South-east Asia, Australia, New Zealand, and Asian (China, Japan, Taiwan) regions (Titlyanov et al., 2017).

1.10. Objectives

Globally, seaweed production was worth around $12 billion in 2019 and is expected to grow to $26 billion by 2025. Previous literature reports showed that small molecular bioactive compounds and polysaccharides isolated from brown marine macroalgae were endowed with potential pharmacological properties against progressive lifestyle disorders. Phaeophyceae (phylum Ochrophyta) encompasses more than 10,000 species residing in marine habitations. Among the phaeophytan marine macroalgae, *Sargassum* and *Turbinaria* are predominantly ubiquitous genera distributed throughout the temperate and tropical oceans. These are abundantly available marine macroalgal species in various parts of the World and could be utilized to develop high-value compounds and nutraceuticals of biomedical significance. Considering the promising perspective for the utilization of these species, and limited research reports on utilization as potential health food, its pharmaceutical potential began to receive considerable attention. Further, marine natural products with small molecular bioactive and polysaccharides with their pleiotropic molecular frameworks are valuable sources of pharmacophore leads and were ubiquitous among the seaweeds. Given this, the research work

conceptualized a systematic approach involving chemical profiling of four species of marine macroalgae, such as *Turbinaria conoides*, *Turbinaria ornata*, *Sargassum ilicifolium* and *Sargassum tenerrimum* (belonging to the family Sargassaceae) for small molecular weight lead pharmacophores and polysaccharides coupled with the evaluation of target biological activities against different disease models, particularly concerning type-2 diabetes mellitus, inflammation, hypertension, and a library of molecules with bioactive potential. Consequently, it was conceptualized to isolate the lead molecules and characterize those using extensive spectroscopic experiments, whereas the novel leads were validated through bioassay.

Based on this background, the objectives of the Thesis are as follows:

1. To screen the extracts from marine macroalgae *Turbinaria conoides*, *Turbinaria ornata*, *Sargassum ilicifolium* and *Sargassum tenerrimum* (belonging to the family Sargassaceae), collected from the coastline of India, for bioactive properties against varieties of oxidative stress-induced disorders.

2. To isolate small molecular weight lead molecules and substituted polysaccharides from extracts/fractions, coupled with the evaluation of biological activities using selective pharmacological properties by various *in vitro* models.

3. To elucidate the structures of purified compounds by spectroscopic techniques.

4. To predict the biological properties by chemi-informatic tools, structure-activity correlation analysis and generation of database of potential lead molecules.

1.11. Thesis outline

Based on the objectives mentioned above, the current Thesis is classified into eight chapters. The importance of the study on bioactive potentials of the selected marine macroalgae, along with objectives, was discussed in the introductory Chapter 1. Chapter 2 reviews the importance of marine macroalgae as bioactive sources, the characterized bioactive compounds, and their medicinal values. Chapter 3 described the *in vitro* evaluation of the antioxidant, anti-hyperglycemic, antihypertensive and anti-inflammatory potentials of the crude organic extracts of marine macroalgae *Turbinaria conoides*, *Turbinaria ornata*, *Sargassum ilicifolium* and *Sargassum tenerrimum* belonging to the family Sargassaceae. The isolation and characterization of secondary metabolites responsible for antioxidant, anti-hyperglycemic, anti-hypertensive and anti-inflammatory activities from *Turbinaria conoides*, *Turbinaria ornata* and *Sargassum ilicifolium* were described in Chapter 4, 5, and 6 respectively. Chapter 7 explained the bioactive polysaccharides from *Turbinaria conoides, Turbinaria ornata and Sargassum tenerrimum.* The summary and conclusion of the work and significant research findings from the current study are detailed in Chapter 8.

CHAPTER 2: REVIEW OF LITERATURE

The significance and background of marine macroalgae belonging to the family Sargassaceae as potential sources of bioactive compounds and their benefits were described in this chapter. Marine macroalgae found to be a rich source of secondary metabolites with pluralities of health benefits. Bioactive pharmacophores were reported from brown marine macroalgae due to terpenoids, phenolic compounds and sulfated polysaccharides. The biologically active pharmacophores in marine macroalgae also include polysaccharides comprising fucoidan, laminarin and alginates

majorly. The marine macroalgal polysaccharides, especially sulphated polysaccharides were reported to have potential antioxidative properties and have greater prospective to be utilized in the food and pharmaceutical industries. Marine macroalgae are biochemically distinctive, and were found to produce wide collection of natural products with prominent bioactivities. Adverse effects of synthetic drugs demand naturally obtained potential bioactive pharmacophores for the treatment of persistent metabolic syndromes, and this recognized the relevance of marine macroalgae as natural sources of bioactive components. Bioactive constituents of brown algae also revealed their nutritional and bioactive properties against various life style disorders, which include hypertension, diabetes mellitus and inflammation. They were found to possess active metabolites with some novel chemical structures, which belong to diverse chemical classes, such as alkaloids, phenols, steroids, terpenoids etc. However, the scientific information about the biological effects of the small molecular weight bioactives and polysaccharides from brown algae were not documented in a proper manner. A detailed literature survey on the secondary metabolites isolated and characterized from the marine macroalgae belonging to the family family Sargassaceae with antioxidant, antidiabetic and anti-inflammatory functionalities were described in this Chapter.

CHAPTER 3: PHARAMACOLOGICAL POTENTIAL OF ORGANIC SOLVENT EXTRACTS FROM SELECTED MARINE MACROALGAE

3.1. Background

Marine macroalgae are known for adapting natural defence strategies to sustain in highly stressed aquatic ecosystems, resulting in an enormous collection of secondary metabolites from diverse biosynthetic pathways. Bioactive pharmacophores obtained from marine macroalgae can be used as remedial therapies against several non-communicable diseases (NCDs) (Biris-Dorhoi et al., 2020). Extensive research on the defence mechanism of macroalgae and natural product chemistry has recognized the occurrence of numerous pharmacophores with promising biological activities (Pradhan et al., 2021). The formation of reactive oxygen species (ROS) through different metabolic routes can cause the prevention of natural physiological regulatory functions by involving in the pathogenesis of several diseases in living organisms. The presence of excess ROS leads to oxidative stress generation and cellular death in the living system (Alfadda et al., 2012). The consequences of oxidative stress-induced damage are cellular apoptosis, myocardial infarction, neurological disorders, chronic obstructive pulmonary disease, chronic inflammatory disorders, and renal function disorders (Pizzino et al., 2017). Adverse side effects due to synthetic drugs necessitated naturally isolated potential bio-actives and antioxidants to combat persistent metabolic diseases. Therefore, macroalgal consumption and isolated secondary metabolites are receiving considerable attention for their usefulness as nutraceuticals, medicines, pigments, and functional foods (El Zokm et al. 2021; Biris-Dorhoi et al., 2020).

Dietary consumption of macroalgae has been reported to the regulation of blood pressure (Cardoso et al., 2015), antioxidant (Chakraborty et al., 2010), antiviral (Liu et al., 2021), and antimicrobial (Silva et al., 2020) activities due to their tremendous bioactivities and nutritional values. Phenolic compounds, including phlorotannins obtained from marine macroalgae have been reported with effective cancer cell apoptosis, and anti-diabetic and anti-inflammatory potentials (Kim et al., 2009; Cotas et al., 2020). Bioactive leads isolated from macroalgae can regulate the level of carbohydrate digestive enzymes and glucose-induced oxidative stress (Lee et al., 2009). Macroalgal bioactive pharmacophores were also observed as angiotensin-I converting enzyme (ACE) inhibitors in renin-angiotensin-aldosterone system (RAAS) (Seca et al., 2018). Many specific macroalgal constituents were found as part of chemical

intermediates (of the cellular pathway) that control the regulation of various inflammatory signals associated with mammalian defence systems (Vo et al., 2012).

For a long time, the consumption of marine macroalgae has been a part of the regular diet among the people of coastal communities. It is extensively consumed in East Asian countries, mainly in China, Japan, and Korea, resulting in better and healthier lifestyles and a lesser mortality rate (Murai et al., 2011). Lipids (such as fatty acids, phospholipids, and glycolipids) derived from macroalgal species with high nutritional value also positively impact overall health and can be utilized in food and biopharmaceuticals industries (Domingues et al., 2022). Phycocolloids are another group of biomolecules obtained from macroalgae, which exhibited promising bioactive potentials (Maneesh et al., 2018; Stranska-Zachariasova et al., 2017; Ngo et al., 2013). Functional foods derived from marine macroalgae are endowed with multiple beneficial properties against several diseases. *Sargassum* and *Turbinaria* are two genera belonging to the rich biodiversity of brown marine macroalgae with significant biomedical and pharmacological applications. The crude extract or purified compound of *Sargassum* spp. showed a wide range of pharmacological properties, including anticancer, antiviral, anti-inflammatory, antioxidant, hypolipidemic, bone loss disorders, etc. Therefore, it is considered one of the rich sources of health-promoting and maintaining agents (Liu et al., 2012). Various *Sargassum* species have been used in Traditional Chinese Medicines (TCM) for 2000 years for their healing properties (Liu et al., 2012). Attenuation of insulin resistance and systemic inflammation were observed after the consumption of *Sargassum* species in high-fat diet-induced obese animals (Oh et al., 2016). Another study reported that the condition of stress-induced liver inflammation was improved after the use of *Sargassum hystrix* powder as a functional food (Husni et al., 2019). Cell cycle arrest of the cancer cell line supported the apoptotic effect of the compound isolated from *Turbinaria conoides* (Jacob et al., 2019). Rushdi (2021) reported the pharmacological and chemical diversity in *Turbinaria*. The current study evaluated the pharmacological potencies of four macroalgal species (*Turbinaria conoides*, *Turbinaria ornata*, *Sargassum tenerrimum* and *Sargassum ilicifolium*) belonging to the family Sargassaceae, collected from the Gulf of Manner region (8º48' N, 78º9' E and 9º14' N, 79º14'E) of southern coastal part of Indian Peninsular. Methanol/ethyl acetate (MeOH/EtOAc) organic crude extracts of selected algal species were evaluated for various bioactive properties, such as oxidative radical inhibition, anti-inflammatory, antihypertensive, and antihyperglycemic properties. Proton NMR (^{1}H-NMR) spectroscopic analysis of solvent extracts showed the fingerprinting regions of different functional groups in the organic extracts responsible for bioactive properties. The bioactivities of the algal extracts were performed by various *in vitro* assays and were correlated with different types of functional groups present in studied solvent extracts.

3.2. Materials and Methods

This section primarily divided into chemicals and instrumentation, sample collection, preparation and extraction, antioxidant activities, anti-inflammatory activities, anti-diabetic activities, antihypertensive activity, spectroscopic analyses and statistical analysis. The methods carried out for the various *in vitro* bioactivity studies were described in their respective sections.

3.3. Antioxidant activities of organic extracts from selected marine macroalgae

This section detailed the promising antioxidant activities of crude methanol-ethyl acetate (MeOH-EtOAc) extracts of the studied macroalgal samples such as *Turbinaria conoides* (J.Agardh) Kützing, 1860; *Turbinaria ornata* (Turner) J.Agardh, 1848; *Sargassum tenerrimum* J. Agardh, 1848; and *Sargassum ilicifolium* (Turner) C. Agardh, 1820 by using different *in vitro* antioxidant assays. The *in vitro* antioxidant assays included radical scavenging activities by using oxidants, such as 1, 1-diphenyl-2-picryl-hydrazil (DPPH), 2, 2′-azino-bis-3-ethylbenzothiozoline-6-sulfonic acid

($ABTS^+$), hydroxyl H_2O_2 scavenging, ferrous ion (Fe^{2+} ion) chelating along with thiobarbituric acid reactive species (TBARS) formation inhibitory activity and total phenolic content (TPC). Studied macroalgal species belonging to the family Sargassaceae displayed considerably greater pharmacological potentials with regard to anti-diabetic, anti-inflammatory, antioxidative and anti-hypertensive activities. The EtOAc-MeOH extract of *T. ornata* displayed greater scavenging ability on DPPH radicals (IC_{50} 0.38 mg mL^{-1}) followed by those obtained from *S. tenerrimum* (IC_{50} 0.45 mg mL^{-1}), *T. conoides* (IC_{50} 0.48 mg mL^{-1}) and *S. ilicifolium* (IC_{50} 0.57 mg mL^{-1}), in descending order. The organic extracts of *T. ornata* exhibited higher $ABTS^+$ radical scavenging activity (IC_{50} 0.41 mg mL^{-1}) in comparison with *S. tenerrimum* (IC_{50} 0.51 mg mL^{-1}), *T. conoides* (IC_{50} 0.57 mg mL^{-1}) and *S. ilicifolium* (IC_{50} 0.65 mg mL^{-1}). The EtOAc-MeOH extract of *S. tenerrimum* displayed greater hydrogen peroxide scavenging ability (IC_{50} 0.49 mg mL^{-1}) followed by those obtained from *T. conoides* (IC_{50} 0.51 mg mL^{-1}), *T. ornata* (IC_{50} 0.52 mg mL^{-1}), and *S. ilicifolium* (IC_{50} 0.64 mg mL^{-1}), in descending order. The organic extracts of *T. ornata* exhibited higher Fe^{2+} ion chelating activity (IC_{50} 0.63 mg mL^{-1}) in comparison with *T. conoides* (IC_{50} 0.65 mg mL^{-1}), *S. tenerrimum* (IC_{50} 0.69 mg mL^{-1}) and *S. ilicifolium* (IC_{50} 0.82 mg mL^{-1}). The TBARS formation inhibitory effects of EtOAc-MeOH extract of *S. tenerrimum* was 52.86 mM MDAEQ/kg, whereas other species exhibited the value of 49.68, 49.24 and 45.32 mM MDAEQ/kg for *S. ilicifolium*, *T. ornata* and *T. conoides* respectively. The total phenolic content (TPC) was significantly greater for the EtOAc-MeOH extract of *T. conoides* (232.46 mg GAE/g) than other studied species, and decreased in the order, *T. ornata* (193.01 mg GAE/g) > *S. tenerrimum* (181.78 mg GAE/g) > *S. ilicifolium* (170.68 mg GAE/g).

3.4. *In vitro* anti-diabetic, anti-inflammatory and ant-hypertensive activities of solvent extracts from selected marine macroalgae

The different organic extracts obtained from the studied marine macroalgae (*S. tenerrimum*, *S. ilicifolium*, *T. ornata* and *T. conoides*) were studied for their anti-inflammatory properties with regard to COX-1, COX-2 and 5-LOX inhibition assays (Table 3.1.2). The EtOAc-MeOH extracts of *T. ornata* exhibited greater 5-LOX inhibiting activity (IC_{50} 1.11 mg mL^{-1}) compared to the other studied algal species belonging to family Sargassaceae (*S. tenerrimum* ~ $IC_{50\ 5\text{-}LOX}$ 1.16 mg mL^{-1}; *T. conoides* ~ $IC_{50\ 5\text{-}LOX}$ 1.26 mg mL^{-1} and *S. ilicifolium* ~ $IC_{50\ 5\text{-}LOX}$ 1.35 mg mL^{-1}).

The crude organic extracts obtained from the studied marine macroalgae (*S. tenerrimum*, *S. ilicifolium*, *T. ornata* and *T. conoides*) were studied for their anti-diabetic properties with regard to *α*-amylase inhibition, *α*-glucosidase inhibition and DPP-4 inhibition assays (Table 3.1.2). Among all studied species, EtOAc-MeOH extract of *T. ornata* revealed greater inhibition of *α*-amylase (IC_{50} 0.42 mg mL^{-1}) than those exhibited by others (*S. tenerrimum* ~ $IC_{50\ \alpha\text{-amylase}}$ 0.46 mg mL^{-1}; *T. conoides* ~ $IC_{50\ \alpha\text{-amylase}}$ 0.50 mg mL^{-1} and *S. ilicifolium* ~ $IC_{50\ \alpha\text{-amylase}}$ 0.59 mg mL^{-1}). Likewise, the EtOAc-MeOH extracts of *S. tenerrimum* exhibited significantly higher *α*-glucosidase inhibiting activity (IC_{50} 0.43 mg mL^{-1}) than other studied species (*T. ornata* ~ $IC_{50\ \alpha\text{-glucosidase}}$ 0.46 mg mL^{-1}; *T. conoides* ~ $IC_{50\ \alpha\text{-glucosidase}}$ 0.52 mg mL^{-1} and *S. ilicifolium* ~ $IC_{50\ \alpha\text{-glucosidase}}$ 0.61 mg mL^{-1}). The DPP-4 inhibitory potential of the EtOAc-MeOH extracts of *S. tenerrimum* (IC_{50} 0.27 mg mL^{-1}) was considerably higher ($P < 0.05$) than those exhibited by other studied species (*T. ornata* ~ $IC_{50\ DPP\text{-}IV}$ 0.29 mg mL^{-1}; *T. conoides* ~ $IC_{50\ DPP\text{-}IV}$ 0.31 mg mL^{-1} and *S. ilicifolium* ~ $IC_{50\ DPP\text{-}IV}$ 0.36 mg mL^{-1}).

The different organic extracts obtained from selected marine macroalgae (*S. tenerrimum, S. ilicifolium, T. ornata and T. conoides*) were also studied for their anti-hypertensive properties with regard to ACE-1 inhibition assay (Table 3.1.2). The EtOAc-MeOH extract of *S. tenerrimum* (IC_{50} 0.24 mg mL^{-1}) exhibited considerably higher antihypertensive activities as displayed by the higher ACE-I inhibiting potential than those exhibited by other studied species (*T. conoides* ~ $IC_{50\ ACE\text{-}I}$ 0.28 mg mL^{-1}, *T. ornata* ~ $IC_{50\ ACE\text{-}I}$ 0.29 mg mL^{-1} and *S. ilicifolium* ~ $IC_{50\ ACE\text{-}I}$ 0.31 mg mL^{-1}) (Table 3.1.2).

Table 3.1. Percentage yield (%), phenolic content, antioxidant, anti-inflammatory, anti-diabetic, and ACE inhibitory activities of the of EtOAc-MeOH extracts of marine macroalgae belonging to family Sargassaceae

	T. conoides	*T. ornata*	*S. tenerrimum*	*S. ilicifolium*
Yield (%)	$8.55^{a} \pm 0.04$	$8.14^{a} \pm 0.12$	$6.06^{b} \pm 0.04$	$5.88^{c} \pm 0.31$
Total phenolics	$232.46^{a} \pm 0.05$	$193.01^{b} \pm 0.22$	$181.78^{c} \pm 0.07$	$170.68^{d} \pm 0.02$
Antioxidant activities				
DPPH radical scavenging	$0.48^{b} \pm 0.02$	$0.38^{c} \pm 0.31$	$0.45^{b} \pm 0.25$	$0.57^{a} \pm 0.22$
$ABTS^{+}$ radical scavenging	$0.57^{b} \pm 0.15^{a}$	$0.41^{c} \pm 0.24$	$0.51^{b} \pm 0.13$	$0.65^{a} \pm 0.07$
Fe^{2+} ion chelating	$0.65^{b} \pm 0.16$	$0.63^{b} \pm 0.05$	$0.69^{b} \pm 0.23$	$0.82^{a} \pm 0.25$
H_2O_2 scavenging	$0.51^{b} \pm 0.32$	$0.52^{b} \pm 0.28$	$0.49^{c} \pm 0.51$	$0.64^{a} \pm 0.27$
Lipoperoxidation inhibition	$45.32^{c} \pm 0.26$	$49.24^{b} \pm 0.11$	$52.86^{a} \pm 0.41$	$49.68^{b} \pm 0.33$
Anti-inflammatory activities				
COX-1 inhibition	$1.70^{b} \pm 0.23$	$1.74^{b} \pm 0.44$	$1.87^{a} \pm 0.04$	$1.78^{b} \pm 0.34$
COX-2 inhibition	$1.21^{a} \pm 0.28$	$1.09^{c} \pm 0.34$	$1.18^{b} \pm 0.17$	$1.25^{a} \pm 0.52$
LOX-5 inhibition	$1.26^{b} \pm 0.17$	$1.11^{c} \pm 0.05^{b}$	$1.16^{c} \pm 0.21$	$1.35^{a} \pm 0.04$
COX-1/ COX-2 (SI)	1.40	1.59	1.57	1.42
Anti-diabetic activities				
α-Amylase inhibition	$0.50^{b} \pm 0.06$	$0.42^{c} \pm 0.17$	$0.46^{c} \pm 0.08$	$0.59^{a} \pm 0.14$
α-Glucosidase inhibition	$0.52^{b} \pm 0.02^{a}$	$0.46^{c} \pm 0.32^{b}$	$0.43^{c} \pm 0.28^{c}$	$0.61^{a} \pm 0.12$
DPP-4 inhibition	$0.31^{b} \pm 0.35^{a}$	$0.29^{c} \pm 0.21^{a}$	$0.27^{c} \pm 0.31^{a}$	$0.36^{a} \pm 0.27$
Anti-hypertensive activities				
ACE-I inhibition	$0.28^{a} \pm 0.12$	$0.29^{a} \pm 0.08^{b}$	$0.24^{b} \pm 0.14$	$0.31^{a} \pm 0.26$

EtOAc-MeOH: ethyl acetate-methanol solvent extract of brown algal samples. The fractions were analyzed in triplicate (n = 3) and expressed as mean ± standard deviation. Means followed by the different superscripts (a-d) within the same row indicate significant difference ($p < 0.05$). Total phenolic contents were determined at 5 mg/mL, and presented as mg of gallic acid equivalence (GAE)/g. The IC_{50} values were expressed as mg mL^{-1}. Lipid peroxidation inhibitory (TBARS assay) was expressed as mM MDAEQ/kg.

3.5. Correlation analysis

The variances (ANOVA) between various results were analyzed by Statistical Program for Social Science (SPSS, ver. 13.0, SPSS Inc., Quarry Bay, HK), and was used for assessing the significant differences between the means. The significant differences were represented as $P < 0.05$, and the readings were presented as mean of triplicates ± standard deviation. Principal component analysis (PCA) was used to recognize the mean variances in the data set. This section explained the relations between various bioactivities based upon statistical evaluations.

3.6. Spectroscopic labelling of the functional groups of solvent fractions of selected ma

The ^{1}H spectra were mainly categorized in six different regions, including saturated hydrocarbons (RCH_3, R_2CH_2 and R_3CH) from δ_H 0.5-2.0, $RC(=O)-CH_3$ (acetyl) or $-CH_2=CH-CH_3$ (allylic) from δ_H 2.0-2.5, RCH_2-X (alkyl halide) or $-OCH_3$ (methoxy) or RCH_2OH (alkanols) from δ_H 2.5-3.5, anomeric protons are seen at δ_H 3.5-4.5, directly attached protons to oxygen of ester linkages or $RCH_2C(=O)-OCH_3$ (alkyl alkanoates) and olefinic ($RCH=CHR_1$) from δ_H 4.5-6.5, and aromatic protons from δ_H 6.5-8.5. The ^{1}H-NMR spectrum of the crude extract of *S. tenerrimum* exhibited maximum proton integrals (35.95) due to the saturated hydrocarbon groups (δ_H 0.5-2.0). The total number of protons at δ_H 2-2.5, apparently for $(RCH_2C-(=O)\ OR_1)/(CH_2=CH-CH_3)/(RC(=O)CH_3)$ were found to be greater in *S. tenerrimum* (proton integral of 3.18).

The proton integrals at δ_H 2.5-3.5 for methoxy (-OCH_3)/functionalized hydride H/substituted alkanol (RCH_2OH) were found to be higher in *T. ornata* (proton integral of 80.88). The proton integrals at olefinic/alkanoates regions (δ_H 4.5-6.5) were found higher for the solvent extracts of *T. conoides* (792.98). The total no of protons at δ_H 3.5-4.5 apparently for anomeric proton of polysachharides, was higher in *T. ornata* (48.98). The proton integrals at aromatic region were found greater for the crude extract of *T. conoides* (proton integral 2.21) (Table 3.1.4).

Table 3.2. Proton integral of crude algal extracts

	Proton integral (Σ H) at specified chemical shift (δ_H)					
Algal species	**δ_H 0.5-2.0[a]**	**δ_H 2.0-2.5[b]**	**δ_H 2.5-3.5[c]**	**δ_H 3.5-4.5[d]**	**δ_H 4.5-6.5[e]**	**δ_H 6.5-8.5[f]**
T. ornata	22.08	1.32	80.88	48.98	627.62	1.12
T. conoides	15.93	2.05	73.90	10.92	762.98	2.21
S. tenerrimum	35.95	3.18	22.17	5.08	166.69	0.93
S. ilicifolium	18.03	1.89	13.05	14.83	133.01	2.20

[a] Saturated hydrocarbons

[b] Alkyl alkanoates/allylic/acetyl groups ($RC\underline{H}_2C(=O)OR_1$)/ ($CH_2=CH-C\underline{H}_3$)/($RC(=O)C\underline{H}_3$)

[c] ($OC\underline{H}_3$)/($RC\underline{H}_2$-X)/ ($RC\underline{H}_2OH$)

[d] Anomeric protons for polysaccharides

[e] Alkanoates/olefinic ($RCH_2C(=O)$-$OC\underline{H}_3$)/ ($RC\underline{H}=C\underline{H}R_1$)

[f] Aromatic proton (Ar-$\underline{H}$)

3.6. Conclusions

Marine macroalgae are often considered ‘wonder herbs’ of aquatic biomes due to their enormous pharmacological potential, and algal biomass also plays an essential role in developing the blue economy. Oceanic waters of the Gulf of Mannar area located in the South-eastern coastal region of the Indian subcontinent have ample resources of marine macroalgae, which have been recognized as a natural defence mechanism because of their saline habitats and ability of these species to withstand oxidative stress conditions. Anti-hyperglycemic, anti-hypertensive, anti-inflammatory, and antioxidant properties of EtOAc/MeOH extracts of four different species belonging to the family Sargassaceae (*T. conoides*, *T. ornata*, *S. tenerrimum* and *S. ilicifolium*) were assessed by using various *in vitro* methods. EtOAc/MeOH crude extracts of *T. ornata* and *T. conoides* were recorded with superior activities against oxidant radical species, and those displayed inverse correlations with lipid peroxidation inhibition and total phenolic constituents. This inferred the role of non-phenolic components (that might be present in crude extracts) towards antioxidant activities, which was also positively correlated with anti-inflammatory, anti-hyperglycemic, and anti-hypertensive properties of those studied macroalgal extracts. The presence of TPC and TBARS in a similar quadrant of component analysis led to the idea that phenoxide anion or free hydrogen of hydroxyl groups could be responsible for entrapping the free radicals formed by peroxidation of lipid molecules in our system. The relative abundance of critical functional groups (accountable for bioactivities) with their characteristic signals in the crude macroalgal extracts have been demonstrated by spectroscopic studies. Overall activities of organic extracts of *Turbinaria* species were more significant than those of *Sargassum* species. The targeted bioactivities of crude extracts of four macroalgal samples were directly associated with polar/or electron donating groups observed in the downfield region of ^1H NMR spectra. The result of this study recognized that *T. conoides* and *T. ornata* might be prospective sources of bioactive metabolites that can be used as promising pharmacophores to combat various lifestyle disorders. Bioactivity-guided fractionation of these marine macroalgae's crude extracts could isolate different classes of secondary metabolites, as illustrated in the following chapters

CHAPTER 4: ISOLATION AND CHARACTERIZATION OF BIOACTIVE SECONDARY METABOLITES FROM *TURBINARIA CONOIDES*

4.1. Materials and methods

This section described the instruments used for the present study along with the reagents and solvents.

4.1.1. Sample Preparation

The brown marine macroalga *T. conoides* (10 kg) were collected from Gulf of Manner of Mandapam region located between 8º48' N, 78º9' E and 9º14' N, 79º14'E on the southwest coast of India. Subsequently, the samples were washed with tap water to remove the surface-associated salt and sand particles. After that macroalgal sample were spread on blotting paper to remove excess water and dried, stored in airtight containers at room temperature for further work. The washed and shade dried leaves of *T. conoides* were powdered (1.2 kg, yield 20 %). Initially the powdered algal sample was extracted with *n*-hexane (300 mL × 2), at RT for 24 h, until the pigments were removed, before being filtered through whatmann No. 1 filter paper. Thereafter, the residue was extracted with solvents EtOAc-MeOH (1:1, v/v, 500 mL × 3) at 40 °C followed by shaking (8 h) and sonication (8 h). The extracts were filtered over anhydrous Na_2SO_4 (100 g), before being evaporated in vacuum using a rotary vacuum evaporator (50 °C) (Heidolf, Germany) to afford a dark brown viscous residue, which was considered as the crude organic extract of *T. conoides* (55 g, yield on dry basis 4.58 %).

4.1.2. Chromatographic purification and spectral analysis of pure compounds from *T. conoides*

The purification of crude organic extract of *T. conoides* was achieved by using sequential chromatographic methods. Initially, the solvent fraction was mixed in silica (3 g, 60-120 meshed) and packed with an adsorbent (60-120 meshed silica gel, 50 g) into a glass column of 90 cm × 4 cm size, before subjecting to liquid chromatographic fractionation. To avoid the interference of waxy materials in the loaded aliquot, the column was primarily purged with *n*-hexane. The solvent polarity was slowly increased by adding solvent EtOAc {*n*-hexane:EtOAc (9:1-3:7, v/v)} to provide 25 fractions (25 mL each) before being divided into 6 groups (TC_1-TC_6) based on TLC analyses (*n*-hexane:EtOAc, 9:1, v/v). The column fraction, TC_2 (2.9 g) that was attained by the elution of *n*-hexane:EtOAc (4:1, v/v) solvent system, was a mixture, and thus subjected to flash chromatographic fractionation (Biotage AB SP1-B1A, 230-400 meshed, 12 g; Biotage AB, Uppsala, Sweden) on 230-400 meshed silica (Biotage, 12 g; Sweden, Biotage No. 25+M 0489-1) using gradient elution of EtOAc/*n*-hexane (0-5% EtOAc) at 236 nm (collection wavelength) to acquire a total of 45 fractions (25 mL each). Based upon analytical TLC patterns, similar fractions were combined to six homogenous fractions ($TC_{2\text{-}1}$-$TC_{2\text{-}6}$). The selected fraction, $TC_{2\text{-}3}$ on successive flash chromatography (10 % MeOH/EtOAc followed by 10 % EtOAc/*n*-hexane) afforded the purification of compound **1** and **2**. The acquired compounds were checked for their purities by TLC (GF_{254} silica gel of 15 mm size) using 10 % EtOAc/*n*-hexane (9:1, v/v) along with RP-C_{18}-HPLC (MeOH/ACN, 3:2 v/v) analysis. Another fraction, $TC_{2\text{-}5}$ was also flash chromatographed (70 % EtOAc/*n*-hexane followed by 10 % MeOH/EtOAc) to yield a total of 37 fractions (50 mL each), which were reduced to eight separate groups of $TC_{2\text{-}5\text{-}1}$-$TC_{2\text{-}5\text{-}8}$ by analytical TLC-guided fractionation. The pooled sub-fraction $TC_{2\text{-}5\text{-}4}$ was fractionated over preparatory TLC (PTLC) (GF_{254} silica using $CHCl_3$/MeOH 9:1, v/v) to yield compound **3** The homogeneity of compound **3** was checked by analytical TLC (on GF_{254} silica) by using EtOAc/*n*-hexane (4:1, v/v) as the solvent system along with RP-C_{18}-HPLC (MeOH/ACN, 3:2 v/v) analysis. The column fraction, TC_3 was further eluted with less polar solvent (*n*-hexane), followed by an increase of polarity (EtOAc to MeOH) to collect twenty-five fractions (10 mL/fraction), which were combined to five ($TC_{3\text{-}1}$ through $TC_{3\text{-}5}$) based upon TLC (8:2 v/v, *n*-

hexane:EtOAc) and RP C_{18}-HPLC (MeOH/acetonitrile MeCN, 3:2 v/v) analysis, and those fractions (TC_{3-1} - TC_{3-5}) were assessed for their bioactivities. The fractions TC_{3-3} (EtOAc:*n*-hexane 2:3 v/v) and TC_{3-4} (EtOAc:*n*-hexane 7:3 v/v) displayed greater bioactive potential in comparison with other fractions, and therefore, were selected for downstream purification. Likewise, the sub-fraction TC_{3-3} was put through fractionation on a silica gel (230-400 mesh) loaded glass column. Step-wise gradient elution with *n*-hexane-EtOAc (9:1 to 3:2, v/v) yielded four sub-fractions (TC_{3-3-1}-TC_{3-3-4}), after TLC (*n*-hexane-EtOAc, 4:1 v/v) and RP-C_{18} HPLC (MeOH-MeCN, 3:2 v/v) experiments. Based on the bioactivity, TC_{3-3-4} was further sub-fractionated with flash chromatographic system by increasing gradient of *n*-hexane/EtOAc/MeOH to acquire twelve sub-fractions (15 mL/fraction). The latter fractions were combined to three ($TC_{3-3-4-1}$-$TC_{3-3-4-3}$) after TLC (*n*-hexane-EtOAc, 8:2 v/v) and RP-C_{18} HPLC (MeOH/MeCN, 3:2 v/v). $TC_{3-3-4-1}$ was purified on silica gel GF_{254} by *n*-hexane: EtOAc (25:1, v/v) solvent system using the preparatory TLC (PTLC) system to yield compound **4** and **5**, and their homogeneities were reinforced by TLC (EtOAc/*n*-hexane, 1:9 v/v) and RP-C_{18} HPLC (MeOH/MeCN, 3:2 v/v). The fraction TC_{3-4} was subjected to flash chromatography on a silica gel column (230-400 mesh), which were combined into three (TC_{3-4-1}-TC_{3-4-3}) after TLC (EtOAc-*n*-hexane, 1:4 v/v). TC_{3-4-2} displayed greater bioactive potential than other column sub-fractions, and flash chromatographic separation using a gradient elution of *n*-hexane/EtOAc yielded eleven fractions (13 mL/fraction), which were compounded into three ($TC_{3-4-2-1}$-$TC_{3-4-2-3}$). The bioactive fraction $TC_{3-4-2-3}$ was a mixture, and was further purified by PTLC (EtOAc: *n*-hexane, 1:26, v/v) to obtain compound **6**. The homogeneity of the latter was reinforced by RP-C_{18} HPLC.

Another one fraction TC_4 upon purification yielded four column sub-fractions (TC_{4-1}-TC_{4-4}). Owing to comparatively greater inhibition potential of TC_{4-3} against inflammatory enzymes LOX-5 and COX-2, compared to others, the column sub-fraction was put through further chromatographic separation to yield eight resultant fractions (TC_{4-3-1}-TC_{4-3-8}). The resultant TC_{4-3-6} exhibited comparatively better enzyme inhibitory potential and upon further flash chromatographic purification yielded furanyl-substituted isochromanyl metabolite, named as turbinochromanone, which was characterized as methyl-4^a-((8-(6′-ethyl-2′, 3′-dihydrofuran-2′-yl)-methyl)-1-oxoisochroman-3-yl)-butanoate (compound **7**).

4.1.3. Bioactive potentials of secondary metabolites isolated from *T. conoides* and structure-activity correlation analyses

The bioactive potentials of six pure compounds isolated from *T. conoides* were checked by various *in vitro* antioxidants (DPPH and $ABTS^+$), anti-diabetic, antihypertensive and anti-inflammatory (5-LOX) assays and their bioactivities were expressed as IC_{50} values in mg mL^{-1} and mM. Several physicochemical parameters of the pure compounds were analyzed to study the structure-activity relationship. The structural descriptors, such as electronic (polarizability/PI, topological polar surface area/tPSA), hydrophobic (octanol-water partition coefficient/log P_{ow}), and steric/bulkiness (molar refractivity/MR, molar volume/MV, parachor/P) descriptors using ACD ChemSketch (version 2019.1; Advance Chemistry Development, Inc., Toronto, Canada) and ChemDraw Ultra (Cambridge Soft Corporation, USA; version 12.0) softwares.

4.1.4. Statistical analysis

Statistical Program for Social Sciences 13.0 (SPSS Inc, Chicago, USA, version 13.0) was used to carry out the statistical calculations. Analyses were performed in triplicate and the significant means of all parameters were examined by analysis of variance (ANOVA). The level of significance for all analyses was $P < 0.05$.

4.2. Results and Discussion

4.2.1. Chromatographic purification and spectral analysis of secondary metabolites from *T. conoides*

Repeated chromatographic purifications of the solvent fractions obtained from *T. conoides* led to the isolation of seven previously unreported secondary metabolites. The novelty of isolated compounds has been verified with those described in the SciFinder databases. The structures were elucidated and confirmed by detailed analyses of the the ^{1}H NMR and ^{13}C NMR, including two-dimensional nuclear magnetic resonance spectroscopy (2D NMR) experiments such as correlation spectroscopy (^{1}H-^{1}H COSY); heteronuclear single-quantum correlation spectroscopy, HSQC; heteronuclear multiple-bond correlation spectroscopy (HMBC) and nuclear Overhauser effect spectroscopy (NOESY) along with mass spectra and Fourier transform infrared (FTIR) analyses.

4.2.1.1. Structural Characterization of Compound 1

Repeated chromatographic fractionation of *T. conoides* yielded compound **1** as a brown oily substance. The molecular ion peaks was appeared at *m/z* 418, with the molecular formula $C_{24}H_{34}O_6$. The compound exhibited eight degrees of unsaturation, which include two carbonyls, three double bonds of the aromatic ring, one double bond and two rings. The ^{13}C NMR in combination with the DEPT experiment confirmed the occurrence of twenty four carbon atoms with three methyls, one methoxy, six methylenes, eight methines and four quaternary (carboxylate and olefinic) carbons. The spectroscopic data of **1** revealed the occurrence of olefinic (δ_C 129.74/δ 5.27), methoxy (δ_C 51.39/δ 3.58) and deshielded methylene {δ_C 65.53/δ 4.23 for $\underline{CH_2}$-O-(-C=O)} functionalities. Highly deshielded ^{13}C resonances at δ_C 174.29 and 132.52 were accounted for carbonyl (-$\underline{C}$=O(O)-) and 4° alkene (>$\underline{C}$=CH-), respectively. The FTIR spectra displayed absorption bands at 3228 (-O-H stretching), 2744 (C-H stretching), 1559 (-C=C- stretching), 1742 (-C=O stretch for ester). The methylene proton at δ 4.01 and methine proton at δ 5.08 exhibited a deshielding shift, which implies the attachment of these protons with oxygen atom. Intense COSY correlation was observed between δ 4.01/1.95 and δ 5.27/1.95.The long range HMBC cross peak between δ 4.01 to δ 38.05, 72.36; δ 1.95 to 132.52 with the COSY correlation between δ 4.01/1.95/5.27 suggested the possibilities of an oxygenated hexacyclic ring (dihydro-pyran) in compound **1**

methyl-2^{1}-yl-[5', 6'- dihydro-5'-yl-{5^{4}-(4-hydroxybenzoyl)-oxy-(5^{2}-methylbutyl)}-3'-methyl-2H-pyran]-2^{1}-methyl butanoate

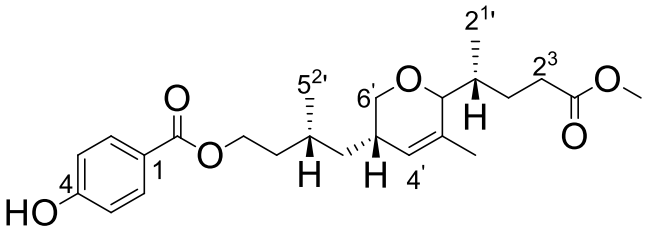

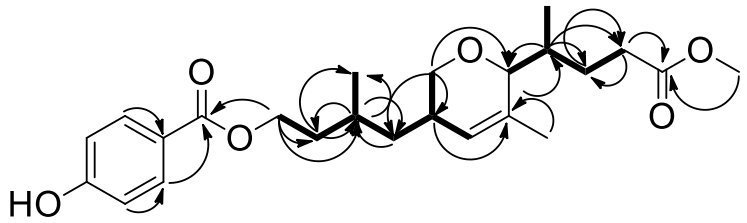

Fig. 4.2.1.1. Key ^{1}H-^{1}H COSY and HMBC correlations of methyl-2^{1}-yl-[5′, 6′- dihydro-5′-yl-{5^{4}-(4-hydroxybenzoyl)-oxy-(5^{2}-methylbutyl)}-3′-methyl-2H-pyran]-2^{1}-methyl butanoate. The key ^{1}H-^{1}H COSY couplings have been represented by the bold face bonds; the HMBC couplings are indicated as single barbed arrow.

4.2.1.2. Structural Characterization of Compound 2

The chromatographic separation of the solvent extract of *T. conoides* yielded compound as a yellow oil. The molecular ion peak appeared at m/z 344 $[M]^{+}$, while the molecular formula $C_{21}H_{28}O_4$, implying eight degrees of unsaturation (two carbonyl groups, three double bonds in aromatic ring, one double bond, and two ring systems). The ^{13}C NMR spectra in connection to DEPT spectra recorded the occurrence of five methylene sp^2 carbons (δ_C 22.6, 24.4, 30.5, 65.5, 69.9), two carbonyl carbons (δ_C 167.7, 179.9), methine sp^2 carbons (δ_C 128.8, 130.0, 129.4, 19.1, 29.3, 34.0, 129.7), three sp^3 carbons (δ_C 14.1, 13.7, 31.8) and two quaternary carbons (δ_C 130.9, 132.3), which apparently validated the existence of C-21 skeleton of **2**. ^{1}H-^{1}H COSY of δ_H 0.80/1.22 and HMBC between δ_H 0.80 to δ_C 22.6, δ_H 1.26 to δ_C 22.6 corroborated the presence of 10-methylhexyl group. Intense ^{1}H-^{1}H COSY correlation was observed between δ_H 5.27/4.01 and the HMBCs between δ_H 2.27 to δ_C 132.3, 179.7; δ_H 5.27 to δ_C 69.9; δ_H 4.01 to δ_C 179.7 supported the presence of dihydro-pyranone framework. The ^{13}C NMR signal at δ_C 130.9 was assigned to the quaternary carbon in aromatic ring, and its higher chemical shift was attributed to the presence of strong electron withdrawing ester group at δ_C 167.7. HMBC signal at δ_H 7.65 to δ_C 167.7 confirmed the connection between aromatic ring with the carbonyl ester group. Based on the exhaustive spectral analyses, the structure of the compound **2** was found to be 11-[(3′, 6′-dihydro-4′-methyl-2′-oxo-2*H*-pyran-3′-yl)methyl]-10-methylhexyl benzoate.

11-[(3', 6'-dihydro-4'-methyl-2'-oxo-2H-pyran-3'-yl)methyl]-1'-methylhexyl benzoate

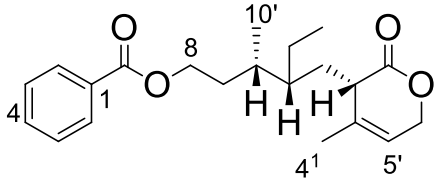

Fig. 4.2.1.2. Key ^{1}H-^{1}H COSY and HMBC correlations of 11-[(3', 6'-dihydro-4'-methyl-2'-oxo-2H-pyran-3'-yl)methyl]-1'-methylhexyl benzoate. The key ^{1}H-^{1}H COSY couplings have been represented by the bold face bonds; the HMBC couplings are indicated as single barbed arrow.

4.2.1.3. Structural Characterization of Compound 3

The chromatographic fraction of the crude extract of *T. conoides* yielded compound as brown liquid. The molecular ion peak was appeared at *m/z* 348, whereas the molecular formula $C_{22}H_{36}O_3$, implying five five degrees of unsaturation (three due to cycloheptene ring, one for carbonyl group and one for ring systems). The absence of signals at δ_C 115.7, 134.9, 82.0 and 179.6 in the DEPT spectrum, and their presence in the ^{13}C NMR spectrum appropriately suggested the occurrence of four quaternary carbons. Two spin systems were recorded at δ_H 0.88/2.81/5.35; δ_H 1.33/2.02/5.15 due to the seven membered, 3,4-dimethyl cyclohepta-2,5-diene ring system and one spin system (δ_H 0.99/1.99) was due to the ethyl side chain. The attachment of one ethyl group at C-6 position was established by the HMBC signal from δ_H 0.99 to δ_C 26.7 and δ_H 1.99 to δ_C 115.7. The presence of a carbonyl ester group at δ_C 179.6 was supported by ^{13}C NMR experiment, and the absence of signal in the corresponding DEPT spectrum. HMBCs between δ_H 4.03 to δ_C 39.5, 26.7; δ_H 1.97, 1.62 to δ_C 26.7; δ_H 1.68, 1.31 to δ_C 62.7; and δ_H 3.63 to δ_C 82.0, 22.1 attributed to tetrahydro-pyran fragment part. Dimethyl groups at δ_H 1.26 were found as singlet, which showed HSQC correlation with δ_C 31.9/29.0, and attached to the quaternary carbon at δ_C 82.06. This was apparent from HMBC correlation from δ_H 1.26 (H-2^2) to δ_C 82.0. Based on the spectral analyses, the structure of the compound **3** was elucidated as [6-ethyl-3,4-dimethyl-(tetrahydro-2′, 2′, 6′-trimethyl-2*H*-pyran-3′-yl)-2,5-cycloheptadiene]-1′-propanoate.

[6-ethyl-3,4-dimethyl-(tetrahydro-2', 2', 6'-trimethyl-2H-pyran-3'-yl)-2,5-cycloheptadiene]-1'-propanoate

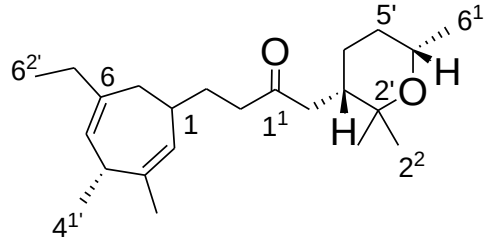

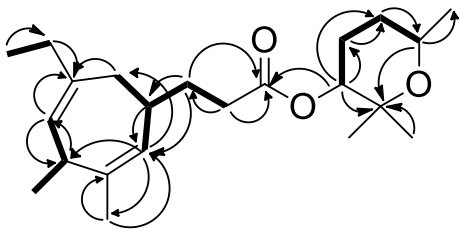

Fig. 4.2.1.3. Key ^1H-^1H COSY and HMBC correlations of [6-ethyl-3,4-dimethyl-(tetrahydro-2′, 2′, 6′-trimethyl-2H-pyran-3′-yl)-2,5-cycloheptadiene]-1′-propanoate. The key ^1H-^1H COSY couplings have been represented by the bold face bonds; the HMBC couplings are indicated as double barbed arrow.

4.2.1.4. Structural Characterization of Compound 4

Compound **4** was obtained as white amorphous, whereas the molecular ion peak was appeared at *m/z* 464, and the molecular formula was determined as $C_{27}H_{45}O_6$. The ^{13}C NMR spectrum exhibited the multiplicities, such as three each of methyl sp^3 and quaternary carbons along with eleven methylene sp^2 and ten methine sp^2 carbons, which were

corroborated by integrated ^{13}C-NMR/DEPT$_{135}$ experiments. Comprehensive analysis of ^{13}C NMR and DEPT spectra supported the occurrence of C-27 skeleton in Compound **4**. ^{13}C NMR signals at δ_C 115-146 designated the presence of olefinic carbons and the absence of ^{13}C signals at δ_C 134.5 and 146.3 in ^{135}DEPT spectrum inferred substitution at these olefinic carbons. The deshielded chemical shift value at δ_C 179.9 stipulated the presence of a carbonyl carbon. The ^{1}H NMR in combination with ^{13}C NMR validated the presence of two terminal methyl signals at δ_H 1.30 and 1.67. The methyl (-CH_3) group at δ_H 1.67 (H-28) appeared downfield due to presence of the olefinic carbon. ^{1}H-^{1}H COSY correlation between δ_H 1.98/0.98 along with the HMBCs between δ_H 1.98 to δ_C 18.0 and δ_H 2.06 δ_C 134.0/39.7 recognized that there was an attachment of ethyl group with the C-6 position of the macrocyclic ring. Presence of three hydroxyl groups were confirmed by the broad stretching vibration band in the IR and deuterium exchange {D_2O (deuterium oxide)} experiment. ^{1}H-^{1}H COSY cross-peaks were inferred between three oxymethines. Based on the spectral analyses, the structure of the compound **4** was elucidated as 6-ethyl-9, 18, 19-trihydroxy-24, 28-dimethyl-22, 25-dioxabicyclo[19.3.1]pentacosa-5, 11, 14-triene-1-one (conoidecyclic A).

6-ethyl-9, 18, 19-trihydroxy-24, 28-dimethyl-22, 25-dioxabicyclo[19.3.1]pentacosa-5, 11, 14-triene-1-one

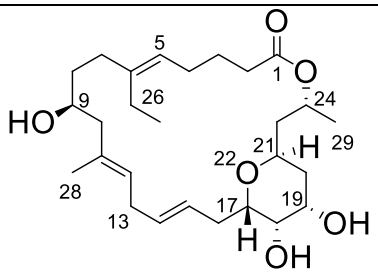

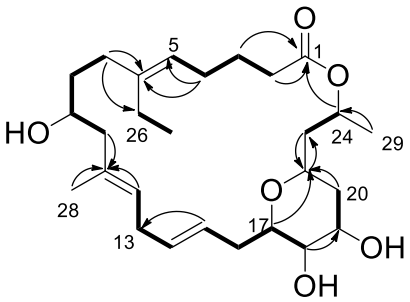

Fig. 4.2.1.4. Key ^{1}H-^{1}H COSY and HMBC correlations of 6-ethyl-9, 18, 19-trihydroxy-24, 28-dimethyl-22, 25-dioxabicyclo[19.3.1]pentacosa-5, 11, 14-triene-1-one (conoidecyclic A). The key ^{1}H-^{1}H COSY couplings have been represented by the bold face bonds; the HMBC couplings are indicated as single barbed arrow.

4.2.1.5. Structural Characterization of Compound 5

The compound **5** was characterized as 6-ethyl-9,18,19-trihydroxy-28-dimethyl-22,25-dioxabicyclo[19.3.1]pentacosa-5,11,14-triene-1-one-29-yl)isobutyl acetate (conoidecyclic B), with molecular ion peak *m/z* at 565 {HRESIMS *m/z* 565.3747 $[M+H]^+$}. Combined NMR/FTIR analyses, inferred its chemical composition as $C_{32}H_{53}O_8$. The ^{1}H NMR in combination with DEPT$_{135}$ and ^{13}C NMR data ascribed the occurrence of four each of methyl sp^3 and quaternary carbons, thirteen methylene sp^2 carbons, and eleven methine sp^2 carbons in the compound. Complete study of ^{13}C NMR and DEPT signals revealed the presence of C-32 skeleton in conoidecyclic B. The basic skeleton of cyclic ether containing macrocycle was similar and the chemical shift values of this fragment were analogous with conoidecyclic A. Apart from the macrocyclic framework, one extra isobutyloxycarbonylmethyl side

chain was attached with the C-29 position. ^{1}H-^{1}H COSY cross-peaks were spotted between δ_H 4.11/2.65 and δ_H 4.05/1.90. Intense ^{1}H-^{13}C HMBC couplings were recorded between δ_H 2.65 to δ_C 173.9; δ_H 4.05 to δ_C 173.9/ 27.15; δ_H 0.88 to δ_C 27.15; δ_H 0.90 to δ_C 27.9, which along with ^{1}H-^{1}H COSY correlations suggested the presence of an isobutyloxycarbonylmethyl side chain in this compound. The connection of side chain with the macrocyclic ring was confirmed by the ^{1}H-^{1}H COSY correlation at δ_H 4.11/2.65. The titled compound exhibited seven degrees of hydrogen deficiencies (two from carbonyl, three from olefinic, along with one each from the cyclic ether and macrocyclic ring system in conoidecyclic B). The molecular ion peak at *m/z* 564 (HREIMS) experienced sequential elimination of water (three molecules) to form fragmentation at *m/z* 510.

6-ethyl-9,18,19-trihydroxy-28-dimethyl-22,25-dioxabicyclo[19.3.1]pentacosa-5,11,14-triene-1-one-29-yl)isobutyl acetate

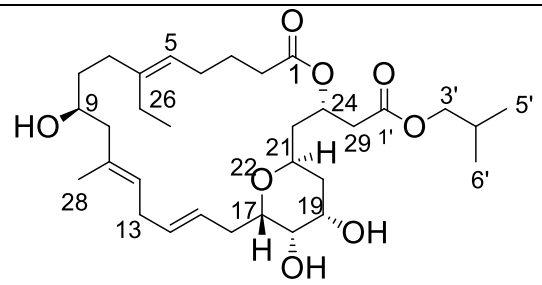

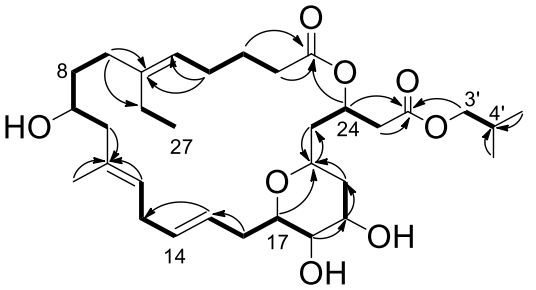

Fig. 4.2.1.5. Key ^{1}H-^{1}H COSY and HMBC correlations of 6-ethyl-9,18,19-trihydroxy-28-dimethyl-22,25-dioxabicyclo[19.3.1]pentacosa-5,11,14-triene-1-one-29-yl)isobutyl acetate (conoidecyclic B). The ^{1}H-^{1}H COSY couplings have been represented by the bold face bonds; the HMBC couplings are indicated as double barbed arrow.

4.2.1.6. Structural Characterization of Compound 6

Compound **6** was purified as white amorphous solid, with elemental composition as $C_{29}H_{46}O_8$ established by recorded molecular ion peak at *m/z* 523.3276 $[M+H]^+$. The integrated experiments encompassing ^{13}C NMR combined with DEPT$_{135}$/HSQC displayed the carbon signals with reference to two methyl sp^3, twelve methylene sp^2, nine methine sp^2, and four quaternary carbons. Combined ^{13}C NMR/DEPT$_{135}$ experiments supported the occurrence of C-29 skeleton in conoidecyclic C, wherein the deshielded carbon traces at δ_C 179.9 and δ_C 171.2 attributed the presence of two carbonyl moieties. The chemical shift values of the studied compound were comparable with conoidecyclic A, and one extra methoxycarbonylmethyl side chain was found to be attached with the C-29 position of the compound. Intense ^{1}H-^{1}H COSY correlations were spotted between δ_H 4.13/2.67). ^{1}H-^{13}C HMBC couplings were recorded between δ_H 4.13 to δ_C 171.2; δ_H 2.67 to δ_C 171.2; δ_H 3.68 to δ_C 171.2 along with one singlet owing to the methoxy group at δ_H 3.68. The connectivity of methoxycarbonylmethyl moiety with macrocyclic ring system was recognized by the ^{1}H-^{1}H COSY correlation between δ_H 4.13/2.67. The index of unsaturation was recorded as seven, which include two carbonyl groups,

three olefinic group, along with one cyclic ether and macrocyclic ring moiety. The molecular ion peak was recorded at *m/z* 522. The ^{1}H NMR signals in conjugation connection with ^{13}C NMR signal recorded exhibited the presence of one terminal methyl signal at δ_H 1.67. The methyl group at δ_H 1.67 shifted downfield due to the occurrence of the adjacent olefinic carbon at C-11. The Intense ^{1}H-^{1}H COSY correlation was observed between δ_H 1.98/0.97 along with the long range HMBCs correlations between δ_H 1.98 to δ_C 18.0 and δ_H 2.06 to δ_C 134.9, 39.7 implied that there was the attachment of an ethyl group attached with to the C-6 position of the macrocyclic ring. Based on the spectral analyses, the structure of the compound **6** was elucidated as (6-ethyl-9, 18, 19-trihydroxy-28-dimethyl-22, 25-dioxabicyclo[19.3.1]pentacosa-5,11,14-triene-1-one-29-yl)methyl acetate (conoidecyclic C).

(6-ethyl-9, 18, 19-trihydroxy-28-dimethyl-22, 25-dioxabicyclo[19.3.1]pentacosa-5,11,14-triene-1-one-29-yl)methyl acetate

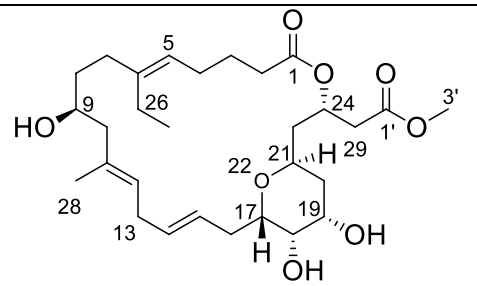

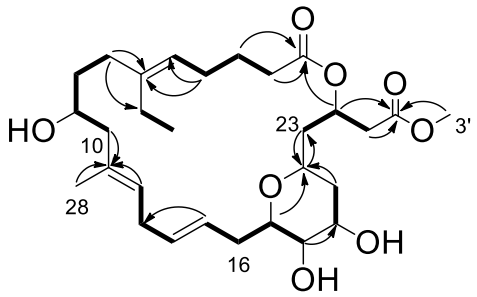

Fig. 4.2.1.6. Key ^{1}H-^{1}H COSY and HMBC correlations of (6-ethyl-9, 18, 19-trihydroxy-28-dimethyl-22, 25-dioxabicyclo[19.3.1]pentacosa-5,11,14-triene-1-one-29-yl)methyl acetate (conoidecyclic C). The key ^{1}H-^{1}H COSY couplings have been represented by the bold face bonds; the HMBC couplings are indicated as double barbed arrow.

4.2.1.7. Structural Characterization of Compound 7

Turbinochromanone (compound **7**) was purified as colorless oily substance. Spectroscopic analyses (mass, 1D and 2D FTIR, and NMR) recognized its elemental composition as $C_{21}H_{26}O_5$ (*m/z* 359.1863 $[M+H]^+$). The titled compound demonstrated nine indices of hydrogen deficiencies (four olefinic, two carbonyl and three rings). ^{13}C NMR signals in combination with DEPT-135 recorded the presence of two sp^3 methyl, seven sp^2 methylene, six each of sp^2 methine and non-protonated carbons, which corroborated the presence of C-21 skeleton. Spectroscopic report of turbinochromanone attributed the manifestation of olefinic (δ_H 5.96/δ_C 149.1) and methoxy (δ_H 3.53/δ_C 52.3) functionalities, whereas deshielded ^{13}C NMR chemical shifts at δ_C 166.6 and δ_C 174.6 were accounted for the carbonyl ester. ^{1}H-^{1}H correlation spectroscopy (COSY) relations were perceived between δ_H 7.02/7.35 and δ_H 4.16/2.83. Heteronuclear multiple bond correlation (^{1}H/^{13}C HMBC) signals between δ_H 4.16/δ_C 166. 6, 35.5; δ_H 2.83/δ_C 123.1, 132.8; δ_H 7.02/δ_C 125.1; δ_H 7.35/δ_C 137.4, 128.0; δ_H 7.11/δ_C 128.02 along with COSYs assigned the isochromen-1-one moiety in turbinochromanone. Presence of a methyl butanoate moiety was established by HMBC's from δ_H 2.27/δ_C

174.6, 33.8; δ_H 3.53/δ_C 174.6; δ_H 1.65/δ_C 174.6. The attachment of butanoate moiety with isochromen-1-one system at C-3 was deduced by COSY correlation between H-3/H-1^a. Other HMBCs from δ_H 2.92/δ_C 117.9; δ_H 4.29/δ_C 149.1; δ_H 5.96/δ_C 117.9 in combination with COSY correlation at δ_H 2.92/4.29 corroborated the presence of a furan moiety in turbinochromanone. ^{1}H-^{1}H COSY at δ_H 1.98/1.22 and HMBC's from δ_H 1.22/δ_C 117.9; δ_H 1.98/δ_H 117.9 substantiated the occurrence of an ethyl moiety at C-6′ locus of the furan ring. The connection between the furan ring with the isochromen-1-one was established by COSY interaction between δ_H 2.52/2.92 in combination with HMBCs from δ_H 2.52/δ_C 128.0, 47.1. Characteristic IR absorption bands at 1736, 2844 and 1537 cm^{-1} were observed for -C=O, -C=C- and -C-H stretching, respectively. Based on the comprehensive spectroscopic characterization, the purified compound from *T. conoides* was identified as methyl-4^a-((8-(6′-ethyl-2′, 3′-dihydrofuran-2′-yl)-methyl)-1-oxoisochroman-3-yl)-butanoate.

Methyl-4^a-((8-(6'-ethyl-2', 3'-dihydrofuran-2'-yl)-methyl)-1-oxoisochroman-3-yl)-butanoate

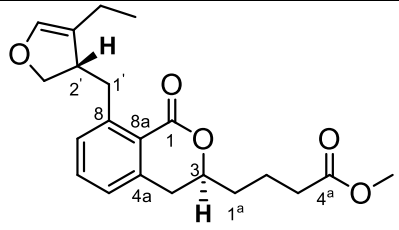

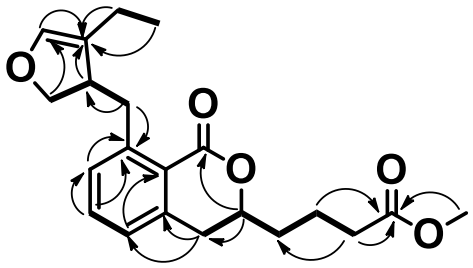

Fig. 4.2.1.7. Key ^{1}H-^{1}H COSY and HMBC correlations of methyl-4^a-((8-(6′-ethyl-2′, 3′-dihydrofuran-2′-yl)-methyl)-1-oxoisochroman-3-yl)-butanoate (compound **7**). The key ^{1}H-^{1}H COSY couplings have been represented by the bold face bonds; the HMBC couplings are indicated as double barbed arrow.

4.3. Bioactivities of Secondary Metabolites Isolated from *T. conoides* and SAR analyses

This section describes the antioxidant, antidiabetic, antihypertensive and anti-inflammatory potentials of the secondary metabolites isolated from *T. conoides* and their activities expressed as IC_{50} values. These results were compared and discussed in this section. Bioassay guided chromatographic fractionation of solvent fractions afforded potential secondary metabolites. Compound **1** exhibited higher scavenging activities against DPPH (IC_{50} 0.54 mg mL^{-1}) and ABTS$^+$ (IC_{50} 0.58 mg mL^{-1}) than those displayed by **2** (IC_{50} 0.59 and 0.69 mg mL^{-1}, respectively) and **3** (IC_{50} 0.68 and 0.76 mg mL^{-1}, respectively). The pro-inflammatory 5-lipoxygenase and cyclooxygenase-2 inhibitory activities of 2*H*-pyranoids (**1** and **2**) were greater (IC_{50} ~ 1 mg mL^{-1}) compared to those displayed by **3** (IC_{50} > 1.1 mg mL^{-1}). There were no significant difference for hydrophobic properties of compounds **1** (log P_{OW} ~ 4.62) and **2** (log P_{OW} ~ 4.58) compared to compound **3** (log P_{OW} ~ 4.4). The steric bulk of compound **1** was greater (P = 942.4 cm^3) than **2** and **3** (P < 800 cm^3) due to the presence of oxo-pyran, carboxylate, and aryl moieties. The polarities induced by electron-rich centres of **1** appeared to increase the electronic properties, which were reflected by its higher tPSA (61.83) compared to other studied compounds (tPSA 35-52). These factors might lead to the potentially greater interaction with the pro-

inflammatory inducible biocatalysts at their active reaction centres, The optimum lipophilic-hydrophilic balance of the studied 2*H*-pyranoids, as determined by the log P_{OW} values also might ascribe towards their effective permeability through inter-membrane barrier in the cellular network. Conoidecyclic A exhibited dual attenuation property against inducible inflammatory enzymes COX-2 and 5-LOX (IC_{50} 1.75 and 4.24 mM, respectively). The anti-inflammatory activities of conoidecyclic A were higher than those displayed by conoidecyclic B (IC_{50} > 1.9 mM) and conoidecyclic C ($IC_{50\ 5\text{-}LOX}$ 5.07 mM). Therefore, it could possibly be concluded that conoidecyclic A, with higher SI and greater specificity towards COX-2 was noteworthy towards development of selective anti-inflammatory therapeutic lead. Conoidecyclic A exhibited significantly greater attenuation properties against ACE-I and PTP-1B (IC_{50} 1.23 and 1.39 mM, respectively), in a comparison with other studied conoidecyclics (IC_{50} > 1.80 mM). The radical scavenging activities (IC_{50DPPH} 1.20 and IC_{50ABTS} 1.48 mM) exhibited by conoidecyclic A were greater when compared with those displayed by conoidecyclic B (IC_{50} 1.35-1.54 mM), conoidecyclic C (IC_{50} 1.54-1.81 mM) and commercially available standards (IC_{50} 1.46-1.69 mM). The steric factors of the studied compounds might play pivotal roles towards their potential bioactivities. Notably, the electronic properties of conoidecyclic B and C, were higher than those of conoidecyclic A, This could be explained by the comparatively lesser steric bulkiness of conoidecyclic A (P 1092.7 cm^3, MV 447.4 cm^3) than those recorded for conoidecyclic B (P 1316.5 cm^3, MV 534.9 cm^3) and C (P 1198.4, MV 522.0 cm^3) owing to the presence of bulkier side chain in the latter. These inferences were appropriately corroborated by the efficiency of conoidecyclic A towards the conformationally favorable interaction with active binding sites of the target enzymes. Notably, the hydrophobicity of conoidecyclic A and B (log P_{OW} 3.13-3.83) were found to reside within the permissible limit of hydrophobic-lipophilic threshold which could attribute to their prospective bioactive properties. Turbinochromanone (compound **7**) possessed attenuation potential against 5-LOX (IC_{50} 3.70 μM). Considerably higher index of anti-inflammatory selectivity of turbinochromanone recognizing the superior selectivity related to COX-2 inhibition. In addition, turbinochromanone showed effective enzyme inhibition property against COX-2 (IC_{50} 1.47 μM) that was lesser. Antioxidant potential of turbinochromanone (IC_{50} ~ 24.4 μM) further supported its potential anti-inflammatory property. Superior electronic parameters (topological polar surface area, tPSA 61.8) along with optimum lipophilic-hydrophilic balance (partition coefficient of logarithmic octanol-water, log P_{OW} ~3.43) of the studied compound **7** recognized its anti-inflammatory potential, and could attribute its effective permeability in celular network.

4.4. Conclusions

Three bioactive 2*H*-pyranoid derivatives characterized as methyl-2^1-yl-[5′,6′-dihydro-5′-yl-{5^4-(4-hydroxybenzoyl)-oxy-(5^2-methylbutyl)}-3′-methyl-2*H*-pyran]-2^1-methyl butanoate (**1**), 11-[(3′,6′-dihydro-4′-methyl-2′-oxo-2*H*-pyran-3′-yl)methyl]-10-methylhexyl benzoate (**2**) and [6-ethyl-3,4-dimethyl-(tetrahydro-2′,2′,6′-trimethyl-2*H*-pyran-3′-yl)2,5-cycloheptadiene]-1-propanoate (**3**) with potential antioxidative activities were isolated from the organic extract of brown seaweed *T. conoides*. The antioxidant and anti-inflammatory activities of substituted 2*H*-pyranyl- 5^2-methylbutyl-hydroxybenzoate analogue (**1**) were greater than the other studied 2*H*-pyranoid metabolites. Additionally, the compounds exhibited greater anti-inflammatory selectivity index as compared to those exhibited by synthetic non-steroidal anti-inflammatory drugs implying the greater anti-inflammatory selectivity of the 2*H*-pyranoids towards pro-inflammatory inducible COX-2. The current study envisaged the potential of 2*H*-pyranoid metabolites isolated from *T. conoides* as natural anti-inflammatory and antioxidant lead molecules in the medicinal formulations.

Three unreported macrolide derivatives, named as compounds **4-6** with potential anti-inflammatory activities were isolated by sequential chromatographic separation from the solvent extract of the brown macroalga *T. conoides*. Compound **4** exhibited potential inhibition against pro-inflammatory enzyme 5-LOX (IC_{50} 4.24 mM) with higher selectivity index (~1.8) than that displayed by the anti-inflammatory agent ibuprofen (0.44). Likewise the compound

could effectively attenuate ACE-I (IC_{50} 1.23 mM) and negative regulator of insulin signaling PTP-1B (IC_{50} 1.39 mM) thereby recognizing its selective bioactive potential to regulate multiple mechanisms implicated in the pathogenesis of inflammation, hypertension, and type-2 diabetes. Structure-activity relation studies showed that the optimum lipophilic-hydrophobic balance coupled with lesser steric bulkiness could play paramount roles to ascribe the greater bioactivities of compound **4** over that of other analogues. Reaction kinetic studies showed that compound **4** exhibited lesser inhibition constant against the studied enzymes than those displayed by other studied metabolites thereby recognizing that the former could efficiently bind with the targeted enzyme. Furthermore, compound **4** displayed acceptable drug-likeness and pharmacokinetic parameters including acceptable oral bioavailability. These results showed that compound **4** enclosing pentacosa macrocyclic frameworks could be developed as a prospective therapeutic lead for use against various chronic diseases towards utilization of the commercially significant marine macroalga *T. conoides* and development of algal bioprocess technology to derive valuable bioactive agents.

An undescribed furanyl-substituted isochromanyl metabolite, compound **7** fractionated from the crude solvent extract of *Turbinaria conoides* demonstrated potential attenuation properties against inflammatory 5-lipoxygenase and cyclooxygenase-2 enzyme. Significantly greater index of anti-inflammatory selectivity of compound **7** compared to the anti-inflammatory agent diclofenac could account for the greater anti-inflammatory selectivity of the studied compound towards the cyclooxygenase-2 isoform. Ideal binding means for compound **7** with inflammatory enzymes showed lesser binding energy with the amino acid residues. Prospective attenuation properties of the studied compound against 5-lipoxygenase and cyclooxygenase-2, in addition to greater electronic properties combined with balanced hydrophobic properties attributed the seaweed-derived isochromanyl derivative as promising source of anti-inflammatory agent with pharmaceutical and biotechnological applications.

CHAPTER 5: ISOLATION AND CHARACTERIZATION OF BIOACTIVE SECONDARY METABOLITES FROM *TURBINARIA ORNATA*

5.1. Materials and Methods

This section described the instruments used for the present study along with the reagents and solvents.

5.1.1. Sample Preparation

The brown marine macroalgal material, *T. ornata* (10 kg) was obtained from the region of south east coastal region of Indian peninsular, specifically, from the Mannar region of Mandapam 8º48'N, 78º9'E and 9º14'N, 79º14'E. The sample was washed and shade-dried for one week at room temperature before being ground to homogeneity (1 kg). Powdered algal material was subjected to extraction with solvent hexane (500 mL × 2), at room temperature for 20 h, until the removal of pigment materials, and filtered through Whatman No. 1 filter paper over anhydrous sodium sulfate. The residues were extracted with equimolar amount of EtOAc/MeOH (1:1, v/v, 450 mL × 4) at 70 °C. The extract was filtered over anhydrous sodium sulfate (150 g), and the combined organic layer was evaporated in vacuum using a rotary vacuum evaporator (~50 °C) (IKA, Germany) to afford a dark brownish viscous residue, and was labeled as crude extract of *T. ornata* (32 g, yield based on dry basis 3.20 %).

5.1.2. Chromatographic Purification and Spectral Analysis of Pure Compounds from *T. ornata*

Crude extract of *T. ornata* (28 g) was purified with a series of chromatographic techniques. Initially 60-120 mesh silica gel (~ 3.8 g) was used to make slurry of the organic extract and loaded into a pre packed (with 60-120 mesh, silica, 350 g) glass column (100 cm × 4 cm). The separation was initiated by the elution with *n*-hexane followed by more polar ones (EtOAc and MeOH) to obtain the total of seven combined fractions (TO_1-TO_7). Based upon the bioactivity, various sub-fractions were selected for the process of chromatographic separation, and the potentially bioactive sub-fractions were purified. Bioactive fraction TO_4 upon fractionation with 100 % *n*-hexane followed by polar solvents (EtOAc-MeOH), resulted to six homogenous fractions ($TO_{4\text{-}1}$-$TO_{4\text{-}6}$) after TLC (9:1, *n*-hexane/EtOAc) and RP C_{18}-HPLC (MeOH/acetonitrile MeCN, 3:2 v/v). Fractions $TO_{4\text{-}4}$ and $TO_{4\text{-}5}$ possessed higher bioactive potentials against ACE-I, and were therefore, shortlisted for further downstream fractionation. The sub-fraction, $TO_{4\text{-}4}$ was fractionated by step-wise gradient elution of *n*-hexane/EtOAc (9:1 to 3:2, v/v) to three fractions ($TO_{4\text{-}4\text{-}1}$-$TO_{4\text{-}4\text{-}3}$). The bioactive fraction $TO_{4\text{-}4\text{-}3}$ was sub-fractionated by flash chromatography over silica gel adsorbent (230-400 mesh) to obtain three sub-fractions ($TO_{4\text{-}4\text{-}3\text{-}1}$-$TO_{4\text{-}4\text{-}3\text{-}3}$). Based on comparatively greater bioactivity, $TO_{4\text{-}4\text{-}3\text{-}3}$ was subjected to preparative HPLC using (MeOH-ACN, 3:2 v/v, 4 ml min^{-1} flow rate) to yield spirornata A (compound **8**, 75 mg), spirornata B (compound **9**, 92 mg). The fraction, $TO_{4\text{-}5}$ was flash chromatographed using step gradient elution of *n*-hexane/EtOAc/MeOH on a silica gel column to afford three fractions ($TO_{4\text{-}5\text{-}1}$-$TO_{4\text{-}5\text{-}3}$). Based upon bioactivity, the fraction $TO_{4\text{-}5\text{-}2}$ was flash chromatographed to combine three fractions ($TO_{4\text{-}5\text{-}2\text{-}1}$-$TO_{4\text{-}5\text{-}2\text{-}3}$). The bioactive sub-fraction, $TO_{4\text{-}5\text{-}2\text{-}3}$ was fractionated by reverse-phase (RP)-HPLC (ACN-MeOH, 8:2 v/v) to acquire spirornata C (compound **10**, 72 mg). The fraction TO_5 (3:7 v/v, *n*-hexane/EtOAc) exhibited considerably higher carbolytic enzyme inhibitory properties compared to other studied fractions, and was therefore, subjected to further separation. Sub-fraction TO_5 was flash chromatographed using *n*-hexane/EtOAc/MeOH step gradient elution on silica gel (Biotage 25 + M) column, and the purified fractions were combined into five fractions ($TO_{5\text{-}1}$-$TO_{5\text{-}5}$). The sub-fraction $TO_{5\text{-}4}$ exhibited comparatively greater bioactivities than those recorded with others, and was therefore, chosen for downstream fractionation by flash chromatography (collection wavelength of 254 nm), which resulted in three combined ($TO_{5\text{-}4\text{-}1}$-$TO_{5\text{-}4\text{-}3}$) fractions after TLC (EtOAc/*n*-hexane 1:4, v/v). Further PTLC fractionation of the bioactive sub-fraction, $TO_{5\text{-}4\text{-}3}$ using EtOAc/*n*-hexane (3:1, v/v) resulted in the separation of turbinafuranone A (compound **11**, 75 mg), turbinafuranone B (compound **12**, 95 mg) and turbinafuranone

C (compound **13**, 92 mg) as pure compounds, which were homogeneous after RP-C_{18} HPLC (MeOH/MeCN 3:2, v/v) and TLC (EtOAc/*n*-hexane, 1:4, v/v).

5.1.3. Bioactive Potentials of Secondary Metabolites Isolated from *T. ornata*

The bioactive potentials of fifteen pure compounds isolated from *T. ornata* were checked by various *in vitro* antioxidants (DPPH and $ABTS^+$), antihypertensive and anti-hyperglycemic assays and their bioactivities were expressed as IC_{50} values (mM). The structural descriptors, such as electronic (polarizability/PI, topological polar surface area/tPSA), hydrophobic (octanol-water partition coefficient/log P_{ow}), and steric/bulkiness (molar refractivity/MR, molar volume/MV, parachor/P) descriptors using ACD ChemSketch (version 2019.1; Advance Chemistry Development, Inc., Toronto, Canada) and ChemDraw Ultra (Cambridge Soft Corporation, USA; version 12.0) softwares.

5.1.4. Statistical analysis

Statistical Program for Social Sciences 13.0 (SPSS Inc, Chicago, USA, version 13.0) was used to carry out the statistical calculations. Analyses were performed in triplicate and the significant means of all parameters were examined by analysis of variance (ANOVA). The level of significance for all analyses was $P < 0.05$.

5.2. Results and Discussion

5.2.1. Chromatographic Purification and Spectral Analysis of Secondary Metabolites from *T. ornata*

Repeated chromatographic purifications of the solvent fractions obtained from *T. ornata* led to the isolation of six new secondary bioactive metabolites. The structures were elucidated and confirmed by extensive analysis of the ^1H NMR, ^{13}C NMR, ^1H-^1H COSY, HSQC, HMBC and NOESY and mass spectra along with FTIR analyses.

5.2.1.1. Structural Characterization of Compound 8

The 6, 6-spiroketal, spirornata A (compound 8) was isolated by repetitive chromatographic purification of crude extract of *T. ornata*. Molecular formula of the compound was determined as $C_{22}H_{34}O_6$ {*m/z* 395.2439 $[M+H]^+$}. Detailed NMR analysis was carried out for the structural interpretation of the compound. The ^1H-^{13}C NMR along with ($DEPT^{135}$) spectra deduced the presence of twenty two carbons. The non-protonated carbons were assigned by the absence of ^{13}C NMR signals in DEPT spectrum and chemical shifts at δ_C 179.2 and 175.6 were attributed to the occurrence of electron withdrawing ester group {-C(=O)O-}. The spectroscopic data assigned the presence of olefinic (δ_C 120.6/δ_H 5.20 for =<u>CH</u>-) and deshielded methylene {δ_C 64.2/δ_H 4.17 for <u>CH_2</u>-O-(-C=O)} functionalities. ^1H-^1H COSY correlations were exhibited between δ_H 3.83/2.82; δ_H 4.12/2.32/2.18/1.02; δ_H 2.42/1.67; δ_H 1.52/3.75/1.11. These findings in connection with intense HMBC correlations from δ_H 3.83 to δ_C 101.4; δ_H 2.82 to δ_C 35.2/179.2; δ_H 4.38 to δ_C 179.2; δ_H 2.18 to δ_C 101.4, and δ_H 1.67 to δ_C 43.1 attributed the presence of the 4′,6′,6-trimethyl-3-oxodecahydrospiro [furo-3,4-c] pyran-7,2′-pyran-3-one moiety in spirornata A. ^1H proton integral inferred the presence of three terminal methyl groups in 4′,6′,6-trimethyl-3-oxodecahydrospiro [furo-3,4-c] pyran-7,2′-pyran-3-one moiety, at 4′, 6′ and 6 position. Long range ^1H-^{13}C HMBC correlation between δ_H 1.02 to δ_C 37.7; δ_H 1.11 to δ_C 68.5; δ_H 0.96 to δ_C 27.7 established the occurrence of three terminal methyl groups. The CH_2 proton at δ_H 4.17 exhibited a downfield shift, which could recognize the connection of these protons with oxygen atom. Assignment of 6^a-methylpent-5^a-en-1^a-yl acetate side chain at C-3′ position was made by intense HMBCs between δ_H 2.27 to δ_C 175.6; δ_H 4.17 to δ_C 175.6; δ_H 2.24 to δ_C 120.6; δ_H 5.20 to δ_C 64.2/131.7; δ_H 1.79 to δ_C 131.7; δ_H 1.76 to δ_C 131.7. Another one spin system between δ_H 4.17/2.24/5.20 was observed. COSY correlations along with the strong HMBC validated the presence of 6^a-methylpent-5^a-en-1^a-yl acetate side chain in spirornata A. The attachment of 6^a-methylpent-5^a-en-1^a-yl acetate side chain at C-3′

position was assigned by the intense HMBCs between δ_H 2.42 to δ_C 33.4. The compound exhibited six degrees of hydrogen deficiencies, with two carbonyls, three rings, and one double bond. The NMR experiments including IR and mass spectroscopic data unambiguously elucidated the structure of spiroketal as 6[a]-methylpent-5[a]-en-3[a]-yl-1[a]-(4′,6′,6-trimethyl-3-oxodecahydrospiro [furo-3,4-c] pyran-7, 2′-pyran-3′-yl) acetate.

6[a]-methylpent-5[a]-en-3[a]-yl-1[a]-(4',6',6-trimethyl-3-oxodecahydrospiro [furo-3,4-c] pyran-7, 2'-pyran-3'-yl) acetate

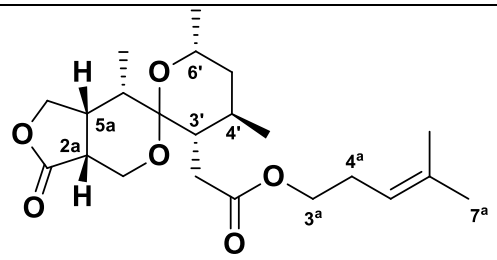

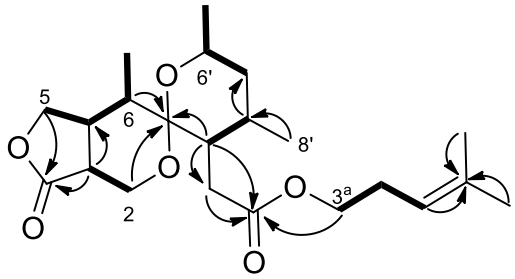

Fig. 5.2.1.1. Key ^{1}H-^{1}H COSY and HMBC correlations of 6[a]-methylpent-5[a]-en-3[a]-yl-1[a]-(4′,6′,6-trimethyl-3-oxodecahydrospiro [furo-3,4-c] pyran-7, 2′-pyran-3′-yl) acetate. The key ^{1}H-^{1}H COSY couplings have been represented by the bold face bonds; the HMBC couplings are indicated as single barbed arrow.

5.2.1. 2. Structural Characterization of Compound 9

Repeated column chromatographic fractionation of *T. ornata* yielded compound **9**, The molecular formula of second spiroketal, spirornata B was determined as $C_{23}H_{32}O_7$ with six degrees of unsaturation {*m/z* 421.2229 $[M+H]^+$}, and the structure was elucidated by detailed NMR analysis. The ^{1}H NMR spectrum exhibited the presence of a methyl singlet (δ_H 1.11 and 1.02) and two olefinic (δ_H 5.37 and 5.28) groups. ^{13}C NMR including DEPT^{135} signals, inferred the presence of C-23 framework with two sp^3 methyls, eight sp^2 methylenes, five sp^3 methines and three non-protonated carbons. Characteristic signals of olefinic functionalities at δ_C 129.5 and 135.1 were observed in ^{13}C NMR. Highly deshielded ^{13}C resonance at δ_C 174.1 and 203.5 were accounted for carbonyl carbonyl [-C=O(O)-] group. Another one deshielding quaternary carbon was observed at δ_C 98.6, which designated its proximity towards an electronegative group. This indicated the linkage of that carbon to an oxygen atom and resulting in downfield resonance. In long range HMBCs, key couplings were observed that validated the connectivity found in ^{1}H-^{1}H COSY. Other HMBC correlations were observed at δ_H 4.05 to δ_C 127.9/98.6; δ_H 2.90 to δ_C 127.9/203.5; δ_H 2.27 to δ_C 125.7; δ_H 5.53 to δ_C 125.7/98.6; δ_H 3.68 to δ_C 98.6, and δ_H 2.37 to δ_C 98.6. Presence of an acetoxy group at C-7 was validated by ^{1}H-^{13}C HMBC correlations between δ_H 2.23 to δ_C 170.9. Attachment of an acetoxy group at C-7 was affirmed by the HMBC correlation δ_H 5.53 to δ_C 170.9. These correlations put forward the presence of a 7-acetoxy-6′-methyl-4-oxodecahydrospiro [isochromene-8,2′-pyran] group in the titled compound **2**. Another two spin systems were perceived at δ_H 4.64/5.37 and δ_H 5.28/2.01/1.02. Intense HMBC correlations were observed at δ_H 2.30 to δ_C 174.1; δ_H 4.64 to δ_C 174.1/129.5; δ_H 5.37 to δ_C 135.1, which along with COSY cross peaks inferred the presence of a pent-4[a]-en-1-yl-acetate side chain. Connection

of pent-4[a]-en-1-yl-acetate side chain with 7-acetoxy-6′-methyl-4-oxodecahydrospiro [isochromene-8,2′-pyran] group was corroborated by intense HMBC correlation at δ_H 2.37 to δ_C 36.7. Based on the detailed spectral experiments the structure of the compound elucidated as pent-4[a]-en-3[a]-yl-1[a]-(7-acetoxy-6′-methyl-4-oxodecahydrospiro [isochromene-8,2′-pyran]-3′-yl) acetate.

pent-4[a]-en-3[a]-yl-1[a]-(7-acetoxy-6'-methyl-4-oxodecahydrospiro [isochromene-8,2'-pyran]-3'-yl) acetate

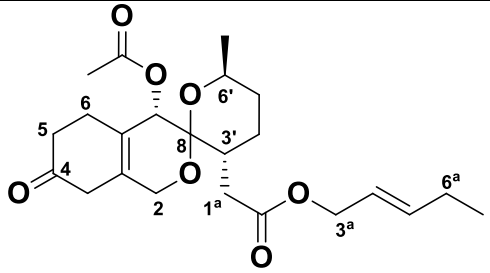

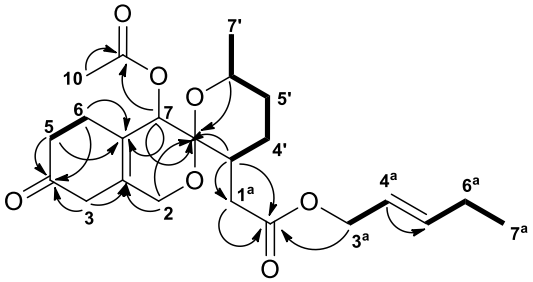

Fig. 5.2.1.2. Key ^{1}H-^{1}H COSY and HMBC correlations of pent-4[a]-en-3[a]-yl-1[a]-(7-acetoxy-6′-methyl-4-oxodecahydrospiro [isochromene-8,2′-pyran]-3′-yl) acetate. The key ^{1}H-^{1}H COSY couplings have been represented by the bold face bonds; the HMBC couplings are indicated as double barbed arrow.

5.2.1.3. Structural Characterization of Compound 10

The third 6, 6-spiroketal, spirornata C (compound 10) was obtained with the molecular formula of $C_{25}H_{36}O_5$ with eight degrees of unsaturation {*m/z* 417.2647 $[M+H]^+$}, and the structure was interpreted by NMR analysis. The ^{1}H NMR spectrum of spirornata C exhibited the occurrence of three methyl singlets (δ_H1.84, 1.74 and 1.81) and two olefinic (δ_H 5.23 and 5.33) groups. ^{13}C NMR along with the DEPT^{135} and HSQC data displayed the presence of C-25 carbon skeleton that were consistent with three sp^3 methyls, eight sp^2 methylenes, together with five sp^3 methines and six non-protonated carbons. Characteristic ^{13}C signals of double bond at δ_C 123.5 and 132.4 were observed in the deshielded region. Highly deshielded ^{13}C resonance at δ_C 170.8 and 202.4 were accounted for carbonyl carbonyl [-C=O(O)-] functionalities. Another one deshielding non-protonated carbon was observed δ_C 97.8 (C-8), which suggested its vicinity towards an electronegative oxygen group. The connectivity within the molecule was established by interpretation of the ^{1}H-^{1}H COSY and HMBC spectrum. Presence of an acetoxy group at C-4′ was confirmed by the ^{1}H-^{13}C HMBC correlations between δ_H 2.21 to δ_C 170.8. These correlations proposed the presence of a 4′-acetoxy-6′-methyl-4-oxodecahydrospiro-[isochromene-8, 2′-pyran] group in spirornata C. Spectroscopic data elucidated the structure of the spiroketal as 6[a]-methylocta-1[a]-(4′-acetoxy-6′-methyl-4-oxodecahydrospiro-[isochromene-8, 2′-pyran]-3′-yl)-1[a], 5[a]-diene.

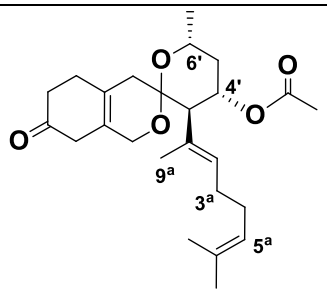

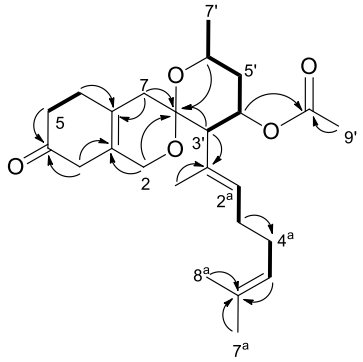

Fig. 5.2.1.3. Key ^{1}H-^{1}H COSY and HMBC correlations of 6ª-methylocta-1ª-(4′-acetoxy-6′-methyl-4-oxodecahydrospiro-[isochromene-8, 2′-pyran]-3′-yl)-1ª, 5ª-diene. The key ^{1}H-^{1}H COSY couplings have been represented by the bold face bonds; the HMBC couplings are indicated as double barbed arrow.

5.2.1.4. Structural Characterization of Compound 11

The furanone analogue attached with cyclooctane ring, turbinafuranone A (compound **11**), characterized as 6, 7-dihydroxy-8-methyl-3-(5'-methyloct-4'-en-1'-yl)-3, 4, 5, 6, 7, 8-hexahydrocyclooct-1-en-[1, 2-c]furan-11-one, was deduced as $C_{20}H_{32}O_4$ with the molecular ion peak at *m/z* 337.2383, and FTIR/NMR experiments. The ^{13}C NMR spectrum along with DEPT of compound **4** recorded the presence of twenty carbon signals with six each of methylene and methine sp^2 carbons, along with four sp^3 and three quaternary and one carbonyl carbon, wherein the quaternary carbons in turbinafuranone A were assigned by their absence in DEPT, which were present in ^{13}C NMR spectrum (δ_C 161.7, 128.4, 135.6). The studied diterpene exhibited five degrees of unsaturation (two each of olefinic bonds and ring systems and one carbonyl group), wherein the olefinic (δ_C 124.6/δ_H 5.19 for =CH-) and chemically deshielded methylene {δ_C 70.2/δ_H 4.78 for CH$_2$-O-(-C=O)} functionalities were attributed. The deshielded ^{13}C NMR signals at δ_C 71.8 and 67.4 ascribed the possibility of the presence of oxymethine carbons, and that at δ_C 175.5 was ascribed to the presence of electronegative ester group. The observed ^{1}H-^{1}H COSY correlations between δ_H 2.26/1.48; δ_H 1.33/1.51/3.28; δ_H 3.42/2.44 along with the intense ^{1}H/^{13}C HMBC correlations from δ_H 2.26 to δ_C 161.7, 128.4; δ_H 1.51 to δ_C 26.4, 71.8; δ_H 3.42 to δ_C 67.4; δ_H 2.44 to δ_C 161.7 inferred the presence of a hexahydro eight membered ring system in turbinafuranone A. Other HMBC correlations between δ_H 2.26 to δ_C 175.5; δ_H 4.78 to δ_C 161.7, 128.4, 175.5 attributed the presence of five membered ring that could be attached with the previous eight membered ring, and corroborated the presence of hexahydrocyclooct-1-en-[1, 2-c]furan-11-one moiety. Presence of hydroxyl group was confirmed by the broad stretching vibration band at 3430 cm^{-1} in IR and deuterium exchange experiment. The connectivity of 5'-methyloct-4'-en side chain with the hexahydrocyclooct-1-en-[1, 2-c]furan-11-one fragment was corroborated by the COSY correlation between δ_H 2.26/1.57 and intense HMBC cross peak at δ_H 2.26 to δ_C 37.5. The attachment of a terminal methyl group in hexahydrocyclooct-1-en-[1, 2-c]furan-11-one fragment at C-8 was inferred with the help of COSY between δ_H 2.44/1.16 and long range HMBC connectivity at δ_H 1.16 to δ_C 33.4.

6, 7-dihydroxy-8-methyl-3-(5'-methyloct-4'-en-1'-yl)-3, 4, 5, 6, 7, 8-hexahydrocyclooct-1-en-[1, 2-c]furan-11-one

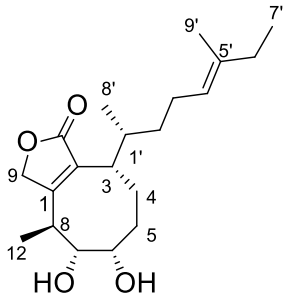

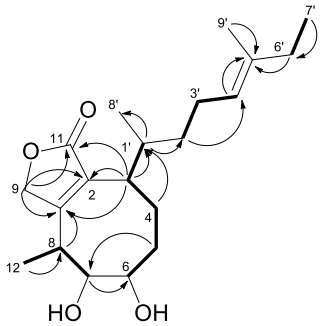

Fig. 5.2.1.4. Key ^{1}H-^{1}H COSY and HMBC correlations 6, 7-dihydroxy-8-methyl-3-(5'-methyloct-4'-en-1'-yl)-3, 4, 5, 6, 7, 8-hexahydrocyclooct-1-en-[1, 2-c]furan-11-one. The key ^{1}H-^{1}H COSY couplings have been represented by the bold face bonds; the HMBC couplings are indicated as double barbed arrow.

5.2.1.5. Structural Characterization of Compound 12

Another cyclooctafuranone derivative, named as turbinafuranone B (compound 12) {4-hydroxy-3-isopropyl-7, 8-dimethyl-6-(pentan-2'-acetate)-3, 4, 5, 6, 7, 8-hexahydrocycloocta-1-en-[1, 2-c]furan-11-one}, with molecular ion peak at *m/z* 381.2648 $[M+H]^{+}$ with combined NMR/FTIR analyses resulted in chemical composition as $C_{22}H_{36}O_5$ with five degrees of hydrogen deficiencies. Combined analysis of ^{13}C NMR/^{135}DEPT spectra attributed the occurrence of 22 carbon atoms. The basic cyclooctafuranone skeleton of turbinafuranone B was analogous with turbinafuranone A, except some major differences in chemical shift value. The increased chemical shift value (+Δ 43.9 of the corresponding carbon in turbinafuranone A) of turbinafuranone B at δ_C 70.3 could be due to the presence of oxygenated group. The ^{13}C and ^{1}H NMR value of C-6 (δ_C 32.5/δ_H 1.46) and C-7 (δ_C 42.2/δ_H 1.62) in turbinafuranone B experienced a lower chemical shift (-Δ 34.9, -Δ 29.6 for ^{13}C and -Δ 1.82, -Δ 1.8 for ^{1}H shift respectively) from turbinafuranone A, which clearly suggested the presence of aliphatic side chain in C-6 and methyl group in C-7. Connection of an isopropyl group at C-3 position was confirmed after COSY at δ_H 2.23/1.75/0.89 and HMBC cross peaks from δ_H 0.89 to δ_C 26.2; δ_H 0.99 to δ_C 26.2; δ_H 1.75 to δ_C 51.1. The connectivity between pentan-2'-acetate side chain at C-6 position with 4-hydroxy-3-isopropyl-7, 8-dimethyl-hexahydrocycloocta-1-en-[1, 2-c]furan-11-one system was inferred by intense HMBC at δ_H 1.46 to δ_C 39.4.

4-hydroxy-3-isopropyl-7, 8-dimethyl-6-(pentan-2'-acetate)-3, 4, 5, 6, 7, 8-hexahydrocycloocta-1-en-[1, 2-c]furan-11-one

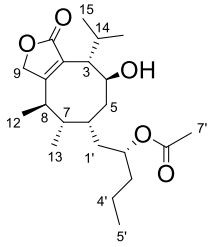

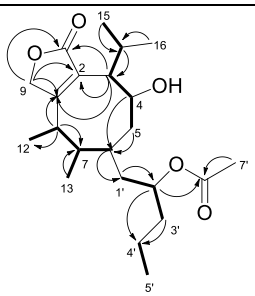

Fig. 5.2.1.5. Key ^{1}H-^{1}H COSY and HMBC correlations of 4-hydroxy-3-isopropyl-7, 8-dimethyl-6-(pentan-2'-acetate)-3, 4, 5, 6, 7, 8-hexahydrocycloocta-1-en-[1, 2-c]furan-11-one. The key ^{1}H-^{1}H COSY couplings have been represented by the bold face bonds; the HMBC couplings are indicated as double barbed arrow.

5.2.1.6. Structural Characterization of Compound 13

The molecular formula of turbinafuranone C (compound 13) was inferred as $C_{22}H_{32}O_5$ from the molecular ion peak at *m/z* 377.2337 $[M+H]^+$, with combined NMR/FTIR experiments. ^{13}C-NMR signals along with ^{135}DEPT experiment confirmed twenty-two carbon signals including five methylene sp^2 carbons, seven methine sp^2 carbons, along with five each of sp^3 and quaternary (with two carbonyl) carbons. The studied compound possessed seven degrees of hydrogen deficiencies including two ring systems, olefinic groups and two carbonyl functionalities. The chemical shift value of δ_H 3.64 (+Δ 2.13 and 2.26 upfield shifts than the corresponding proton in turbinafuranone A) at H-5 and δ_H 4.52 (+Δ 1.24 upfield shift than the corresponding proton in turbinafuranone A) at H-6, with their corresponding carbon shift value δ 69.3 (+Δ 39.0 from turbinafuranone A) and δ 71.3 (+Δ 3.9 from turbinafuranone A) respectively, suggested the presence of oxygenated functionalities at these centers. Another one increased chemical shift value with a difference (from turbinafuranone A) of +Δ 2.11 (for ^{1}H shift) and +Δ 56.5 (for ^{13}C shift) was observed in turbinafuranone C, could be indicated the presence of electronegative olefinic group at H-7/C-7. The deshielded singlet at δ_H 3.34 in the ^{1}H-NMR spectrum was connected at C-5 position with HMBC { δ_H 3.34 to δ_C 69.3} correlation, which established the presence of methoxy protons at C-5 position. The acetoxy group at C-6 position was established by intense HMBC cross peaks between δ_H 4.52 to δ_C 170.6 and δ_H 2.23 to δ_C 170.6.

6-acetoxy-8-ethyl-5-methoxy-3-(2'-methylhex-4'-en-1'-yl)-3, 4, 5, 6, 7-pentahydrocycloocta-1, 7-dien-[1, 2-c]furan-11-one

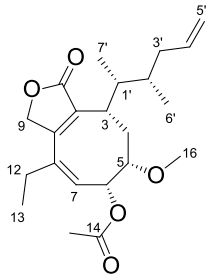

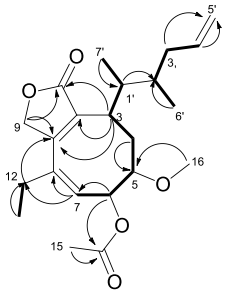

Fig. 5.2.1.6. Key ^{1}H-^{1}H COSY and HMBC correlations of 6-acetoxy-8-ethyl-5-methoxy-3-(2'-methylhex-4'-en-1'-yl)-3, 4, 5, 6, 7-pentahydrocycloocta-1, 7-dien-[1, 2-c]furan-11-one. The key ^{1}H-^{1}H COSY couplings have been represented by the bold face bonds; the HMBC couplings are indicated as double barbed arrow.

5.3. Bioactivities of Secondary Metabolites Isolated from *T. ornata* and SAR analyses

The antioxidant and antihypertensive potentials of the six pure compounds isolated from *T. ornata* were checked by *in vitro* assays and their IC_{50} values were calculated. Spirornata A (compound **8**) showed noticeably greater ACE-I inhibitory property (IC_{50} 4.5 µM) compared to those exhibited by spirornata B (IC_{50}4.7µM) and C (IC_{50} 4.8µM). The electronegative groups in the oxodecahydrospiro [furo-3,4-c] pyran-7, 2′-pyranyl framework along with the esterfied side chain in spirornata A could evidently form hydrogen bonding interfaces with the aminoacyl residues in the active site of ACE-I, and could form co-ordinate bond with binding site Zn^{2+} ion. Conspicuously greater number of electronegative centers in spirornata A might lead to its greater antihypertensive activity. Also, free radical quenching activities (IC_{50DPPH} 1.14 and IC_{50ABTS} 1.28 mM) exhibited by spirornata Awere greater when compared to those exhibited by other analogues (IC_{50} 1.25-1.71 mM) and commercially available standard (IC_{50} 1.46-1.69 mM). The electronic property of spirornata B (tPSA 88.13) was higher than that displayed by spirornata A. However, the steric parameters of spirornatas B and C (P > 900) were higher than that displayed by spirornata A (P 882). Higher steric bulkness of spirornatas B and C could result into their unfavorable condition to react with targeted enzyme leading to their lesser bioactivity than spiroketal A. The *in vitro* anti-hyperglycemic properties of the studied cyclooctafuranone analogous (compounds 11-13) were determined by their attenuation potential against PTP-1B as well as carbolytic enzymes *α*-amylase and *α*-glucosidase. It was recorded that turbinafuranone B exhibited higher inhibiton potential against PTP-1B (IC_{50} 2.42 × 10^{-2} mM) compared to those displayed by other studied compounds (IC_{50} > 2.55 × 10^{-2} mM), which explained the greater selective attenuation property of turbinafuranone B towards PTP-1B enzyme. Likewise, the *α*-amylase and *α*-glucosidase inhibitory potential of the isolated metabolites named after turbinafuranone B were found to be greater (IC_{50} 0.31 and 0.27 mM, respectively) compared to turbinafuranones A and C. Conspicuously, turbinafuranone B exhibited potential quenching properties against the oxidant species (IC_{50} 1.05-1.24 mM), which also reinforced its potential capacity to contain the oxidant species. The target bioactivities of the studied compounds were correlated with various physicochemical parameters. This could properly be explained by greater tPSA value of turbinafuranone B (72.83) than those calculated for turbinafuranone A (66.67) and C (61.83). Notably, the electron-rich centers of turbinafuranone B could be responsible for its inducible polarity and also towards the favorable interaction with enzyme active site leading to attenuate PTP-1B inhibitory activity. The hydrophobicity of turbinafuranone A-C (log P_{OW} 3.12-3.49) were obtained to reside within the thresold permissible limit of hydrophobic-lipophilic balance.

5.4. Conclusions

Bioactivity-assisted chromatographic purification of the organic extract of *T. ornata* yielded three spiroketal-type compounds, compound **8-10**. Structure-activity relationship analysis recognized that higher topological polar surface area along with optimum hydrophobicity of compound **8** favored the interaction with the allosteric site of ACE-I enzyme, and also predominantly contributed towards greater antioxidant activities, which were corroborated by lesser docking parameters. *In silico* predictions of physicochemical parameters along with absorption, distribution, metabolism, and excretion could recognize the acceptable oral bioavailability of compound **8**. The results illustrated that compound **8** could be developed as a promising marine-originated spiroketal-type compound for use against hypertensive diseases.

Organic extract of the intertidal macroalga, *T. ornata* was subjected to repetitive chromatographic fractionation to obtain three unreported cyclooctafuranone analogues, named as compounds **11-13**. Among the isolated analogues, compound **12** exhibited greater attenuation properties against PTP-1B (IC_{50} 2.42 mM) over other studied analogues (IC_{50} >2.55 mM). Structure-bioactivity correlation analysis established that higher topological polar surface area along with optimum hydrophobicity of compound **12** favored the interaction with active sites of PTP-1B enzyme, and also predominantly contributed toward greater radical scavenging activities, which was corroborated by lesser docking parameters (binding energy and docking score -11.80 and -12.78 kcal/mol, respectively). The results illustrated the bioactive potentials of compound **12** as prospective marine-originated cyclooctafuranone, which could be utilized as a prospective anti-hyperglycemic lead.

CHAPTER 6: ISOLATION AND CHARACTERIZATION OF BIOACTIVE SECONDARY METABOLITES FROM *SARGASSUM ILICIFOLIUM*

6.1. Materials and Methods

This section described the instruments used for the present study along with the reagents and solvents.

6.1.1. Sample Preparation

The brown marine macroalga *S. ilicifolium* (15 kg) were collected from Gulf of Manner region (8º48' N, 78º9' E and 9º14' N, 79º14'E) of southern coastal part of India. The sample was repetitively cleaned with tap water several times to remove the residual salt, sand and dirt materials. Cleaned algal sample was kept upon blotting paper to remove excess water and dried, before being crushed into the powdered form (1 kg). Initially extraction was started using *n*-hexane (350 mL × 3), at ambient temperature for 16 h, till the removal of pigmentious materials. Afterwards, the liquid extract was filtered through filter paper and the residue was extracted with MeOH-EtOAc solvent system (1:1 v/v, 400 mL × 4) at about 85° C, and the pooled extracts were filtered over Na_2SO_4 (anhydrous, 100 g). A rotary vacuum evaporator (Heidolf, Germany) was used (operated at 45 °C) for the concentration of the organic extract to obtain a brownish viscous concentrate that was termed as the organic extract of *S. ilicifolium* (28 g, yield on dry basis 2.8 %).

6.1.2. Chromatographic Purification and Spectral Analysis of Pure Compound from *S. ilicifolium*

The organic extract of *S. ilicifolium* (20 g) was mixed with silica gel (60-120 mesh, 3 g) to make slurry, and well packed into a glass column which was previously loaded with silica (60-120 mesh) gel. The separation of the fractions was started by eluting with *n*-hexane (100 %) followed by slowly increasing of polarity by using ethyl acetate (EtOAc) and methanol (MeOH) to obtain four combined factions. The fraction SI_3 possessing greater radical scavenging potential compared to other fraction, was further separated through flash chromatographic system (Biotage AB, Biotage AB SP1-B1A Uppsala, Sweden) on a silica gel column (Biotage, 230-400 mesh, 12 g; Sweden, 25+M). The flash chromatography was performed with a stepwise gradient elution to obtain seven sub-fractions (SI_{3-1} to SI_{3-7}) after TLC analyses. The sub-fraction SI_{3-5}, was found to exhibit higher radical scavenging potential, and therefore, was chosen for downstream purification by preparative thin-layer chromatography (PTLC) using silica gel (GF_{254}) with *n*-hexane/EtOAc (42:8, v/v) to yield the xenicate-type diterpenoid (compound **1**, 83 mg). Analytical TLC (on GF_{254} silica) was used to validate the homogeneity of the isolated compound.

6.1.3. Bioactive Potentials of Secondary Metabolites Isolated from *S. ilicifolium*

The bioactive potentials of one pure compound isolated from *S. ilicifolium* was checked by various *in vitro* antioxidants, anti-inflammatory assays their bioactivities were expressed as IC_{50} values (mM). The structural descriptors, such as electronic (polarizability/PI, topological polar surface area/tPSA), hydrophobic (octanol-water partition coefficient/log P_{ow}), and steric/bulkiness (molar refractivity/MR, molar volume/MV, parachor/P) descriptors using ACD ChemSketch (version 2019.1; Advance Chemistry Development, Inc., Toronto, Canada) and ChemDraw Ultra (Cambridge Soft Corporation, USA; version 12.0) softwares.

6.1.4. Statistical analysis

Statistical Program for Social Sciences 13.0 (SPSS Inc, Chicago, USA, version 13.0) was used to carry out the statistical calculations. Analyses were performed in triplicate and the significant means of all parameters were examined by analysis of variance (ANOVA). The level of significance for all analyses was $P < 0.05$.

6.2. Results and Discussion

6.2.1. Chromatographic Purification and Spectral Analysis of Secondary Metabolite from *S. ilicifolium*

Repeated chromatographic purifications of the solvent fractions obtained from *S. ilicifolium* led to the isolation of six new secondary bioactive metabolites. The structures were elucidated and confirmed by extensive analysis of the ^{1}H NMR, ^{13}C NMR, ^{1}H-^{1}H COSY, HSQC, HMBC and NOESY and mass spectra along with FTIR analyses.

6.2.1.1. Structural Characterization of Compound 14

The xenicane diterpenoid (compound **14**), characterized as 3-(17-hydroxy-14-methylhept-13-en-10-yl)-6-methylhexahydro-1*H*-cyclonona[c]furan-4,19-diyl diacetate was deduced as $C_{24}H_{36}O_6$ with the molecular ion peak at *m/z* 421.2596 $[M+H]^+$, and FTIR/NMR experiments. The ^{13}C NMR spectrum along with DEPT of the titled compound recorded the presence of five each of quaternary and methyl along with six methylene and eight methine carbons. The studied diterpene exhibited seven degrees of unsaturation (three olefinic bonds, two ring systems and two carbonyl groups), wherein the deshielded ^{13}C NMR chemical shifts at δ_C 169.3 and 170.8 supported the occurrence of ester group {-C(=O)O-}. The spectroscopic data attributed the presence of olefinic (δ_C 122.7-134.1) and deshielded methylene {δ_C 66.8-69.6 for $\underline{CH_2}$-O-(-C=O)} functionalities. Disappearance of ^{13}C NMR chemical shifts at the regions of δ_C 148.5, 134.1, 131.9, 170.8 and 169.3 in ^{135}DEPT spectrum ascribed the presence of five quaternary carbons. Highly deshielded chemical shift value at δ_H 3.71 to 4.32 region obtained from ^{1}H NMR spectrum suggested that the possibility of proton attached with an electronegative group (assigned with oxygen). The ^{1}H-^{1}H COSY cross peaks among δ_H 2.94/3.71, 1.84/4.18/2.28; 5.33/2.36, 2.71/5.88 in combination with ^{1}H-^{13}C HMBC correlations at attributed the occurrence of a furan attached nine-membered ring system. Another ^{1}H-^{1}H COSY spin system was exhibited by δ_H 4.32/2.03/1.20, 1.32/1.97/5.14. The HMBCs corresponding to δ_H 2.03 to δ_C 36.2; δ_H 1.32 to δ_C 26.5; δ_H 1.97 to δ_C 122.7; δ_H 5.14/1.52/1.62 with δ_C 131.9 in connection with previous COSY cross-peaks suggested the occurrence of 17-hydroxy-14-methylhept-13-en-10-yl fragment. The connectivity of 17-hydroxy-14-methylhept-13-en-10-yl side chain with furan-attached nine-membered ring system at C-3 was established by an intense HMBC correlation at δ_H 1.84 to δ_C 31.6. FT-IR spectrum of xenicane type diterpenoid exhibited peaks at 3428, 2858, 1742 and 1638 cm^{-1}, which established the stretching vibrations due to O-H, C–H, ester {-C(=O)–O-} and >C = C<, respectively. Based on the detailed spectroscopic characterization, the purified compound from *S. ilicifolium* was named as {3-(17-hydroxy-14-methylhept-13-en-10-yl)-6-methylhexahydro-1*H*-cyclonona[c]furan-4,19-diyl diacetate}.

3-(17-hydroxy-14-methylhept-13-en-10-yl)-6-methylhexahydro-1H-cyclonona[c]furan-4,19-diyl diacetate

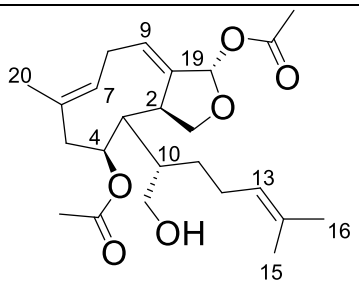

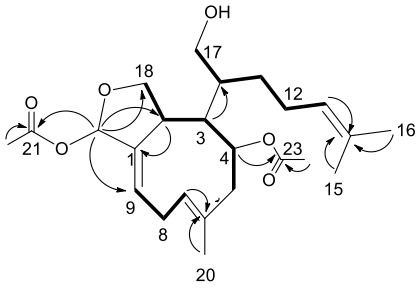

Fig. 6.2.1.1. Key ^{1}H-^{1}H COSY and HMBC correlations of 3-(17-hydroxy-14-methylhept-13-en-10-yl)-6-methylhexahydro-1*H*-cyclonona[c]furan-4,19-diyl diacetate. The key ^{1}H-^{1}H COSY couplings have been represented by the bold face bonds; the HMBC couplings are indicated as single barbed arrow.

6.3. Bioactivities of Secondary Metabolites Isolated from *S. ilicifolium* and SAR analyses

The studied xenicane diterpenoid derivative isolated from *S. ilicifolium* exhibited potential anti-inflammatory and antioxidant activities. The titled diterpenoid demonstrated significant duel inhibition potential against pro-inflammatory enzymes, cyclooxygense-2 (IC_{50} 2.47 mM) and 5-lipoxygenase (IC_{50} 4.70 mM). The compound exhibited significantly greater anti-inflammatory selectivity index which accounted for the greater selectivity of the isolated xenicane diterpenoid towards COX-2. The xenicane analogue exhibited greater antioxidant properties against 2,2'-azino-bis(3-ethylbenzothiazoline-6-sulphonic acid) (IC_{50} 1.38 mM) and 2,2-diphenyl-1-picrylhydrazyl (IC_{50} 1.26 mM) than the antioxidative agent α-tocopherol (IC_{50} 1.4-1.7 mM).

Potential bioactivities of diterpenoid derivative, isolated from brown alga *S. ilicifolium* was analyzed with various structural parameters. Polarity of the studied xenicane diterpenoid was induced by electron-rich centers resulting in its higher topological polar surface area (tPSA 82.06) compared with standards (tPSA < 40). Notably, the electronic parameters could be responsible towards the greater interaction with active sites of enzyme 5-LOX. Similarly its prospective antioxidant properties (IC_{50} < 1.40 mM) could properly be justified by its significantly greater electronic properties in comparison with standard agents.

6.4. Conclusions

Bioassay-directed purification of the organic extract of brown seaweed *S. ilicifolium* resulted in the isolation of a xenicane-type diterpene derivative, characterised as 3-(17-hydroxy-14-methylhept-13-en-10-yl)-6-methylhexahydro-1*H*-cyclonona[c]furan-4,19-diyl diacetate. The studied compound displayed attenuation properties against 5-LOX. Additionally, the higher anti-inflammatory selectivity index of xenicane derivative (> 1) showed the selective attenuation potential against pro-inflammatory COX-2. The studied compound has a greater electronic property coupled with ideal hydrophobicity, and lesser docking parameters (binding energy -9.61 kcal mol^{-1} docking score -11.17 kcal mol^{-1}) with the interactive site of 5-LOX enzyme obtained from the molecular docking studies corroborated the potential anti-inflammatory properties of the xenicane diterpenoid.

CHAPTER 7: ISOLATION AND CHARACTERIZATION OF BIOACTIVE POLYSACCHARIDES FROM *SARGASSUM TENERRIMUM, TURNINATIA CONOIDES AND TURBINARIA ORNATA*

7.1. Isolation and Characterization of Bioactive Polysaccharide from *Sargassum tenerrimum*

7.1.1. Materials and Methods

This section described the instruments used for the present study along with the reagents and solvents.

7.1.2. Preparation of Polysaccharide

Dried and powdered leaves of brown macroalga *S. tenerrimum* (200 g) were pre-treated with acetone (500 mL, 4 h) at about 35 °C followed by 30% formaldehyde solution (600 mL, 14 h) and filtered to obtain pigmentious and phenolic substances respectively. Pigmentous and phenolic materials were removed by filtration followed by concentration at 45°C with the help of a rotary vacuum concentrator (Heidolph, Instruments GmbH & Co., Schwabach, Germany). The residual dried powder was extracted twice with doubly-distilled water (3000 mL) at about 90 °C for a period of 6 h, and was filtered to result in an aqueous extract. The obtained supernatant (1200 mL) was then concentrated to one-eighth of the initial volume (150 mL) by a rotational vacuum evaporator (Martin Christ RVC 2-33 IR, Martin Christ, Germany). The concentrated aqueous extract was treated with trichloroacetic acid (TCA 5%, m/v) and clarified by centrifugation (at 15 min, 6000 rpm, 35°C, Sorvall® Biofuge Stratos, Thermo Scientific, USA) to separate the protein materials. The resultant supernatant was precipitated with ice cold ethanol (1:2, v/v) by keeping at -4 °C (12 h) and carried out centrifugation. The supernatant was subjected for freeze drying with laboratory lyophilizer (Martin Christ alpha 1-4 LD plus, Martin Christ, Germany) to obtain crude polysaccharide 10.08 g (STP, yield based on powdered algal material, 5.04%).

7.1.3. Chromatographic Purification and Chemical Characterization of polysaccharide from *S. tenerrimum*

Crude polysaccharide (~ 2 g) extracted from *S. tenerrimum* was chromatographically fractionated over an anion exchanger {diethylaminoethyl-cellulose, 8 g equilibrated in tris buffer (50 mL, 50 mM, pH 7.4)} to afford the fractions STP-1 through STP-5 (eluted with an increasing gradient of NaCl, 0.05 to 0.25 M) that were assayed for positive chemical reaction of polysaccharide and monosaccharide composition. The eluted column fractions were lyophilized (~65 mg) and were hydrolyzed by a strong acid (trifluoroacetic acid, 1M) before being analyzed for the presence of monosaccharides by an amino column (25 cm × 0.46 cm, 5 μ) connected with an HPLC system coupled with an evaporative light-scattering detector (SofTA model-300^S, Teledyne Tech. Inc., Lincoln, NE). The fraction STP-2 was characterized by extensive spectroscopic analysis built on total content of carbohydrate (> 55%) and monosaccharide composition. Molecular weight of the hydrolyzed polysaccharide was deduced by mass spectral experiment (negative-ion electrospray ionization, ESI$^-$/MS). Dinitrosalicylic acid assay was used to quantify total carbohydrate, whereas contents of sulfate, uronic acid, and protein were assessed using previously described methods. Structural interpretation of the purified polysaccharide was performed by spectroscopic analysis.

7.2. Results and discussion

7.2.1. Extraction, purification, yield and bioactivities of polysaccharide from *S. tenerrimum*

The crude polysaccharide was chromatographically separated into various fractions by anion exchange chromatography (using DEAE cellulose 52) eluted with linear and step-wise gradient of NaCl concentration (0.05 to 0.25 M) and are designated as STP-1, STP-2, STP-3, STP-4 and STP-5, respectively. The percent yield of purified polysaccharide fractions eluted was found to be 2.0 %, 22.3 %, 19.8 %, 16.2 % and 16.1 %, respectively. The crude polysaccharide STP contained of 67.0 % of total carbohydrate and 13.0 % sulfate, while the uronic acid and protein

contents were found to be 5.2 % and 3.1 %, respectively. Among the purified polysaccharide fractions, the major polysaccharide fraction (STP-2) corresponds to 0.1 M NaCl accounted for 58.8 % carbohydrate content and lesser protein content (< 1 %). STP-2 displayed relatively higher sulfate contents than those exhibited by other fractions. Hence the column fraction named STP-2 was freeze-dried and further subjected to monosaccharide composition analysis after depolymerized with trifluoroacetic acid. STP-2 recorded greater yield of carbohydrate (~59%) with lesser protein (< 1%) than other sub-fractions. Radical scavenging (IC_{50} 2.09 mM) and ALP activities (45.3 μM/mL/sec) of STP-2 were found to be superior to those displayed by the remaining fractions, and consequently, STP-2 was put through structural characterization and further biochemical experiments.

7.2.2. Chemical composition analysis of polysaccharide from *S. tenerrimum*

The content of carbohydrate for STP-2 was relatively higher than that of other sub-fractions. The column sub-fraction designated as STP-2 recorded greater percentage of carbohydrate (58.8 %) and a considerable amount of sulfate (13.1 %) with a trace amount of protein (< 1 %). The monosaccharide composition analysis revealed the presence of two major monosaccharide units fucose and galactose. The structural identity of the polysaccharide was deduced to be *α*-(1→3) linked fucopyranose with sulfation at C-2 position and *β*-(1→4) linked galactopyranose with OAc substitution at C-6 position.

7.2.3. Spectroscopic evaluation of polysaccharide from *S. tenerrimum*

Polysaccharide fraction STP-2 was comprised of recurring structural entities of 2-*O*-SO_3-*α*-(1→3)-fucopyranose (unit A) and 6-*O*-acetyl-*β*-(1→4)-galactopyranose (unit B) by comprehensive spectroscopic studies comprising NMR (1D and 2D), FT-IR, and HR(ESI)MS. ^{1}H-NMR of the studied compound exhibited discrete signals at δ_H 4.65-5.71, and was recognized as a wrapper of anomeric protons that were apportioned to pyranose H-1 of unit A and B. The ^{1}H-NMR signals across δ_H 3.58-4.47 were ascribed to the protons at C-2 to C-6 of the pyranoid ring, and the sharp singlet at about δ_H 2.20 was due to the methyl (-OCOC$\underline{H}_3$) proton at C-6 position of *β*-(1→4)-galactopyranose. A distinct doublet at δ_H 1.18 was assigned to the C-6 methyl protons of (1→3)-linked *α*-fucopyranose. Anomeric proton of (1→3)-connected *α*-fucopyranosyl (unit A) exhibited a doublet by reason of coupling with H-2. The *J* value of anomeric proton at δ_H 5.71 was 3.68 Hz characterizing an *α*-fucopyranosyl residue. Coupling constant between axial/axial protons was 7-8 Hz, whereas equatorial/equatorial or axial/equatorial protons exhibited coupling constant of 3-4 Hz. ^{13}C-NMR spectrum displayed the anomeric residues at δ_C 99-106. Characteristic ^{13}C-NMR signals at δ_C 61-79 were characteristic of C-2 to C-6 pyranoid ring carbons. The signal at δ_C 106.4 was assigned to the anomeric carbon of *β*-connected galactopyaranoside. Distinct peaks at δ_C 16-18 were attributed to C-6 methyl. ^{13}C-NMR traces between δ_C 65-80 were accredited to pyranoid C-2 to C-5. A distinct peak at δ_C 106.4 was attributed to C-1 of *β*-galactopyranose. The quaternary carbon at δ_C 178.5 ppm was identified as carbonyl ester group at C-6 substitution of *β*-galactopyranose unit, and was absent in the DEPT spectrum. ^{1}H-^{1}H COSY spectrum of the sulfated galacto-fucopyranose showed H1/H2 connections between δ_H 5.71/4.39, δ 5.33/3.99 and 4.65/3.68. HR(ESI)MS spectrum of sulfated galacto-fucopyranose (resulting after hydrolysis) recorded a molecular ion peak at 671.0799 $[M-H]^-$, which was apportioned to single-charged anion of trisaccharide units comprising of glycosidic remains of 2-*O*-SO_3-*α*-(1→3)-Fuc*p* and 6-*O*-acetyl-*β*-(1→4)-Gal*p*. Detailed structural investigation elucidated the structural motif of the sulfated galacto-fucopyranose [→1)-2-*O*-sulfonato-*α*-Fuc*p*-(3→1)-2-*O*-sulfonato-*α*-Fuc*p*-(3→] units as central branch with [(4→1)-6-*O*-acetyl-*β*-Gal*p*-(4→] unit as lateral segment in that (1→3)-connected *α*-fucopyranose organized the C-2 sulfated central polymeric chain with C-4 *O*-acetyl/C-6 (1→4)-linked *β*-galctopyranose.

7.2.4. Effect on cell viability on human mesenchymal stem cells (hMSC, osteoblast cell line)

Cell viability assessment of human hMSC cell line following treatment with ST-Ag^{NP} (at 1000 μg/mL) displayed 79% viability of the macrophages after 24 h, and 77% after three days of incubation (Table 7.5). The hMSC cell treated with the nanoparticle conjugate at 250 μg/mL exhibited 85% viability after 72 h, whereas that administered with standard displayed 88% cell viability. It was obvious that hMSCs treated with ST-Ag^{NP} even at higher concentration showed no cytotoxicity. Greater than 70% cell viability of osteoblast hMSC cell lines at all concentrations of ST-Ag^{NP} exhibited in different incubation time period (24-72 h), which recognized ST-Ag^{NP} as non-cytotoxic.

7.2.5. ALP activity and mineralization study of STP-2 and ST-Ag^{NP}

ALP activity of ST-Ag^{NP} (250 μg/mL) treated hMSCs was considerably increased (63.3 mU/mg) after 21 days in comparison with polysaccharide alone (30.4 mU/mg). Similarly, after 21 days, mineralized nodule formation in STP-2 treated (250 μg/mL) cells were significantly lesser than those in the ST-Ag^{NP} treated cells, which supported lesser osteogenic potential of STP-2. ALP activity was considerably increased (63.3 mU/mg) in hMSCs after 21 days following treatment with ST-Ag^{NP} (250 μg/mL) as also exhibited by sodium alendronate (standard, 72.8 mU/mg) resulting in osteoblastic differentiation of the cell, whereas in control, the ALP expression was significantly lesser (30.4 mU/mg, $p < 0.05$). Likewise, formation of calcium mineralized nodule was apparent on osteoblastic hMSCs treated with ST-Ag^{NP}, and was considerably higher than that displayed by the untreated control.

7.2.6. Osteocalcin and BMP-2 expression

Flow cytometric (FCM) analysis displayed a uniform distribution of cell size (forward scatter) and reasonably regular cell granularity (side scatter). Expression of osteocalcin positive cell population (49.6% of aggregate cell counts) and average fluorescence intensity of osteocalcin expression was considerably increased in hMSCs following treatment with ST-Ag^{NP} (250 μg/mL), whereas in control, the fluorescence intensity (14.11) was significantly lesser. Fluorescence-activated cell sorting (FACS) study of hMSCs following treatment with ST-Ag^{NP} (at 250 μg/mL) showed an increase in cell population of BMP-2 positive hMSCs (up to 23.02% of total counts). Expression of BMP-2 positive cell population and average fluorescence intensity of BMP-2 expression was considerably increased (25.88) in hMSCs following treatment with ST-Ag^{NP} (250 μg/mL), whereas in control, the fluorescence intensity (10.12) was significantly lesser.

7.2.7. Effect of ST-Ag^{NP} on body weight and food consumption

Dexamethasone-induced (glucocorticoid-induced) rats displayed substantial reduction in body weight than that exhibited by normal control ($p < 0.001$). However, there were no significant reduction and gain of body weight as well as average weekly food consumption and water intake in ST-Ag^{NP} treatment groups during the study period (Tables 7.6, 7.7). No considerable alterations in water and food consumption pattern as well as body weight, over two weeks on acute toxicity study, were apparent (Table 7.8).

7.2.8. Effect on hematological parameters

A marginal reduction in hematological parameters in osteoporotic control group was apparent compared to the normal control animals, whereas statistically significant increase was noted in total leukocyte (WBC) ($p < 0.01$) and platelet count ($p < 0.05$) in ST-Ag^{NP} and sodium alendronate-treated animals at higher dose (1 g/mg BW) (Table 7.9).

Osteoporosis-induced rats treated with ST-Ag^{NP} did not effect in any noteworthy difference in glucose plasma random (GPR, 84 mg/dL), γ-glutamyl transferase (<10 U/L) and other parameters when compared to those treated with standards and normal control rats (Table 7.10).

7.2.9. Biochemical parameters in plasma

Glucocorticoid produced an elevated levels of serum ALP, TC and HDL (648 U/L, 57 and 43 mg/dL, respectively), when compared to the normal control group (338 U/L, 39, 26 mg/dL, respectively) (Table 7.9). Treatment with ST-Ag^{NP} (1 g/kg BW) resulted significant reduction in ALP (386 u/L), HDL (28 mg/dL) and TC levels (44 mg/dL) of glucocorticoid treated animals. Triglyceride (TG) is the most abundant lipid in the human body, the level of TG was lowered in glucocorticoid-induced osteoporosis group (49.7 mg/dL) than in the normal group (61.1 mg/ dL) (Table 7.9). Conspicuously, ST-Ag^{NP} treated group (1 g/kg BW) resulted in up- regulation of serum TG level (59.7 mg/dL), which was comparable with sodium alendronate treated group (58.26 mg/dL) (Table 7.9). Glucocorticoid treatment caused significant decrease in calcium level (6.98 mg/dL) when compared to the normal control group (9.51 mg/dL) and those treated with sodium alendronate (8.54 mg/dL, 3 mg/kg BW) and ST-Ag^{NP} at higher dose (8.14 mg/dL, 1 g/kg BW) (Table 7.9). Serum creatinine and urea levels in osteoporosis-induced group were higher (0.44 and 54.43 mg/dL, respectively) than normal control group (0.38 and 43.23 mg/dL, respectively), and those treated with ST-Ag^{NP} could normalize the serum creatinine and urea levels (0.37 and 47.73 mg/dL, respectively) (Table 7.9). Serum sodium, potassium and chloride levels were lower in the glucocorticoid treated groups when compared to the normal control, although the difference was statistically insignificant (Table 7.11). No significant changes of intracellular hepatocyte enzymes, such as GPT/ALT, GOT/AST of glucocorticoid-treated groups when compared to the normal control was apparent (Tables 7.10-7.11), which inferred no hepatotoxicity following administration of ST-Ag^{NP}. Estradiol (E2) levels were diminished in the glucocorticoid-administered osteoporosis-induced groups (46.5 pg/mL) compared with normal control group (77.5 pg/mL) (Table 7.9). Improvement in the level of E2 was recorded in the disease-induced animals treated with ST-Ag^{NP} (76 pg/mL at 1 g/kg BW) and sodium alendronate (75 pg/mL) (Table 7.9). Notably, a significant elevation in serum PTH (parathyroid hormone) level was observed in glucocorticoid-treated groups (13 pg/mL) (Table 7.9), and those administered with ST-Ag^{NP} significantly suppressed serum PTH levels (7.4 pg/mL) as with standard (7.5 pg/mL).

7.2.10. Antioxidant indices of left femur homogenate

Osteoporosis-induced animals displayed reduced activities of antioxidant indices, such as catalase (0.37 U/mg protein), glutathione (GSH, 4.2 mg/gT), glutathione S-transferase (GST, 1220.3 U/gT) and glutathione peroxidase (GPx 71.2 U/gT) in the left femur homogenate compared to normal (Table 7.9). Treatment with ST-Ag^{NP} (1 g/kg BW) resulted in significant improvement in the catalase activities (0.9 U/mg protein) along with GSH (7.1 mg/gT), GST (1805.3 U/gT), and GPx concentrations (143.1 U/gT) ($p < 0.001$), which were comparable with standard sodium alendronate (Table 7.9). Osteoporosis-induced groups developed significant lipid peroxidation, as proved by a discernible increase in MDA (38.6 nmol/gT). ST-Ag^{NP} (1 g/kg BW) resulted a significant decrease in MDA (20 nmol/gT) in the left femur homogenate (Table 7.9).

7.2.11. Histopathological evaluation

Histopathology of the right femur sections in control group displayed surface hyaline articular cartilage, overlying lamellar bone forming cortex and trabecular bone. The trabecular bone of osteoporotic control exhibited anisotropy, thinning, micro-fracture and trabecular disconnection. Disconnected trabeculae of distal metaphysis and

wide bone marrow spaces in between the trabeculae were filled with fat cells, whereas interspersed marrow was predominantly composed with mature adipocytes along with foci of hemorrhagic suffusion. However, disease-induced groups treated with ST-Ag^{NP} and sodium alendronate showed disappearance of osteoporotic cavities and nearly normal content and distribution of collagen fibers in the trabecular bone. Furthermore, rat femur showed mild increase of thickness of cortical and trabecular bone following the treatment with mid dose of ST-Ag^{NP}. However, higher dose of ST-Ag^{NP} preserved cortical bone thickness and absence of erosion cavities, normal architecture of bone trabeculae, and trabecular bone thickness were maintained. On detailed histopathological examination of tissues, no pathologically significant lesions were observed in normal control and treatment groups. Histopathology of the liver in control animals and disease-induced groups treated with ST-Ag^{NP} exhibited normal hepatic cells with conserved nucleus, central vein, sinusoids, and portal tracts. The sections showed liver parenchyma composed of congested central veins with hepatocytes radiating outwards from the central veins to the portal tract. The histology of the renal tissues in normal control animals and osteoporosis-induced groups treated with ST-Ag^{NP} showed normal renal parenchyma composed of mature glomeruli and surrounding tubules. The cells of the tubules showed normal morphology of cells. Interstitium of kidney was not expanded, and vessels showed normal morphology. The histology of the brain section of normal control rats and osteoporotic groups treated with ST-Ag^{NP} showed normal brain parenchyma with cortical neurons and subcortical white matter. The ventricles appeared normal in contour. Histopathology of the spleen sections of normal control rats and osteoporotic groups treated with ST-Ag^{NP} showed capsule enclosing splenic parenchyma with hyperplastic lymphoid follicles in white pulp and red pulp with extramedullary hematopoiesis. None of the animals in normal control and treatment groups showed any histological changes during evaluation. These findings could suggest that, treatment with ST-Ag^{NP} did not induce any overt adverse effects on the treated animals, significantly improved the indices of increased bone formation and decreased bone destruction, greater antioxidant effect, and improvement of oxidative stress conditions.

7.2.12. Discussion

Glucocorticoids are considered as essential hormones for the treatment of various metabolic disorders, but their excessive presence could bring about severe side effects, especially bone fissures. Previous reports demonstrated that long-term glucocorticoid therapy (~ 2 months) could interfere with the body's handling of calcium and levels of sex hormones resulting in bone loss and osteoporosis (Briot et al., 2015). Owing to the potential pharmacological properties of marine macroalgae belonging to the genus Sargassum (Maneesh et al., 2017a, 2018; Chakraborty et al., 2020; Surabhi et al., 2021), it might be an important marine flora to develop novel bioactive polysaccharides with anti-osteoporotic properties. Structural modification of polysaccharide by synthesizing nanoparticles could increase their pharmaceutical uses and easy target-based drug delivery with lesser toxicity and reproducibility (Swierczewska et al., 2016). The present study isolated a sulfated galacto-fucopyranose characterized as [→1)-2-*O*-sulfonato-*α*-Fuc*p*-(3→1)-2-*O*-sulfonato-*α*-Fuc*p*-(3→] units as central branch with [(4→1)-6-*O*-acetyl-*β*-Gal*p*-(4→] entity as side chain (abbreviated as STP-2) isolated from *S. tenneremum*, and synthesis of polysaccharide-structured nanoparticle (ST-Ag^{NP}). Functional properties (anti-osteoporotic) of ST-Ag^{NP} were evaluated by *in-vitro* followed by *in vivo* experimental animal model. Structural characterization of hydrolyzed polymeric unit isolated from *S. tenerrimum* was accomplished by detailed NMR (1D and 2D), FT-IR, HR(ESI)MS and UV spectroscopic techniques.

The ^{1}H NMR signals between δ_H 5.1-5.7 recognized *α*-anomeric protons, whereas those at δ_H 4.5-4.9 were ascribed to *β*-anomeric protons. Presence of chemical shift values at δ_H 5.71 and 5.33 assigned the presence of (1→3)-connected *α*-L-fucopyranosyl in the polysaccharide, whereas that at δ_H 4.65 was accredited to *β*-galactopyranosyl (Ale

et al., 2011), which was reported to be common structural unit of polysaccharides from brown macroalgae (Nishino et al., 1994). Signals between δ_H 3.58 and 4.47 were due to C-2 to C-5 pyranoid protons. Another signal at δ_H 2.2 was accredited to the methyl (-CH_3) protons of *O*-acetyl group of *β*-galactopyranose unit (unit C). A distinct doublet at δ_H 1.18 was assigned to the C-6 methyl protons of (1→3)-linked *α*-fucopyranosyl (unit A) (Synytsya et al., 2010). Major IR absorption band at 839 cm^{-1} reinforced the presence of C-2 sulfate group with equatorial positioning (Bilan et al., 2002). Anomeric carbon of sulfated galacto-fucopyranose were found between δ_C 99-106, and it was observed that chemical shift of *α*-anomeric carbon had been lesser than that of the *β*-anomeric carbon (Maneesh et al., 2018; Ponce et al., 2003). NOE correlation was observed between δ_H 4.39 (H-2A)/3.99 (H-2B), which authenticated the typical spatial correlation (axially oriented) between (1→3)-linked fucose motif (Bilan et al., 2007). Other axial correlations were exhibited by strong NOE correlations between δ_H 4.39 (H-2A)/4.06 (H-4A), 3.99 (H-2B)/3.79 (H- 4B), and 4.65 (H-1C)/3.93 (H-5C).

$AgNO_3$ was treated with various concentrations of polysaccharide solutions (0.1 through 0.3%) for nanoparticle formation, and the solution of 0.3% with greater yield was designated for advanced characterization of ST-Ag^{NP} of sulfated galacto-fucopyranose. It was observed that with an increase in the concentration of the native polysaccharide (STP-2), the absorbance in UV was increased with a shift of absorption maximum towards the lower wavelength region. The blue shift (decrease in wavelength) of λ_{max} could appropriately recognize the decrease in particle size (Zargar et al., 2014). According to previous report of literature, nanoparticles with different size ranges would demonstrate variable optical properties attributable to the difference in SPR bands (Heath et al., 1989). Mean particle size of ST-Ag^{NP} (0.3% polysaccharide solution) as determined by DLS after 2 h of ultrasonication was 27 nm, whereas PDI was recorded as 0.340. PDI was aimed to evaluate the particle size distribution on surface, which also acknowledged the degree of uniformity in size of nanoparticles. The PDI of 0.01-0.70 was considered as monodispersed system, and a value lesser than 0.50 comprehended the homogeneous dispersion of nanoparticles, whereas PDI of larger than 0.70 indicated aggregation (Danaei et al., 2018). Zeta potential is contemplated as an essential tool to measure the stability of ST-Ag^{NP} by ascertaining the electrostatic repulsion between nanoparticles of the resulting dispersion system and surface charge. Conspicuously, zeta potential of nanoparticle dispersion system possessing more negative value than (-) 30 mV or more positive than (+) 30 mV might be deemed stable (Gericke et al., 2020). Zeta potential of ST-Ag^{NP} was determined to be -35.4, and that possibly would be guided by the increased surface charge caused by the presence of charged sulfate group.

The polysaccharide (STP-2) and polysaccharide-based nanoparticle (ST-Ag^{NP}) have distinctive physico-chemical characteristics as a result of their variable size and shape. Morphological attributions of STP-2 and ST-Ag^{NP} were analyzed using SEM. STP-2 consisted of thread-molded fibrous polymeric elements. SEM micrograph represented that STP-2 had a structure arranged in disorganized manner, although separately formed particles in nano-range were observed in case of ST-Ag^{NP} on an even surface (Elsupikhe et al., 2015). The spherical-shaped uniform nanoparticles of ST-Ag^{NP} with no aggregation were established by TEM.

Four intense X-ray diffraction peaks at 38.06, 44.32, 64.58 and 77.30 were perceived in 2θ 10-80°, which could index the angle values of (111), (200), (220), and (311) conforming to face-centered cubic (fcc) silver pattern of ST-Ag^{NP} (Rao et al., 2020). Furthermore, the manifestation of elemental silver was observed by EDX analysis, wherein an intense signal of metallic silver was observed by an optical absorption peak at approximately 3 KeV (Rao et al., 2020). Other than that, the remaining peaks of O, C and S, which might be originated from the STP-2, could cap ST-Ag^{NP} and also imparted stability. Notably, the sulfate FTIR peak at 839 cm^{-1} was found to be suppressed in ST-Ag^{NPs}.

The sulfate group might play an important role in stabilization of ST-Ag^{NP} with surface atom interaction (He et al., 2003).

Noticeably, reduced size of nanoparticle could result in greater dispersion of particles with lesser degree of agglomeration. ST-Ag^{NP} prepared with 0.3% of polysaccharide was found to exhibit greater bioactive potentials (*in vitro* ALP and antioxidant activities) than those displayed by the native polysaccharide alone, and other studied nanoparticle fractions (Table 7.4). Based on this outcome, ST-Ag^{NP} (with 0.3% polysaccharide) was selected for ALP and mineralization studies on the hMSC cells, and the results were compared with those obtained with the native polysaccharide (STP-2). Following 21 days of experiment, it was observed that osteoblast differentiation potential (ALP activity) and mineralized nodule formation (alizarin red S study) ability of STP-2 were considerably reduced than that exhibited by ST-Ag^{NP}. Therefore, we have selected ST-Ag^{NP} over STP-2 for further detailed experiments on account of its smaller particle size and greater osteogenic potential.

To appraise the effect of ST-Ag^{NP} on cytotoxicity and cell viability, MTT assay was carried out with hMSC cells (Table 7.5). Sodium alendronate and ST-Ag^{NP} treated hMSCs (at 150 μg/mL) resulted in ~90% of viability of the cells even after three days of incubation. Viability of hMSCs was decreased to 77% after three days following treatment with higher concentration (1000 μg/mL) of ST-Ag^{NP}, and the result was comparable to that displayed by the standard alendronate (Table 7.5). Greater than 75% survival of hMSCs clearly directed to the cyto-compatibility of the nanoparticle ST-Ag^{NP}, as advocated by ISO 7405:2008. It was found that ST-Ag^{NP} with concentration as high as 1000 μg/mL exhibited no significant cellular and morphological alterations as well as cytotoxicity in the macrophage cells even after three days of incubation period.

Quantification of osteoblast differentiation of hMSCs was depicted by expression of ALP. The bones of mammalian origin are able to produce isoenzyme ALP-2, wherein development of bones could be directly proportional with the increasing levels of this enzyme (Prajatelistia et al., 2021). ALP activity of hMSC cells exhibited significant improvement after three weeks of osteoblast differentiation ($p < 0.05$) compared with the untreated control.

Alizarin red marker was used to identify the formation of calcium containing osteocyte in differentiated culture of hMSCs by the development of red-colored alizarin red-calcium complex. Intense deposition of calcium on hMSCs treated with ST-Ag^{NP} could attribute that the polysaccharide-nanoparticle construct played a supportive function for osteogenic differentiation. Thus, it could be theorized that the comparable trend of primary cell adhesion was followed by hMSCs treated with ST-Ag^{NP} following the formation of calcium nodule, and helped to conserve their essential cell adhesion events (Liu et al., 2013). An increase in intracellular lipidic globules was found in hMSCs treated with ST-Ag^{NP} as evidenced by oil red O staining. Thus, ST-Ag^{NP} could act as a prospective bone mineralization surface thereby improving cell osteogenesis.

The bone γ-carboxyglutamate (bgalp) gene has been recognized to biosynthesize bone γ-carboxyglutamic acid-enclosing protein (BGALP), which is also a well-known osteocalcin precursor. Osteocalcin, which comprise about 10% of the noncollagenous protein found in bone, was reported to possess potential calcium binding capacity and bone extracellular matrix mineralization, is produced by osteoblast cells. Consequently, serum bone turnover indicators might well be directly associated with the osteocalcin positive cells (Abe, et al., 2019). Osteocalcin positive macrophage cell population exhibited a shift from M1 to M2-phase following treatment of hMSCs with the polysaccharide-nanoparticle construct ST-Ag^{NP}.

Human BMP-2, which is inherent in the family of transforming growth factor-beta (tgF-β), is a bioactive protein that prompts osteogenesis in extra-skeletal location. Formation of bone matrices could be induced with BMP-2 by intensifying the differentiation of osteoblasts. The considerable shift of population profile of BMP-2 positive cells in M2-phase with ST-Ag^{NP} treated hMSC macrophages was depicted in, and the results were compared with normal control and sodium alendronate-treated macrophages No significant difference in expression of BMP-2 and osteocalcin was apparent between the hMSCs administered with ST-Ag^{NP} and sodium alendronate. Greater than two-fold increase in fluorescence active macrophages treated with ST-Ag^{NP} was apparent than that displayed by the untreated hMSCs, and was exemplified by increased osteocalcin and BMP-2, which reinforced the differentiation of osteoblast cells.

Glucocorticoids were reported to affect the metabolisms of osteoclasts and bone marrow stromal cells, which lessen the formation of osteoblast cells. The latter is central to form bone and hematopoiesis, and its loss could result in reduction of cellularity of bone marrow (Kim et al., 2011). Osteoblast differentiation is primarily affected by glucocorticoids leading to a reduction in bone formation. Notably, the differentiation of bone marrow stromal cells could be redirected from osteoblastic to adipocyte lineage by glucocorticoids. In this study, glucocorticoid-induced osteoporotic rats displayed a marked reduction in total counts of electrolyte, leucocyte, and platelet along with hemoglobin A1c levels compared to normal control (Table 7.9). Conspicuously, administration of ST-Ag^{NP} (1 g/kg BW) could result in a significant improvement on total counts of electrolyte (7.19×10^6 cells/μL), leucocyte (6.65×10^6 cells/μL), platelet (869.83×10^3 cells/μL), and hemoglobin A1c (6.9%) compared to those recorded in the diseased control (Table 7.9).

Serum ALP is considered as an important biochemical indicator of bone formation. The risks of enhanced bone turnover and fracture were related to ALP activity, and the present study demonstrated that the osteoporotic group increased activity of ALP indicating lesser bone mineral density (BMD). Noticeably, bone strength is directly proportional to BMD and bone quality. Oral administration of ST-Ag^{NP} showed its protective nature by significantly reducing the elevated levels of ALP in comparison with glucocorticoid-induced osteoporotic rats. Higher level of cholesterol was found to decrease BMD, and significantly increased the levels of bone resorption markers to result in osteoclast-facilitated bone resorption, which increased the risk of osteoporosis in rodents (Chen et al., 2018).

The concentration of serum estradiol (E2) and serum parathyroid hormone (PTH) were assessed by enzyme linked immunosorbent assay (ELISA). It has been known that PTH is closely regulated by serum calcium concentrations. Serum calcium metabolism is directly affected by glucocorticoids as a result of the poor absorption in GI (Rickers et al., 1982). Urinary calcium elimination and lower calcium absorption could result in the increase of parathyroid hormone (PTH) secretion. Low level of serum calcium could cause the increase of PTH (Elkomy et al., 2015), which is one of the most important stimulators of osteoclastic bone resorption, was considerably elevated in the glucocorticoid-treated groups compared to normal control (7.3 pg/mL). Treatment with ST-Ag^{NP} reduced serum PTH (Table 7.9) and protected the bone by corresponding increase in bone mineral. Reduced level of PTH could promote osteoblastogenesis and decreased osteoblast apoptosis by reacting upon osteoblasts (Silva et al., 2015). Characteristic osteogenic markers, such as alkaline phosphatase (ALP), osteocalcin (OCN), and bone morphogenetic protein (BMP), which were recognized for signaling of bone formation, were also stimulated by PTH (Silva et al., 2015). It was known that long-term glucocorticoid treatment decreased bone mass and increased bone marrow adiposity by enlarged adipogenic differentiation. Conspicuously, the estrogen deficiency in women was reported to be directly associated with rapid trabecular bone loss (Riggs et al., 2002) by increasing the formation of osteoclasts leading to bone resorption. Concerning serum estradiol levels, it was found that dexamethasone (osteoporosis-inducing drug) caused reduction in serum estradiol level compared to normal control. The declining levels of estrogen could cause increased incidence of

osteoporosis. With an increasing level of serum estradiol, the size of pre-osteoclasts was reduced, thereby resulting in the stimulation of important bone regulating cytokines (Riggs et al., 2000). Evidently, all doses of ST-Ag^{NP} augmented the level of estradiol in serum (Table 7.9), and that could account for an increased bone strength.

Bone loss is mainly caused by the lack of estrogen, and it has been recognized that glucocorticoids inhibited the responses of the steroid hormone, which promotes the activity of osteoblasts. TC levels would be associated with the lower levels of stored estrogen, thereby affecting the pathogenesis of osteoporosis. In animal model study, glucocorticoid treatment showed a significant increase in HDL and TC level (43 and 58 mg/dL, respectively) in osteoporotic groups compared to the normal control (26 and 39 mg/dL, respectively). Therefore, higher cholesterol could damage bone microstructure and decreases bone mechanical strength leading to a higher risk of osteoporosis. Upon treatment with ST-Ag^{NP} (1 g/kg BW) in dexamethasone-treated rats, the HDL and TC levels were reduced to 28 and 45 mg/dL, respectively. Obviously, loss of BMD in osteoporotic group was corroborated by the reduction of serum calcium levels, whereas a substantial reduction in calcium content (~7 mg/dL) was perceived upon glucocorticoid treatment by reason of reduced intestinal absorption of calcium and its urinary excretion. Treatment with ST-Ag^{NP} resulted in an appreciable recovery in the levels of calcium (8.1 mg/dL) when compared to the positive control group (8.5 mg/dL) (Table 7.9).

There were ample evidences to show that oxidative stress prompted by overproduction of reactive oxygen species (ROS) could increase bone marrow adiposity and bone loss, resulting in osteoporosis (Domazetovic et al., 2017). Under normal physiological conditions, osteoblasts and osteoclast bone cells can combat oxidative stress by promoting antioxidant defenses, which include the enzymes GPx, GPX, GSH, GST, GR, and catalase (Soelaiman et al., 2017), which were quantified using bone homogenates derived from the distal portion of the femur. Dexamethasone treatment had significantly reduced the antioxidant enzyme activities in the femur compared to normal group (Table 7.9). Also, an increase of lipid peroxidation was observed by increasing malondialdehyde (MDA) level in osteoporosis-induced rats (Table 7.9). This could recognize higher degree of free radical production and oxidative stress owing to estrogen deficit and increased ROS that could activate osteoclasts to result in oxidative damage of bone. Diseased rats treated with ST-Ag^{NP} recovered the antioxidant levels, which could restore osteoblastic mineralization in the treated groups (Domazetovic et al., 2017).

Histopathology of the right femur sections in normal control animals revealed surface hyaline articular cartilage, overlying lamellar bone forming cortex and trabecular bone. Interspersed marrow was predominantly composed with mature adipocytes. In contrast, osteoporotic control trabecular bone exhibited anisotropy, thinning, microfracture, and trabecular disconnection. However, disease-induced groups treated with higher dose of ST-Ag^{NP} and sodium alendronate standard showed disappearance of osteoporotic cavities with nearly normal distribution and content of collagen fibers in trabecular bone. High dose of ST-Ag^{NP} preserved cortical bone thickness and absence of erosion cavities, normal architecture of bone trabeculae, and trabecular bone thickness were maintained. On detailed histopathological examination of tissues, no pathologically significant lesions were perceived in normal control and treatment groups.

The differences between normal control, osteoporosis-induced group, and ST-Ag^{NP} treated group were also established by ^{1}H NMR of serum of the experimental subjects (Pontes et al., 2019). The ^{1}H NMR spectra suggested that the lipid content of osteoporosis-induced group was different from that in the normal control group. Signals at δ_H 3.12-3.35 were accredited to taurine and choline, whereas those at δ_H 0.88-1.36 were due to methyl/methylene groups of LDL/VLDL. The control group exhibited greater proton integral at δ_H 3.16-3.75, and proton integration value (~7) of

this group was larger than in the diseased group (Table 7.12). Osteoporosis-induced group displayed an increased integration value (3.3) at δ_H 0.88-1.50, which recognized the decrease in bone mineral density (Lv et al., 2016). Proton integration values of sodium alendronate and ST-Ag^{NP} treated groups (5.99 and 9.89, respectively) (Table 7.12) at δ_H 3.16-3.75 was considerably greater than in the diseased group (3.85), which indicated that serum choline and taurine levels of healthy groups were higher than the osteoporosis-induced group (Lv et al., 2016; Long et al., 2009). Taurine is considered as one of the richest amino acids in bone, and was reported to inhibit the formation of osteoclast cells (Ahmed et al., 2009). Proton integration of unsaturated lipid levels of osteoporosis-induced group was also found to be higher (0.83) than normal control group and other treated groups (< 15) at δ_H 5.00-5.35, which corroborated the records of the previous study (Briot et al., 2015).

7.3. Isolation and Characterization of Bioactive Polysaccharide from *Turbinaria conoides*

7.3.1. Materials and Methods

This section described the instruments used for the present study along with the reagents and solvents.

7.3.2. Preparation of Polysaccharide

Dried powdered leaves of *T. conoides* material (250 g) was pre-treated at 35°C with acetone (500 mL, 5 h) followed by the treatment with 30% (v/v) formaldehyde solution (650 mL, 14 h), before being filtered to acquire pigmented and phenolic constituents, respectively. Pre-treated extracted materials were filtered and concentrated at about 45 °C by a rotary vacuum evaporator (Heidolph, Instruments GmbH & Co., Schwabach, Germany). Residual algal material was then extracted twice with double distilled water (1250 mL x 2) at 95 °C for 6 h, followed by filtration to obtain aqueous extract. The aqueous supernatant (1600 mL) was reduced to one-fifth of the initial volume (~ 340 mL) by rotational vacuum concentrator. The concentrated aqueous extract was then added with trichloroacetic acid (TCA, 5%, w/v) and centrifuged (10 min, 6500 rpm, 5°C, Sorvall® Biofuge Stratos, Thermo Scientific, USA) to separate the proteinaceous substances. The clarified supernatant was subjected to precipitate with ice cold ethyl alcohol (2.5 volume) (kept for overnight at - 4°C) followed by centrifugation. The clarified part was freeze dried (Martin Christ beta 2-8 LSCbasic, Martin Christ, Germany) to yield crude polysaccharide (TCP, 11.65 g; yield based on dry weight, 4.66 %).

7.3.3. Chromatographic Purification and Chemical Characterization of polysaccharide from *T. conoides*

Crude polysaccharide (TCP, 11.65 g; yield based on dry weight, 4.66%) was isolated from thalli (leaves) of *T. conoides* was fractionated with ion exchange chromatographic technique by using diethylaminoethyl cellulose (DEAE, anion exchanger) on a glass column (25 cm x 4 cm). Column chromatographic fractionation of TCP was resulted with five fractions (TCP-1 to TCP-5 isolated with increasing concentration of NaCl, 0.0 to 0.45 M), which were assessed for presence of carbohydrate and monosaccharide compositional analysis. The column purified fractions were freeze dried and depolymerized with trifluoroacetic acid (3 mL, 1M) before being subjected to monosaccharides composition analysis by an evaporative light-scattering detector (ELSD, SofTA model-300^S, Teledyne Tech. Inc., Lincoln, NE) attached to an high-pressure liquid chromatographic (HPLC) system. Other chemical compositional analysis of column purified along with crude fractions, such as total content of carbohydrate, sulfate, protein and uronic acid were quantifiably estimated using previous methodologies. Based on the compositional analysis of monosaccharide and carbohydrate content, the fraction TCP-3 was structurally characterized with the help of spectroscopic analysis. Molecular mass of the TCP-3 was deduced by HR(ESI)MS in negative mode. The disappearance of sulfate group was further confirmed by Fourier-transform infrared (FT-IR) spectral analysis, whereas completion of methylation was

initially confirmed by FT-IR and structural characterization by nuclear magnetic resonance (NMR) spectroscopic analysis.

7.4. Results and discussion

7.4.1. Extraction, purification, yield and bioactivities of polysaccharide from *T. conoides*

The crude polysaccharide was chromatographically separated into various fractions by anion exchange chromatography (using DEAE cellulose 52) eluted with linear and step-wise gradient of NaCl concentration (0.0 to 0.45 M) and are designated as TCP-1, TCP-2, TCP-3, TCP-4 and TCP-5, respectively. The percent yield of purified polysaccharide fractions eluted was found to be 12.5 %, 16.1 %, 23.1 %, 17.3 % and 18.7 %, respectively. Among the purified polysaccharide fractions, the major polysaccharide fraction (TCP-3) corresponds to 0.2 M NaCl accounted for ~ 80 % carbohydrate content and lesser protein content (< 0.9 %). Hence the column fraction named TCP-3 was freeze-dried and further subjected to monosaccharide composition analysis after depolymerized with trifluoroacetic acid. Free radical quenching (IC_{50DPPH} ~1.7 mM) potential of TCP-3 was superior to those displayed by other fractions (IC_{50DPPH} > 1.9 mM). TCP-3 exhibited higher attenuation potential of pro-inflammatory 5-LOX (IC_{50} 4.2 mM) compared to other column fractions (IC_{50} > 4.4 mM).

7.4.2. Chemical composition analysis of polysaccharide from *T. conoides*

The content of carbohydrate for TCP-3 was relatively higher than that of other sub-fractions. The column sub-fraction designated as TCP-3 recorded greater percentage of carbohydrate (~ 80 %) and a considerable amount of sulfate (7.2 %) with a trace amount of protein (< 0.9 %). The monosaccharide composition analysis revealed the presence of two major monosaccharide units fucose (58 %) and galactose (41 %). The structural identity of the polysaccharide was deduced to be [→1)-*O*-4-sulfonato-*α*-fucopyranose-(3→1)-*O*-2-sulfonato-*α*-fucopyranose-(3→] as main backbone with 6-*O*-acetylated [→1)-*β*-galactopyranose-(4→] as side chain.

7.4.3. Spectroscopic evaluation of polysaccharide from *T. conoides*

Chemical structure of TCP-3 was interpreted by spectroscopic analyses, with the help of NMR (1D and 2D), FTIR, and HR(ESI)MS. Purified TCP-3 was composed with 4-*O*-SO_3-*α*-(1→3)-Fuc*p* (unit A) and 2-*O*-SO_3-*α*-(1→3)-Fuc*p* (unit B) as key skeletal branch and *β*-(1→4)-Gal*p* (unit C) as lateral branch with -OAc substitution at C-6 of unit C. FTIR spectrum of TCP-3 recorded peaks at 3442, 2946 cm-1, which were allocated as O-H and C-H functionalities, respectively. Furthermore, asymmetric S=O and sulfate ester stretching (C-O-S) were confirmed by the IR frequencies at 1231 and 841 cm-1, respectively. Presence of carbonyl ester moiety was confirmed with IR frequency at 1739 cm^{-1}. Proton (^1H) NMR spectrum indicated signals at δ_H 4.55-5.32 analogous to the protons of anomeric region (for *β* and *α*), which was attributed to H-1 of the pyranose sugar of 4-*O*-SO_3-*α*-(1→3)-Fuc*p* (unit A), 2-*O*-SO_3-*α*-(1→3)-Fuc*p* and *β*-(1→4)-Gal*p* with –OAc substitution at C-6 (unit C) units. Anomeric proton at δ_H 5.33 represented the H-1 proton of fucopyranose residue in TCP-3. Other ^1H-NMR signals at δ_H 3.15-4.02 were characterized as the protons of C-2 to C-5/C-6 pyranoid ring. Intense signals around δ_H 1.2-1.3 were attributed to C-6 methyl protons of units A and B (fucopyranose residue), respectively. The signals appeared at δ_H 2.14-2.58 were observed due to the presence of *O*-acetyl protons. ^{13}C-NMR spectrum revealed anomeric signals at δ_C 92.0-99.5. ^{13}C signals at δ_C 60.6-76.0 were characteristics of pyranoid ring carbon and at δ_C 20.6 and 19.8 were accredited to C-6 methyl carbons of units A and B, respectively. Position of the anomeric proton and C-2 to C-6 ring protons in 4-*O*-SO_3-*α*-(1→3)-Fuc*p* was also established by ^1H-^1H COSY and ^1H-^{13}C HSQC correlations. COSY correlations that observed between δ_H 5.33/3.56/3.82 and δ_H 3.90/3.61, which attributed to the fragment of C-1 to C-3 and C-4/5 in 4-*O*-SO_3-*α*-(1→3)-Fuc*p*.

Correspondingly, another one (H-B1) anomeric proton at δ_H 5.15 exhibited coupling constant (*J*) value of 3.75 Hz was recognized as anomeric proton of unit B. Deshielded signal in proton NMR at δ_H 4.55 with coupling constant (*J*) value of 8.06 Hz was attributed to the anomeric proton of *β*-(1→4)-Gal*p* fragment (unit C). Single-charged anion was ascribed by intense peak at m/z 629.0693, which resulted in glycosidic residues of unit A, B and C. Linkage pattern analysis in polysaccharide was established by desulfation, methylation reaction followed by reductive cleavage and acetylation. An all-inclusive spectroscopic study of the homogenous polysaccharide ascribed the structure as [→1)-*O*-4-sulfonato-*α*-fucopyranose-(3→1)-*O*-2-sulfonato-*α*-fucopyranose-(3→] as main backbone with 6-*O*-acetylated [→1)-*β*-galactopyranose-(4→] as side chain.

7.4.4. Effect of TCP-3 on hematological and immunomodulating parameters in CTX-induced immunosuppressed mice

The relative weights of the spleen and thymus (lymphoid organs) along with total WBC count were significantly reduced in animals administrated with CTX (0.179, 0.098%, and 2300 cells/cu mm, respectively) (Table 7.28) and it displayed considerable recovery following the treatment with TCP-3 (0.271, 0.143%, and 4300 cells/cu mm, respectively; @100-400 mg/kg BW) (Table 7.28), which signified the triggered immune response by lymphocytes. Administration of TCP-3 at 200 mg/kg BW resulted a notable recovery of bone marrow cells and *α*-esterase activity (13.54 cells/femur/mL x 10^6 and 1680 positive cells/4000 BMC, respectively $p > 0.01$). Not much change was observed for other hematological parameter (Table 7.29). Bone marrow is a stem cell pool, which provides a constant supply of various immune cells including lymphocytes and macrophages to the blood and lymph, and can be considered as the reservoir of immune stem cells. The *α*-esterase is considered as a cytochemical marker for differentiating bone marrow cells, wherein non-specific esterase activity was possessed entirely by stem cells, nonetheless the monocytes differentiation possesses *α*-specific esterase activity (McClean et al., 1995).

The level of serum IFN-*γ* and IL-2 in CTX-induced animals resulted in a substantial decline (0.59 and 2.32 pg/mL, respectively), whereas those treated with TCP-3 at 100 mg/kg BW recovered the reduced serum IFN-*γ* and IL-2 level up to 1.49 and 3.99 pg/mL, respectively. IFN-*γ* is type-II interferon, which coordinates a diverse array of immunological activities, interferes with viral replication, and its upregulation is associated with greater resistance to bacteria and viruses (Kang et al., 2018). IL-2 (generated from T cells) is known for enhancing natural killer (NK) cell activity and B cell immunoglobulin function (Hipp et al., 2017), by regulating activities of WBCs for growth and proliferation of T cells.

Hematopoietic stem cells of bone marrow are the preliminary source of cell types that involves in the immune system. The microenvironment of antigen-independent maturation of B-cells is also provided by the bone marrow. IFN-*γ* is a pleiotropic cytokine (of activated T lymphocytes) that stimulates both immune networks, which is one of the effective macrophage activators. Other than playing a multitude of roles in pathogen defense and immune modulation, IFN-*γ* can act as a secretory factor that interferes in viral replication. Specific immune cells upon infection or stimulation with antigen or mitogen can produce IFN-*γ*, which makes it a useful anti-microbial cytokine in the antiviral defense system. The development and growth of peripheral immune cells (instigation of the immune response) are promoted by IL-2, which has a homeostatic effect and also promotes antigen-specific division and survival of regulatory T cells.

7.4.5. Protective effect of TCP-3 on CTX-induced suppression of lymphocyte blastogenesis in mice (*in vivo* and *ex vivo*)

The protective effect of TCP-3 on blastogenesis of splenocytes, thymocytes, and bone marrow was evaluated in viable cells. Administration of TCP-3 at 100-400 mg/kg BW resulted in a notable upregulation in the proliferation of spleen cells (1.49), along with mitogenic potential of con A (1.43-fold), PWM (1.51-fold), LPS (1.58-fold), and PHA (1.5-fold) on spleen cell proliferation in comparison with CTX-treated group. Likewise, notable thymus and bone marrow cell proliferation were observed with TCP-3 treated groups after incubating with mitogens (2.24-2.46 and 1.24-2.51-fold, respectively). Similar trend was observed in case of *ex vivo* system. Mitogens (Con A, PWM, LPS, and PHA), which are considered as polyclonal lymphocyte activators, cause Mitogens (Con A, PWM, LPS, and PHA), which are considered as polyclonal lymphocyte activators, cause blastogenic response to lymphocytes, and are recognized as nonspecific stimulants of immune cells. The augmentation of proliferated lymphocytes in bone marrow, thymus, and spleen of TCP-3 administrated animals in comparison with CTX-treated animals evidently demonstrated the activated stimulatory effect of TCP-3 isolated from *T. conoides* extract on the immune system.

7.4.6. Effect of TCP-3 on IL-2 and IFN-γ gene expression

Jurkat cells treated with TCP-3 (6.25-25 μg/mL) displayed appreciable cell viability (up to 80%) besides resulting in a significant upregulation in mRNA expression ($p < 0.05$) of IL-2. The change of mRNA expression of IFN-*γ* was substantially increased up to 2.13-fold at 6.25 μg/mL. These results suggested that IFN-*γ* and IL-2 levels might be increased by TCP-3 through the gene-expressed activation of T-cells. Natural products (polyphenols from *Astragalus* and 6-shogaol) were found to promote IFN-*γ* production in Jurkat human T cells (Ouyang et al., 2021). There was report about induction of IFN-*γ* and IL-2 gene transcription on Jurkat cells was also observed by polysaccharide-protein complex isolated from *Lycium barbarum* L (Chen et al., 2008).

7.4.7. Effect of TCP-3 on inflammatory cytokines in LPS-induced animals and RAW 264.7 cells

The serum TNF-*α* level of LPS-induced animals was increased (4.88 pg/mL) in comparison with normal control (3.25 pg/mL) . Notably, treatment with TCP-3 at 100 and 200 mg/kg BW ($p < 0.01$) repressed the LPS-induced serum TNF-*α* level (3.78 and 3.12 pg/mL, respectively) in experimental mice. The level of serum IL-6 in the normal control group of mice was 5.01 pg/mL, which was elevated up to (8.06 pg/mL) after treatment with LPS. The animals administrated with TCP-3 at 100 and 200 mg/kg BW showed substantial inhibition of the LPS-induced IL-6 production (5.96 and 6.23 pg/mL, respectively). Elevation of IL-1*β* level was marginally inhibited by TCP-3 at 100 mg/kg BW (2.25 pg/mL). Treatment with TCP-3 also significantly inhibited LPS-induced serum NO levels at 200 and 400 mg/kg BW of TCP-3 (0.67 and 0.94 μM, respectively, $p < 0.01$).

No significant reduction in viability was apparent for the cells treated with TCP-3 (10-100 μg/mL) even after 72 h of incubation. Alteration or deformations of cell size and shape were not observed for TCP-3 treated RAW 264.7 cells in comparison with normal control. The elevated LPS-induced cytokines and NO were reduced following treatment with TCP-3 (at 10-25 mg/mL). The gene expression studies showed upregulation of the mRNA expressions of pro-inflammatory cytokines TNF-*α*, IL-6, IL-1*β,* and *i*NOS in LPS-treated macrophages. The LPS-induced upregulation of TNF-*α* and IL-6 genes was reduced (0.46 and 38.74-fold, respectively) following treatment with TCP-3 (@ 50 and 10 mg/mL, respectively.

Pro-inflammatory cytokines (IL-6/1*β*, TNF-*α*) are responsible for the inflammatory response, wherein IL-6 and TNF-*α* production along with some biochemical cascade could be stimulated by IL-1*β*, which possessed diverse physiological and immunological effects. The discharge of NO by activated macrophages is also considered one of the

key cytostatic mechanisms related to nonspecific immunity. The inflammatory response (activated by the production of pro-inflammatory cytokines) is stimulated by LPS, a component obtained from the cell wall of bacteria. There were reports about the isolation of sulfated polysaccharides from *Turbinaria ornata* suppressing LPS-induced inflammatory responses (Bhardwaj et al., 2020)

7.4.8. *In-vitro* anti-inflammatory activities of TCP-3 on human monocyte THP-1 cells

Cell viability study of TCP-3 (6.25-100 µg/mL) were accomplished on THP-1 cells, which resulted > 90% of viability without any structural alteration. The TNF-α expression level of LPS-treated cells appeared as green surrounded by blue color, which clearly indicated the change in cytokine level between normal control and LPS-treated cells. The recovery of THP-1 cells was observed with the treatment with TCP-3 (at 50 µg/mL) TCP-3 treatment on cells resulted in a substantial reduction in IL-1β expression that was corroborated by the change in the blue color of cells. A significant elevation ($p < 0.05$) in TGF-β expression was observed on TCP-3 treated cells. Mean fluorescence intensity of these cytokines further supported this observation. LPS-induced elevated IL-12 expression was also downregulated after the treatment with TCP-3 (at 50 µg/mL). TNF-α is a pro-inflammatory cytokine that is released by macrophages through acute inflammation and is found to be elevated in serum during different inflammatory responses including bacterial infection. A higher TNF-α level was found during septic shock, other inflammatory diseases, and even in the present day, Covid-19 affected patients (Del Valle et al., 2020). IL-1β is also a pro-inflammatory cytokine, which was found to be discharged by immune cells and macrophages during the inflammation. TGF-β creates a lenient environment for the growth of tumor cells, by prompting the effects of immunomodulatory cytokines.

Treatment with TCP-3 (at 50 µg/mL) recorded a substantial downregulation of IFN-γ and IL-2 gene expression levels in LPS-treated THP-1 cells (2.44 and 1.84-fold, respectively). The immunity-enhancing properties of IL-2 and IFN-were further supported by its role in T-cell proliferation and native T-cell differentiation (Bachmann et al., 2007). The present experiment revealed that following the treatment with TCP-3 (at 50 µg/mL), the relative gene expression levels of IL-2 and IFN-γ in THP-1 cells were significantly decreased in comparison with LPS treated cells.

The upregulated LPS-induced NO and IL-6 levels were further significantly reduced ($p < 0.05$) with the treatment with TCP-3 (50 µg/mL). This evidence was further supported by the population shifts of histograms and cell percentage expressions of NO and IL-6. Nitric oxide can regulate the functional activity of different immune cells. IL-6 is considered one of the most important inflammatory cytokines, which can be found elevated during most inflammatory conditions (Del Valle et al., 2020). From the above experimental data, it could be concluded that TCP-3 at 50 µg/mL could effectively reduce the upregulated *i*NOs and IL-6 levels along with relative gene expression levels of IL-2 and IFN-γ in THP-1 cells and regulate inflammatory responses.

7.5. Isolation and Characterization of Bioactive Polysaccharide from *Turbinaria ornata*

7.5.1. Materials and Methods

This section described the instruments used for the present study along with the reagents and solvents.

7.5.2. Preparation of Polysaccharide

Dried and homogenous leaves of *T. ornata* (200 g) was pre-treated with acetone (450 mL, 4 h) and 30% (v/v) formaldehyde solution (600 mL, 14 h) was added at about 35°C before being filtered to acquire pigmented and phenolic substances, respectively. The residual powder was extracted with double distilled water (1000 mL x 2) at about 95 °C for 5 h, and was filtered to yield an aqueous extract. The aqueous supernatant (1600 mL) was concentrated to one-fifth

of the initial volume (320 mL) by rotational vacuum evaporator. The aqueous extract was added with trichloroacetic acid (5%, w/v) and centrifuged (at 10 min, 6500 rpm, 5 °C) to remove the protein materials. The clarified supernatant was made to precipitate with ice cold ethyl alcohol (x 2.5 volume) (kept for overnight at - 4°C) and the contents were centrifuged. The clarified part was lyophilized to afford crude polysaccharide (TOP, 9.58 g; yield on dry weight basis, 4.79%).

7.5.3. Chromatographic Purification and Chemical Characterization of polysaccharide from *T. ornata*

Crude polysaccharide (TOP, 9.58 g; yield on dry weight basis, 4.79%) was isolated from thalli (leaves) of *T. ornata* was fractionated with ion exchange chromatographic technique by using diethylaminoethyl cellulose (DEAE, anion exchanger) on a glass column. Column chromatographic fractionation of TOP was resulted with five fractions (TOP-1 to TOP-5 isolated with increasing concentration of NaCl, 0.05 to 0.25 M), which were assessed for presence of carbohydrate and monosaccharide compositional analysis. The column purified fractions were freeze dried and depolymerized with trifluoroacetic acid before being subjected to monosaccharides composition analysis by an evaporative light-scattering detector attached to an high-pressure liquid chromatographic (HPLC) system. Other chemical compositional analysis of column purified along with crude fractions, such as total content of carbohydrate, sulfate, protein and uronic acid were quantifiably estimated using previous methodologies. Based on the compositional analysis of monosaccharide and carbohydrate content, the fraction TOP-3 was structurally characterized with the help of spectroscopic analysis. Molecular mass of the TOP-3 was deduced by HR(ESI)MS in negative mode. The disappearance of sulfate group was further confirmed by Fourier-transform infrared (FT-IR) spectral analysis, whereas completion of methylation was initially confirmed by FT-IR and structural characterization by nuclear magnetic resonance (NMR) spectroscopic analysis.

7.6. Results and discussion

7.6.1. Extraction, purification, yield and bioactivities of polysaccharide from *T. ornata*

The crude polysaccharide was chromatographically separated into various fractions by anion exchange chromatography (using DEAE cellulose 52) eluted with linear and step-wise gradient of NaCl concentration (0.05 to 0.25 M) and are designated as TOP-1, TOP-2, TOP-3, TOP-4 and TOP-5, respectively. The percent yield of purified polysaccharide fractions eluted was found to be 13.5 %, 17.1 %, 24.1 %, 19.3 % and 16.7 %, respectively. Among the purified polysaccharide fractions, the major polysaccharide fraction (TOP-3) corresponds to 0.15 M NaCl accounted for ~ 85 % carbohydrate content and lesser protein content (< 1 %). Hence the column fraction named TOP-3 was freeze-dried and further subjected to monosaccharide composition analysis after depolymerized with trifluoroacetic acid. TOP-3 was recorded with greater yield of carbohydrate (86%) with lesser protein (0.9%) than other eluted fractions (Table 3.1.2). Free radical scavenging (IC_{50DPPH} 1.57 mg mL^{-1}) potential of TOP-3 was greater than those displayed by other fractions (IC_{50DPPH} > 1.6 mg mL^{-1}). In addition, greater selectivity index of TOP-3 (1.12) could reveal its higher attenuation potential against COX-2 than its constitutive isoform COX-1.

7.6.2. Chemical composition analysis of polysaccharide from *T. ornata*

The content of carbohydrate for TCP-3 was relatively higher than that of other sub-fractions. The column sub-fraction designated as TCP-3 recorded greater percentage of carbohydrate (~ 85 %) and a considerable amount of sulfate (6.9 %) with a trace amount of protein (< 1 %). The monosaccharide composition analysis revealed the presence of two major monosaccharide units fucose (62 %) and galactose (37 %). The structural identity of the polysaccharide was deduced to be as [→1)-*O*-4-sulfonato-*α*-fucopyranose-(3→1)-*α*-fucopyranose-(3→] as the main backbone with *β*-(1→4)-galactopyranose as side branch with –OAc substitution at C-6 position.

7.6.3. Spectroscopic evaluation of polysaccharide from *T. ornata*

The structure of the purified sulfated galactofucan was elucidated by all-inclusive spectroscopic analyses, such as FTIR, NMR (1D and 2D), and HR(ESI)MS. Purified polysaccharide fraction (TOP-3) was built by 4-*O*-SO_3-*α*-(1→3)-fucopyranose (unit A) and *α*-(1→3)-fucopyranose (unit B) as a primary structural branch and 6-*O*-acetyl-*β*-(1→4)-galactopyranose (unit C) as a lateral branch. FTIR peaks at 3441, 2925 cm^{-1} were assigned to the O-H and C-H stretching functionalities, whereas two intense absorption bands at 1636 and 1012 cm^{-1} were due to O-C-O glycosidic and C-O-C intra-molecular linkage stretching. Furthermore, asymmetric S=O stretching and C-O-S sulfate ester stretching was confirmed by 1221 and 844 cm^{-1}, respectively. ^{1}H-NMR spectrum revealed signals at δ_H 4.61-5.64 analogous to the characteristics of anomeric protons (for *β* and *α*), and was attributed to H-1 of pyranose sugar of 4-*O*-SO_3-*α*-(1→3)-fucopyranose (unit A), *α*-(1→3)-fucopyranose (unit B) and 6-*O*-acetyl-*β*-(1→4)-galactopyranose (unit C) motifs. Anomeric proton at δ_H 5.64 exhibited a ^{1}H-NMR coupling constant (*J*) of 3.7 Hz, which was archetypal of H_1 protons in fucopyranose and revealed the occurrence of Fuc*p* residue in TOP-3. Other ^{1}H-NMR signals at δ_H 3.57-4.37 were recognized to C-2 to C-5/C-6 pyranoid ring protons. Sharp proton singlet at δ_H 2.23 was observed due to the methyl (-CH_3) proton of –OCOC$\underline{H_3}$ group at the C-6 position of *β*-(1→4)-Gal*p*. Two different doublets at δ_H 1.13 and 1.16 were allocated to the C-6 methyl protons of unit A and B. ^{13}C-NMR exhibited anomeric traces at δ_C 97.4-105.5. Distinctive ^{13}C signals at δ_C 63.7-78.1 were characteristic of C-2 to C-5/C-6 pyranoid ring carbons. Distinctive peaks at δ_C 25.1, 17.1, and 18.4 were attributed to methyl carbon of *O*-acetyl group and C-6 methyl carbons of 4-*O*-SO_3-*α*-(1→3)-fucopyranose and *α*-(1→3)-fucopyranose motifs. Likewise, the anomeric proton at δ_H 5.28 (H-B1) was ascribed to C_1 of *α*-(1→3)-Fuc*p* (unit B). C-B1 to C-B3 fragment was established by ^{1}H-^{1}H COSYs between δ_H 5.28/3.89/4.34. Furthermore, a strong HMBC signal between δ_H 5.28 to δ_C 68.5 corroborated the establishment. The single-charged anion of trisaccharide entities was ascribed by an intense molecular ion peak at *m/z* 592.1309, which resulted in glycosidic residues of 4-*O*-SO_3-*α*-(1→3)-Fuc*p*, *α*-(1→3)-Fuc*p* and 6-*O*-acetyl-*β*-(1→4)-Gal*p*. The spectrum contained other major peaks at *m/z* 388.0675, 367.1240, 242.0096, 221.0661 and 163.0606 analogous to the fragments [4-*O*-SO_3-*α*-(1→3)-Fuc*p*-*α*-(1→3)-Fuc*p*]$^-$, [*α*-(1→3)-Fuc*p*-6-*O*-acetyl-*β*-(1→4)-Gal*p*]$^-$, [4-*O*-SO_3-*α*-(1→3)-Fuc*p*]$^-$, [6-*O*-acetyl-*β*-(1→4)-Gal*p*]$^-$ and [*α*-(1→3)-Fuc*p*]$^-$, respectively. Based on the spectroscopic analyses, TOP-3 was elucidated as [→1)-*O*-4-sulfonato-*α*-fucopyranose-(3→1)-*α*-fucopyranose-(3→] as the main backbone with *β*-(1→4)-galactopyranose as side branch with –OAc substitution at C-6 position

7.6.4. Evaluation of cellular viability by cytotoxicity assays

Purified sulfated galactofucan (TOP-3) was found to induce cytotoxicity in human ductal and hepatocellular carcinoma cell lines (MCF7 and HepG2, respectively) in a dose-proportional way, as evaluated by SRB, MTT, NRU, and LDH assays. The untreated control MCF7 and HepG2 cells revealed 100% cell viability, while normal 3T3-L1 preadipocytes treated with TOP-3 (12.5-200 μg/mL) cell line did not display any toxicity following overnight incubation (Table 7.18). In the SRB assay, MCF7 and HepG2 cells exhibited 94.8 and 88.6% viability, respectively with treatment with TOP-3 at 12.5 μg/mL (Table 7.18). The SRB assay of the MCF7 and HepG2 cells treated with various concentrations of TOP-3 exhibited a significant reduction in cell viability as the concentration altered from 12.5 to 200 μg/mL (15.5%) (Table 7.18). No such change was observed in the case of 3T3L1 preadipocytes cells. Likewise, a considerable decrease in cell viability was apparent in the case of MTT and NRU assay. Cytotoxicity on MCF7 and HepG2, treated with TOP-3 at higher concentrations resulted in a noteworthy decrease of viable MCF7 and HepG2 cells (12.7 and 15.6% at 200 μg/mL, respectively) in the MTT assay compared to the lower concentrations of TOP-3 and

untreated normal cells. Conspicuously, the untreated control cells revealed high confluency of cell monolayer, while the MCF7 and HepG2 cells administered with TOP-3 showed substantial morphological deformations, such as changes in shape and size of cells, reduction and rounding of cells, development of blebs, debris, and apoptotic bodies. These deformed morphologies were increased upon treatment with an increasing concentration of TOP-3 (12.5-200 μg/mL), which recognized the manifestation of apoptosis. Development of blebs on cell membrane surface and bulge of microspikes from cells could confirm the apoptosis. Morphologically deformed apoptotic cells also could lose connection with neighboring cells (Monga et al., 2013).

Cytotoxicity of TOP-3 was also quantitatively determined by NRU assay (Repetto et al., 2008). Viable cells could absorb and incorporate neutral red into the lysosomes, even though it could not be taken up by non-viable cells (Kuete et al., 2016). In this study, TOP-3 displayed a dose-proportionate decrease in the viability of MCF7 and HepG2 cells. TOP-3 exhibited cell viability of 92.3% at 12.5 μg/mL, in NRU assay, and with an increasing concentration of TOP-3, the cell viability was found to be lesser than 20%. Conspicuously, the test compound (TOP-3) did not show considerable cytotoxicity against the 3T3-L1 cell line. In the case of the LDH assay, higher absorbance values were detected (>0.85 at 200 μg/mL) for TOP-3 treated MCF7 and HepG2 cells, in comparison with untreated. Notably, 47-51% of viable MCF7 and HepG2 cells treated with standard drug camptothecin (CPT) at 7.5 μg/mL, were perceived (Table 7.18). However, LDH leakage was found to increase to some extent at higher concentrations of TOP-3. Depending upon the cytotoxicity evaluated by MTT, IC_{50} values of TOP-3 were determined as 64.5 μg/mL for HepG2 and 47.4 μg/mL for MCF7 cells, and therefore, TOP-3 with these two concentrations was selected for subsequent studies.

7.6.5. Detection of apoptosis and necrosis

Annexin V assay is one of the most widely utilized apoptosis study markers for translocation of phosphatidylserine (PS) from the inner to the outer leaflet of the plasma membrane (Mohammed et al., 2018). Annexin V-FITC/PI assay was performed by flow cytometric analysis to quantify the cell apoptosis with TOP-3 and CPT (standard) treated MCF7 and HepG2 cells. Flow cytometric analysis of TOP-3 treated with MCF7 and HepG2 cells resulted in early and late apoptosis at the IC_{50} concentrations (obtained from MTT assay). The outcome of annexin V/FITC-PI apoptosis demonstrated the distribution of carcinoma cells (MCF7 and HepG2) into four population quadrants, representing annex V-/PI-, annex V+/PI-, annex V+/PI+, and annex V-/PI+(corresponding to viable, early apoptotic, late apoptotic, and necrotic cells, respectively). Maximum numbers of viable cells were observed in untreated control MCF7, HepG2, and 3T3-L1 cells (99.7-99.9%), along with a minimal number of early and late apoptotic cells (<0.2%). Total gated cells in M1 macrophage were 97-98% for MCF7 and HepG2 cell lines. However, treatment with TOP-3 on MCF7 and HepG2 exhibited lesser cell viability (29.9 and 47.6%, respectively), than that of the control cells. The early apoptotic cells were 56.0 and 24.2%, respectively, whereas 14 and 26.02% of late apoptotic cells were observed in TOP-3 treated MCF7 and HepG2 cell lines, respectively. The apoptosis of TOP-3 treated MCF7 and HepG2 cells were also supported by the shifting of macrophage (M1 to M2). Noticeably, 2.15% of the necrotic cells were observed in the case of HepG2, and no such necrosis was noticed for MCF7 cells. Untreated control and TOP-3 treated 3T3-L1 preadipocytes cells resulted in greater than 85% cell viability. Lesser early apoptosis and late apoptosis were observed for TOP-3 treated 3T3-L1 preadipocytes cells. TOP-3 treated MCF7 and HepG2 cells displayed a considerable enhancement in the number of early and late apoptosis, which was comparable with the CPT (standard) treated MCF7 and HepG2 cells but greater than untreated control (p <0.05). The augmentation of cell apoptosis in TOP-3 treated MCF7 and HepG2 cells could attribute to the potential anticancer property of TOP-3 through cell apoptosis. There was a report about the induction of HepG2 cancer cell arrest in the G0/G1 phase of the cell cycle by fucoidan

(Arumugam et al., 2019b). In another study, a polysaccharide isolated from *Undaria pinnatifida* also exhibited apoptosis in the hepatocellular carcinoma SMMC-7721 cells, where annexin V/PI double-staining and flow cytometric study revealed that the population of apoptotic cells could significantly increase from 9.8% in untreated cells to 25.1% in the polysaccharide treated cells (Yang et al., 2013). A polysaccharide isolated from brown seaweed *Sargassum cinereum* also resulted in enhanced early and late apoptosis (82.6%) than those exhibited by the normal control (76.7%) in the colon cancer cell line (Narayani et al., 2019). Annexin V/PI stained MCF-7 cells treated with the water-extracted polysaccharide isolated from *Ecklonia kurome* exhibited a significant augmentation of early apoptosis (58.2%) in comparison with the normal control (Li et al., 2020). Another study revealed the flow cytometric quantification of apoptosis, wherein the percentage of early and late apoptosis was elevated to 42.5 in the case of sulfated polysaccharide-treated HeLa cells, and normal control exhibited 1.17% of apoptosis (Jose et al., 2018). A recent study also revealed that induction of apoptosis was found to increase up to 18.7% from 4.1% in ilimaquinone (a sesquiterpene derivative isolated from a marine sponge)-treated breast cancer cell line (Bai et al., 2021).

7.6.6. Detection of live/dead cells

The percentage of apoptotic and necrotic cells was further quantified by acridine orange/ethidium bromide (AO/ETBR) fluorescence staining (Kasibhatla et al., 2006). The untreated control MCF7, HepG2, and 3T3-L1 cells on AO/ETBR fluorescence staining were shown to be green in color indicating viable cells. The AO/ETBR staining of MCF7, HepG2, and 3T3-L1 cells treated with TOP-3 displayed bright green, orange, and red colors signifying viable cells, early apoptotic, and late apoptotic cells, respectively. A comparable result was observed between TOP-3 and standard CPT treated MCF7, HepG2, and 3T3-L1 cells in terms of the total number of cells after apoptosis. These results supported the fact that cell apoptosis could be successfully induced by TOP-3 in MCF7 and HepG2 (carcinoma) cell lines. A similar pattern was observed in the case of carrageenan-treated HepG2 and Caco2 cells (Ariffin et al., 2014). AO/ETBR-stained fluorescence microscopic study of turbiconol also resulted in induction of apoptosis and cell cycle arrest in A549 and HepG2 cell lines (Jacob et al., 2019). In another study, induction of apoptosis on sulfated polysaccharide-treated human liver and lung cancer cell lines was identified through (AO/ETBR) fluorescence staining (Suresh et al., 2013). A recent study also exhibited the apoptosis changes of colon, cervical, liver, and breast cancer cells treated with crude polysaccharides isolated from marine bivalves by using AO/ETBR staining (Padmanaban et al., 2022).

7.6.7. Gene expression of tumor suppressor protein *p53*

The induction of apoptosis with TOP-3 treated MCF7, HepG2, and 3T3-L1 cell lines were evaluated by the activation of *p53* gene expression. The tumor suppressor *p53* gene is a nuclear transcription factor associated with cell cycle growth or apoptosis, and damage of DNA, which is related in a common manner (uncontrolled proliferation) with human cancers (Gudkov et al., 2003). Studies revealed that pro-apoptotic potential was stimulated by the growth of *p53* in tumor cells and activation of *p53* could be considered as an important therapeutic response against advanced tumor and cancer treatment (Amini et al., 2019; Xue et al., 2007; Ventura et al., 2007). The weakening of *p53* activity (due to the mutation) was interrelated with the spread of tumors and cancer (Vousden et al., 2007). The IC_{50} values of TOP-3 were determined as 64.5 μg/mL for HepG2 and 47.4 μg/mL for MCF7 cells from the MTT assay, and therefore, these particular concentrations were considered for this study. A concentration of 200 μg/mL (for TOP-3) was used for 3T3-L1 and 7.5 μg/mL of CPT (standard). Substantial up-regulation for *p53* gene expression was perceived upon treatment with TOP-3 treated carcinoma cells (MCF7 and HepG2). Melting curves and amplification curves of *p53* and *β*-actin

protein were shown in, which represented the melting of all double standard DNA to single standard DNA, and a total number of cycles respectively, during the qRT-PCR reaction.

The occurrence of the *p53* gene in untreated, TOP-3, and CPT treated MCF-7, HepG2 and 3T3-L1 was confirmed by the gel photograph. Notably, an increase of a 1.5-1.8-fold *p53* gene expression in MCF7 and HepG2 cells was noted upon treatment with TOP-3 in comparison with untreated control cells. Furthermore, CPT (standard) treated MCF7 and HepG2 cells exhibited 5.7 and 2.7-fold increase in expression of *p53* gene. No significant rise in *p53* gene expression was recognized in TOP-3/CPT-treated 3T3-L1 preadipocytes compared to untreated control. Therefore, it could be concluded that TOP-3 could successfully induce apoptosis in MCF7 and HepG2 cell lines by up-regulating *p53* gene expression. Previous reports revealed anticancer activities of an alkaloid isolated from a marine sponge, by modulating *p53*-dependent transcriptional factor in the JB6 Cl41 cells and HepG2 cells (Dyshlovoy et al., 2014; Rajivgandhi et al., 2019). An induction of apoptosis in lung cancer cells through a *p53*-dependent pathway was reported by renieramycin M, which was isolated from the blue sponge *Xestospongia* sp (Halim et al., 2011). Another study reported that the polysaccharide isolated from seaweed *Laurencia papillosa* could result in the induction of apoptosis in breast cancer tumor cells through an activated *p53* gene expression (Ghannam et al., 2018).

7.6. Conclusions

The marine macroalga, *Sargassum tenerrimum*, was found to be an important natural resource of sulfated galacto-fucopyranose, exemplified as [→1)-2-*O*-sulfonato-*α*-Fuc*p*-(3→1)-2-*O*-sulfonato-*α*-Fuc*p*-(3→] units as central branch containing [(4→1)-6-*O*-acetyl-*β*-Gal*p*-(4→] unit as the lateral segment, and a nanoparticle (ST-Ag^{NP}) synthesized from that carbohydrate biopolymer exhibiting potential activities against osteoporosis or related bone disorder. The present work demonstrated that ST-Ag^{NP} produced a dose-dependent, anti-osteoporotic action in glucocorticoid-induced rats by regulating altered serum estradiol and parathyroid hormone levels and antioxidant and serum biochemical parameters are related to a bone health disorder when administered for eight consecutive weeks. ST-Ag^{NP} did not cause any noticeable adverse effects on the treated animals. The hMSC osteoblast cells treated with ST-Ag^{NP} exhibited conspicuous mineralization of the bone matrix, other than up-regulating the expression of ALP, BMP-2, and osteocalcin regarding the untreated control. ST-Ag^{NP} did not display cytotoxicity towards the osteoblast cells and showed considerable osteogenic differentiation activities, proliferating bone cells and increasing mineral deposition. The protective mechanism of ST-Ag^{NP} might be through the improvement in impaired bone structural properties in the *in vivo* osteoporosis model through its related physiological and antioxidant effects. These results suggested that ST-Ag^{NP} might be a good therapeutic lead to reduce the risk of osteoporosis.

The phaeophytan marine macroalga, *T. ornata* was found to be a significant natural source of sulfated galactofucan, represented as [→1)-*O*-4-sulfonato-*α*-fucopyranose-(3→1)-*α*-fucopyranose-(3→] as the main branch with [→1)-6-*O*-acetyl-*β*-galactopyranose-(4→] as side branch exhibiting potential activities against ductal carcinoma (MCF7) and hepatocellular liver carcinoma (HepG2) cells. Sulfated galactofucan resulted in significant cytotoxicity on MCF7 and HepG2 cell lines, which was evaluated by SRB, MTT, NRU, and LDH assays . In contrast, no cytotoxic effect was apparent in the case of 3T3-L1 preadipocytes cells. Sulfated galactofucan treated MCF7 and HepG2 cell lines exhibited a reduction of cell viability than the untreated control cells and were comparable with CPT (standard) treated cells. Quantification of apoptosis was studied by annexin V/FITC-PI-stained flow cytometric method and the early apoptotic cells were significantly greater in the case of sulfated galactofucan treated MCF7 and HepG2 cell lines, than those exhibited by untreated cell lines, and the percent of early apoptotic cells were comparable with standard (CPT). Acridine orange/ethidium bromide fluorescence staining study could further display an enhanced apoptotic

alteration in the sulfated galactofucan-treated ductal carcinoma (MCF7) and liver hepatocellular carcinoma (HepG2) cells in comparison with the untreated control, and no such significant difference was perceived with CPT-treated MCF7 and HepG2 cells. The studied galactofucan resulted in an elevation of *p53* gene expressions in comparison with untreated controls. These findings suggested that sulfated galactofucan isolated from *T. ornata* might be used as an alternate approach for the treatment of ductal and hepatocellular carcinoma. In future research, the apoptotic effect of sulfated galactofucan will be evaluated on in vivo- based model.

The immune system is considered one of the critical factors for human health and well-being, specifically during the era of the novel coronavirus SARS-CoV-2 outbreak. The marine macroalga, *Turbinaria conoides* was found to be a predominantly available natural resource of sulfated galactofucan (TCP-3), characterized as [→1)-*O*-4-sulfonato-*α*-fucopyranose-(3→1)-*O*-2-sulfonato-*α*-fucopyranose-(3→] as the main backbone with [→1)-*β*-galactopyranose-(4→] with 6-*O*-acetyl substitution as a side branch, showing potential immunomodulatory and anti-inflammatory activities. TCP-3 exhibited the immunomodulatory potential by increasing bone marrow stem cell differentiation, *α*-esterase activity, and lymphocyte blastogenesis in CTX-induced immunosuppressed mice. TCP-3 also induced antiviral and immune activation by upregulating serum IFN-*γ* and IL-2 levels in CTX-induced animals. Anti-inflammatory activities of TCP-3 were exhibited by regulating the secretion of pro-inflammatory cytokines, such as TNF-*α*, IL-6/1*β*/12, TGF-*β,* and NO in different *in vitro* and *in vivo* models. Cytopathic effect and viral copy formation on Vero cells (with SARS-CoV-2 infection) were substantially reduced after the treatment with TCP-3. The (1→3) linked fucopyranose and (1→4) linked galactopyranose in TCP-3 could interact with membrane-associated pattern recognition receptors to prevent the virus entry through cellular signaling pathways and stimulate inflammatory cytokine production. In conclusion, these results suggested that treatment with TCP-3 might be a good naturally derived alternative source for health benefits against inflammation and autoimmune disorders. TCP-3 could also be utilized as a potential natural antiviral polysaccharide against SARS-CoV-2 infection, developed from marine organisms.

CHAPTER 8: SUMMARY

Oceans cover approximately more than 70% of the earth's surface. The oceanic ecosystem is a treasure house of natural compounds with their intrinsic biological potentials and usefulness as a functional food. Among various marine flora and fauna, marine macroalgae are often regarded as *wonder plants* of the sea. They are unique marine living resources with various economic applications and ecological significance. Recently, there has been an increasing interest in marine macroalgae due to its copious positive benefits. The sector has attracted a lot of investments the World over and is expanding rapidly. Thus, marine macroalgae offer a considerable opportunity for the blue economy. Marine macroalgae are a rich source of nutrients, bioactive compounds and secondary metabolites. The macronutrients and micronutrients present in the marine macroalgae have the potential to supply sustainable nutrients to meet the ever-increasing nutritional requirements of humankind, and the bioactive compounds form the basis for the production of a broad spectrum of high-value products, such as nutraceuticals, functional foods, cosmeceuticals and chemicals. The versatile secondary metabolites derived from marine macroalgae have interesting functional properties and offer many possibilities for developing novel drugs/ future pharmaceuticals. Marine macroalgae or seaweed-derived active ingredients and structurally diverse bioactive compounds have potential pharmaceutical advantages and are endowed with pluralities of bioactivities against different diseases. Sulfated polysaccharides, lipids, steroids, terpenoids, alkaloids etc., are some of the structurally other bioactive metabolites obtained from marine macroalgae (Barzkar et al., 2020;

Malve et al., 2016). Among various marine macroalgae, brown macroalgae constitute a predominant share of algal resources worldwide. There is immense potential for these florae as a source of potentially beneficial bioactive compounds against various drug targets. Among brown marine macroalgae, those belonging to *Sargassum* and *Turbinaria* (family: Sargassaceae) constitute an essential part of commercially exploited seaweeds in India and various regions of the World. Considering the promising perspective for utilizing these marine macroalgae groups and limited research reports on their utilization as a potential health food, their pharmaceutical potential began to receive considerable attention.

Marine macroalgae are considered one of the essential components of marine habitats (constitute 10% share of all marine flora and fauna) and were reported to comprise minerals, vitamins, carotenoids, phenolics, polysaccharides, amino acids, proteins and other metabolites (Hakim et al., 2020). These chemical entities exhibited diverse biological activities encompassed anti-inflammatory, antiviral, anticancer, antihypertensive, antihyperglycemic etc. (Hakim et al., 2020). Brown algal species belonging to the family Sargassaceae (class Phaeophyceae, phylum Ochrophyta) are the most abundant and diversified class of macroalgae distributed in cold-temperate and tropical ocean water. This specific class of marine plants is found to have substantial ecological importance due to their growth (in the dense belt) in the intertidal zone of several rocky shores of temperate oceans. It also provides valuable habitat to support biological diversity. Therefore, brown algae are accounted as keystone species of marine life. Marine macroalgae naturally protect themselves from hypersaline and oxidative stress conditions in the hostile oceanic ecosystem because they lack an external protective shield. Therefore, these marine florae have been a favourite choice among researchers because the probability of finding bioactive metabolites (for use in health food and pharmaceutical industries) against various oxidative stress-mediated disorders is expected to be higher. The pathophysiologies of various chronic diseases, such as cancer, inflammation, diabetes, and hypertension, are progressed by reactive oxygen species (ROS) induced altered cellular pathways. Excessive production of reactive oxygen species (ROS) can be reduced by antioxidant compounds protecting living organisms from protein damage, lipid peroxidation and DNA damage (Begum et al., 2021). In this current study, four different brown algae (*Turbinaria conoides*, *Turbinaria ornata*, *Sargassum ilicifolium*, and *Sargassum tenerrimum*) belonging to the family Sargassaceae (Order Fucales) were selected from the Gulf of Mannar region, India and their crude methanol-ethylacetate (MeOH/EtOAc) extracts were screened for oxidative radical inhibition, antihypertensive, anti-inflammatory, and antihyperglycemic properties. The crude extract of *T. conoides* and *T. ornata* displayed significantly greater total phenolic content (TPC) (~ 33 and 24 mg GAE/g, respectively) in comparison with *Sargassum* species (< 20 mg GAE/g). Overall antioxidant, anti-inflammatory, antihypertensive, and antihyperglycemic activities of *Turbinaria* species were also superior to *Sargassum* species. The presence of more significant numbers of antioxidants might be responsible for the studied activities of *T. conoides* and *T. ornata* related to inflammation, hyperglycemia, and hypertension. Targeted bioactive potentials of crude macroalgal extracts were further supported by polar/or electron-donating groups in the downfield region of 1H NMR spectra. These results suggested that these crude macroalgal extracts might be sources of the different classes of bioactive pharmacophores, which can be used to combat various lifestyle diseases.

Bioactivity-guided fractionation of *T. conoides* resulted in isolating and characterizing of seven bioactive metabolites (three 2*H*-pyran derivatives, three macrocyclic derivatives and one isochromanone derivative). The structural interpretations of these isolated compounds were confirmed by one-dimensional (1D) nuclear magnetic resonance (NMR) spectroscopy, including carbon (^{13}C NMR), proton (^{1}H NMR), distortionless enhancement by polarization transfer (DEPT NMR) along with two-dimensional (2D) NMR {correlation spectroscopy (^{1}H-^{1}H COSY), heteronuclear single quantum coherence (HSQC), heteronuclear multiple bond correlation (HMBC), nuclear overhauser effect (NOE)}, Fourier-transform-infrared (FTIR), and mass spectroscopic analyses. Among those three 2*H*-pyran derivatives, compound **1** displayed higher free radical scavenging activities against DPPH (IC_{50} 0.54 mg mL^{-1}) and

$ABTS^+$ (IC_{50} 0.58 mg mL^{-1}), followed by **2** (IC_{50} 0.59 and 0.69 mg mL^{-1}, respectively) and **3** (IC_{50} 0.68 and 0.76 mg mL^{-1}, respectively). Also, the pro-inflammatory cyclooxygenase-2 (COX-2) and 5-lipoxygenase (5-LOX) enzyme inhibitory activities of **1** and **2** were considerably greater (IC_{50} ~ 1 mg mL^{-1}) in comparison with compound **3** (IC_{50} > 1.1 mg mL^{-1}). The selectivity index of compound **1** (anti-COX-1_{IC50}/anti-COX-2_{IC50} ~ 1.9) was also higher than other studied analogues, which implied its greater anti-inflammatory selectivity towards pro-inflammatory inducible COX-2 enzyme. Their different structural descriptors further corroborated the antioxidative and anti-inflammatory properties of studied 2*H*-pyranoids. In the case of hydrophobic parameter, no significant difference was noticed between compounds **1**-**3** (log P_{OW} ~ 4.4-4.62). A more substantial number of electron-rich centres in compound **1** resulted in its superior bioactivities, which were reflected by its higher electronic parameters (tPSA ~ 61.83, Pl ~ 44 × 10^{-24} cm^3) than other analogues. These might be the factors responsible for the more significant interactions of compound **1** with pro-inflammatory inducible enzymes and oxidant species at their active reaction sites. Overall bioactivity data, more significant electronic factors, and optimum lipophilic-hydrophilic balance of studied 2*H*-pyranoids suggested compound **1** with substituted dihydropyran, 4-hydroxybenzoate and methyl butanoate units, might constitute a naturally-derived potential anti-inflammatory lead.

The next set of metabolites obtained from *T. conoides* was comprised of macrocyclic framework. All three compounds (**4**-**6**) possessed with basic dioxabicyclo[19.3.1]pentacosa skeleton. Compounds **5** and **6** contained an extra isobutylacetate and methylacetate side chain, respectively. Among those macrocyclic lactones, compound **4** showed dual inhibition properties against COX-2 and 5-LOX (IC_{50} 1.75 and 4.24 mM, respectively) enzymes, which was higher than compounds **5** and **6**. Higher selectivity index (SI) of compound **4** (1.79) was observed in comparison with compounds **5** and **6** (1.65-1.68). From this result, it could be concluded that compound **4**, with greater specificity towards COX-2 enzyme inhibition, was noteworthy towards the development of selective anti-inflammatory therapeutic lead. Compound **4** also exhibited substantial attenuation properties against angiotensin-converting enzyme-I (ACE-I) and protein tyrosine phosphatase-1B (PTP-1B) (IC_{50} 1.23 and 1.39 mM, respectively) compared to other two analogues (IC_{50} > 1.80 mM). Similar trend was observed in case of radical scavenging activities, whereas compounds **5** and **6** (IC_{50DPPH} 1.35-1.54 and IC_{50ABTS} 1.54-1.81 mM) exhibited lesser activity than compound **4** (IC_{50DPPH} 1.20 and IC_{50ABTS} 1.48 mM). In this case, the steric factors played important roles towards these potential bioactivities. Maximum steric bulkiness of compounds **5** and **6** (due to the presence of extra side chain) could make those less efficient towards the conformationally unfavoured interactions with active binding sites of the target enzymes. Notably, the hydrophobicity of compound **4** (log P_{OW} 3.13) was found to reside within the permissible range of hydrophobic-lipophilic threshold, which could also attribute to its prospective bioactivities and effective permeability. Swiss ADME study of these compounds predicted that compound **4** could possess greater oral bioavailability (passed the filter of Lipinski's rule without any violation). Also, comparatively better skin permeability (pharmacokinetic parameter) was observed for compound **4**, than those exhibited by **5** and **6**. *In-silico* molecular docking studies against 5-LOX further corroborated more excellent compound 4, COX-2, ACE-I, and PTP-1B enzyme bioactivities. Compound **4** displayed maximum numbers of hydrogen bonding interactions with these enzyme active sites, minimum binding energies, and docking scores compared to the other two studied compounds. Therefore, it could be concluded that compound **4** with pentacosa macrocyclic moiety could be a promising therapeutic lead against different chronic disorders.

Another isochromanone derivative (compound **7**) obtained from *T. conoides* showed potent attenuation against 5-LOX (IC_{50} 3.70 μM) enzyme, and the bioactivity of this compound was compared with synthetic standard. The chemical structure of compound **7** comprised ethyl dihydrofuran attached oxo-benzopyran ring with a methyl butyrate side chain. Superior electronic parameters (tPSA 61.8) and optimal lipophilic-hydrophilic balance (log P_{OW}~3.43) of compound **7** recognized its anti-inflammatory and free radical scavenging potential (IC_{50}~24 μM). *In-silico* molecular docking of compound **7** recorded binding energies of -11.05 and -9.40 kcal mol^{-1} with COX-2 and 5-

LOX, respectively. The predicted bioavailability radar plot of this studied compound exhibited its acceptable oral bioavailability and drug-likeness.

A total of six bioactive metabolites (three 6,6-spiroketal derivatives and three cyclooctafuranone analogues) were isolated from EtOAc/MeOH extract of *T. ornata*. Among those three spikokrtal analogues (compounds **8**-**10**), compound **8** displayed greater ACE-I inhibitory property (IC_{50} 4.55 μM) than those exhibited by compounds **9** and **10** (IC_{50} 4.72 and 4.86 μM, respectively). It is important to note that presence of electronegative groups in oxodecahydrospiro [furo-3,4-c] pyran-7,2′-pyranyl skeleton with esterified side chain in compound **8** could evidently form hydrogen bonding interactions with the aminoacyl residues ACE-I active site. These results were further supported by molecular docking study, where compound **8** was noted with lesser docking score (-11.55 kcal/mol) and binding energy (-10.55 kcal/mol) in comparison with other studied spiroketals. This finding evidently established its favourable interactions and promising binding affinity with the allosteric sites of ACE-I enzyme than those exhibited by others. Predicted electronic parameter of the compound **9** (tPSA 88.13) was higher than compound **8**. The steric parameters of compound **9** and **10** (P > 900) also exhibited with higher values than compound **8** (P 882), which could be the reason for their lesser bioactivity due to the unfavorable condition to react with the targeted enzyme. Compounds **9** and **10** were composed of a common core unit of oxodecahydrospiro [isochromene-8,2′-pyran] with side chains of pent-4ª-en-1ª-acetate and 6ª-methylocta-1ª,5ª-diene. Based on this analysis, compound **8** could be used as a potential therapeutic lead against hypertensive disorders.

Three cyclooctafuranone analogues (compounds **11**-**13**) isolated from *T. ornata* were tested against PTP-1B, *α*-amylase, and *α*-glucosidase enzymes. Among these studied metabolites, compound **12** exhibited more significant inhibition potential against PTP-1B (IC_{50} 2.42 mM) compared to those exhibited by compounds **11** and **13** (IC_{50} > 2.55 mM), which also explained greater selective attenuation property of compound **12** toward PTP-1B enzyme. Likewise, the attenuation potential of *α*-amylase and *α*-glucosidase enzymes were higher in the case of compound **12** (IC_{50} 0.31 and 0.27 mM, respectively) compared to those displayed by compounds **13** and **11**, in descending order. Molecular docking analysis of compounds **11**-**13** was accomplished with insulin signaling pathway regulator PTP-1B. Among the isolated metabolites, compound **12** exhibited two hydrogen bonding interactions in the catalytic domain of the target enzyme, whereas no hydrogen bonding interactions were observed for compounds **11** and **13**. Additionally, lesser binding energy (-11.80 kcal/mol), inhibition constant (54.79 pM), and docking score (-12.78 kcal/mol) of compound **12** with the binding site of PTP-1B supported its potent anti-hyperglycemic properties. Conspicuously, compound **12** also displayed potential scavenging properties against DPPH and $ABTS^{+}$ radical species (IC_{50} 1.05-1.24 mM), which also reinforced its potencies against free radical oxidant species that could play a major role in hyperglycemia by elevating the production of advanced glycation end products.

One xenicane diterpenoid derivative (compound **14**) was obtained from *S. ilicifolium* showed potent attenuation against cyclooxygenase-2 (IC_{50} 2.47 mM) and 5-lipoxygenase (IC_{50} 4.70 mM) enzyme along with greater anti-inflammatory selectivity index (1.4). The xenicane diterpenoid derivative (compound **14**) showed adequate antioxidant properties against ABTS (IC_{50} 1.38 mM) and DPPH (IC_{50} 1.26 mM). The chemical structure of compound **14** is composed of furan attached nine-membered skeleton with hydroxy methyl-heptene side chain. Suitable electronic parameters (tPSA 82) and optimum lipophilic-hydrophilic (L-H) balance of compound **14** might be attributed towards the effective permeability of the targeted enzymatic cellular network. *In-silico* molecular docking of compound **14** recorded a binding energy of -9.61 kcal mol^{-1} with the 5-LOX enzyme. Predicted drug likeliness nature, acceptable oral bioavailability, and potential bioactivity of compound **14**, suggested its usefulness as naturally-derived anti-inflammatory lead that could prevent the production of inflammatory prostaglandins, thromboxane, and leukotrienes.

Three sulfated polysaccharides were isolated from *S. tenerrimum*, *T. ornata* and *T. conoides*, all of these crude polysaccharides were purified by diethylaminoethyl DEAE anion exchange chromatography. Major carbohydrate-

containing fractions were selected and their structural characterizations were accomplished by detailed spectroscopic studies (1D and 2D NMR, FTIR, mass). A sulfated galacto-fucopyranose was isolated from the marine brown alga *Sargassum tenerrimum* and a nanoparticle (ST-Ag^{NP}) was synthesized from that carbohydrate biopolymer. The particle size and morphology of ST-Ag^{NP} was confirmed by particle size analyzer, SEM, TEM and AFM analyses. Elemental composition and crystallinity of ST-Ag^{NP} was obtained from EDAX and XRD analyses, respectively. The stability of ST-Ag^{NP} was confirmed by its negative zeta potential values (-35.4). ST-Ag^{NP} exhibited potential activities against osteoporosis and related bone health disorder. No cytotoxicity was observed on osteoblast cells after the administration of ST-Ag^{NP} thus, it showed considerable osteoblast differentiation potencies, which proliferates bone cells by increasing calcium mineral deposition. The osteoblast cells (hMSC) administrated with ST-Ag^{NP} displayed noticeable bone matrix mineralization, apart from the elevation of ALP, BMP-2, and osteocalcin expression in comparison with the untreated control. Altered serum parathyroid hormone and estradiol levels of glucocorticoid-induced animals were significantly recovered (including other serum biochemical parameters) upon administration of ST-Ag^{NP} in a dose-dependent manner. Also, ST-Ag^{NP} did not cause any obvious adverse effects on the treated animals. These results suggested that ST-Ag^{NP} might be a promising therapeutic lead for the treatment of osteoporosis.

Another polysaccharide (TOP-3) was obtained from the phaeophytan marine macroalga, *T. ornata*, with potential activities against liver hepatocellular carcinoma (HepG2) and ductal carcinoma (MCF7) cells. Significant cytotoxicity was observed on MCF7 and HepG2 cell lines after the administration of TOP-3, whereas no cytotoxic effect was observed in the case of 3T3-L1 preadipocytes cells. Induction of early apoptotic cells was found to be significantly more significant in the case of TOP-3 treated HepG2 and MCF7 cell lines, and an enhanced apoptotic alteration was noticed in TOP-3 treated MCF7 and HepG2 cells in comparison with untreated control. The studied galactofucan (TOP-3) further showed upregulation of *p53* gene expressions compared with normal cells. These results suggested that TOP-3 might be used as an alternate to the treatment against ductal and hepatocellular carcinoma.

A sulfated galactofucan (TCP-3) was isolated from *Turbinaria conoides* showed potential immunomodulatory and anti-inflammatory activities. Toxicity study of TCP-3 showed its nontoxic nature in *in vivo* and *in vitro* models. The relative lymphoid organs (spleen and thymus) weights along with total WBC count were significantly reduced in cyclophosphamide (CTX)-induced (0.179, 0.098%, and 2300 cells/cu mm, respectively), which showed considerable recovery (which signified the triggered immune response by lymphocytes) after the treatment with TCP-3 (0.271, 0.143%, and 4300 cells/cu mm, respectively; @100-400 mg/kg BW). Administration of TCP-3 at 200 mg/kg BW resulted a noteworthy recovery of bone marrow cells and α-esterase activity (13.54 cells/femur/mL x 10^6 and 1680 positive cells/4000 BMC, respectively). The level of serum IFN-γ and IL-2 in CTX-induced animals was recovered (1.49 and 3.99 pg/mL, respectively) upon treatment with TCP-3 at 100 mg/kg BW. The protective effect of TCP-3 on blastogenesis of splenocytes, thymocytes, and bone marrow was evaluated in viable cells and it showed a notable upregulated cell proliferations with the presence of mitogens. A substantial upregulation in mRNA expression of IL-2 and IFN-γ was observed in TCP-3 treated Jurkat cells. Anti-inflammatory activities of TCP-3 were showed by the regulation pro-inflammatory cytokines secretion, such as TNF-α, IL-6/1β/12, TGF-β, and NO in different *in vitro* and *in vivo* models. Viral copy formation and cytopathic effect on SARS-CoV-2 infected Vero cells were significantly reduced after the treatment with TCP-3. The (1→3) linked fucopyranose and (1→4) linked galactopyranose in TCP-3, could possibly interact with membrane-associated PRRs (pattern recognition receptors) to inhibit the entry of virus through cellular signaling pathways and also stimulate the production of inflammatory cytokines. Therefore, these results suggested that administration of TCP-3 might be a good naturally-derived alternate source against autoimmune and inflammation disorders. In addition, TCP-3 could also be used as algal-derived natural antiviral polysaccharide against SARS-CoV-2 infection.

The present study established that the marine macroalgae or seaweed-derived functional ingredients from those belonging to the family Sargassaceae, particularly *Turbinaria* and *Sargassum*, and structurally diverse bioactive compounds have potential pharmaceutical advantages and are endowed with pluralities of bioactivities against different diseases. The work developed small molecular weight bioactive and those of polysaccharide origin from brown marine macroalgae *Turbinaria conoides*, *Turbinaria ornata*, *Sargassum ilicifolium*, and *Sargassum tenerrimum* towards their utilization as valuable natural leads for use against oxidants, inflammatory cytokines, hypertension, and hyperglycemia. Developing newly reported bioactive compounds from the studied bioactive metabolites would form the basis for new drug leads. Noticeably, there is an increasing share of patent applications from marine-derived bioactive compounds. The recent thrust of an increased list of granted patents concerning marine pharmacophores signifies the importance of research in marine bioactive molecules. Brown macroalgae of *Turbinaria and Sargassum* constitute a predominant share of seaweed resources worldwide. This group of marine flora has immense potential as a source of potentially beneficial bioactive compounds against various drug targets. Considering the promising perspective for utilizing this group of marine macroalgae belonging to the family Sargassaceae, and limited research reports on their utilization as a potential health food, the present study concerning their pharmaceutical potential is significant.

Marine macroalgae have the potential to contribute to sustainable futures. This group of marine flora could be used to address many of the 'Development Challenges' directly linked to the United Nations Sustainability Development Goals (SDG). The macronutrients and micronutrients present in marine macroalgae can meet the population's nutritional requirements. Thus, they could help achieve SDG 2, which involves ending hunger, achieving food security and improving nutrition. The bioactive compounds and specialized secondary metabolites of marine macroalgae could promote well-being and thus support achieving SDG 3, which envisages ensuring a healthy life.

REFERENCES

The references from all the chapters have been cited in this section.